UNCLASSIFIED

AD 268 201

Reproduced
by the

ARMED SERVICES TECHNICAL INFORMATION AGENCY
ARLINGTON HALL STATION
ARLINGTON 12, VIRGINIA

DEPARTMENT OF DEFENSE

UNCLASSIFIED

NOTICE: When government or other drawings, specifications or other data are used for any purpose other than in connection with a definitely related government procurement operation, the U. S. Government thereby incurs no responsibility, nor any obligation whatsoever; and the fact that the Government may have formulated, furnished, or in any way supplied the said drawings, specifications, or other data is not to be regarded by implication or otherwise as in any manner licensing the holder or any other person or corporation, or conveying any rights or permission to manufacture, use or sell any patented invention that may in any way be related thereto.

CATALOGED BY ASTIA
AS AD No. 268 201
268201

AFFTC TECHNICAL REPORT 61-18

STORAGE, SERVICING, TRANSFER, AND HANDLING OF HYDROGEN

May 1961

Directorate of Rocket Propulsion and Missiles

Contract AF 33(616)-7330

ASTIA
DEC 20 1961
TIPDR

AIR FORCE FLIGHT TEST CENTER
AIR RESEARCH AND DEVELOPMENT COMMAND
UNITED STATES AIR FORCE
EDWARDS AIR FORCE BASE, CALIFORNIA

AFFTC TECHNICAL REPORT 61-18

STORAGE, SERVICING, TRANSFER, AND HANDLING OF HYDROGEN

A. W. Adkins
I. A. Black
R. W. Byrnes
R. W. Breckenridge, Jr.
A. A. Fowle
F. Gabron
F. E. Ruccia

Arthur D. Little, Inc.
Cambridge, Massachusetts

May 1961

Directorate of Rocket Propulsion and Missiles

Contract AF 33(616)-7330

Project Number 0(1-8119)

Task Number 60196

AIR FORCE FLIGHT TEST CENTER
AIR RESEARCH AND DEVELOPMENT COMMAND
UNITED STATES AIR FORCE
EDWARDS AIR FORCE BASE, CALIFORNIA

NOTICES

When Government drawings, specifications, or other data are used for any purpose other than in connection with a definitely related Government procurement operation, the United States Government thereby incurs no responsibility nor any obligation whatsoever; and the fact that the Government may have formulated, furnished, or in any way supplied the said drawings, specifications, or other data, is not to be regarded by implication or otherwise as in any manner licensing the holder or any other person or corporation, or conveying any rights or permission to manufacture, use, or sell any patented invention that may in any way be related thereto.

- - - - - - -

Qualified requestors may obtain copies of this report from the Armed Services Technical Information Agency,(ASTIA), Arlington Hall Station, Arlington 12, Virginia.

- - - - - - -

Copies of AFFTC Technical Reports and Technical Notes should not be returned to the Air Force Flight Test Center unless return is required by security considerations, contractual obligations, or notice on a specific document.

FOREWORD

Contract AF 33(616)-5641, initiated by the Aeronautical Accessories Laboratory, Wright Air Development Center, Wright-Patterson Air Force Base, Ohio provided WADC Technical Report 59-386, "Storage, Transfer and Servicing Equipment for Liquid Hydrogen," July 1959 and a "Handbook for Hydrogen Handling Equipment," WADC Technical Report 59-751, February 1960, by Arthur D. Little, Inc. These publications set forth a body of information concerning the proper selection and design of equipment for handling large quantities of liquid hydrogen and the most adequate, safe, and economical procedures for operating ground servicing systems.

Contract AF 33(616)-7330, also initiated by the Wright Air Development Center, provides this Technical Report of following and related work. Its purpose is to reinforce, in certain important areas, the existing information and engineering data relating to the design and use of liquid hydrogen ground handling equipment. This report is submitted by Arthur D. Little, Inc., Cambridge, Mass., per Item IV, Paragraph B, Part I of the contract. Research began April 11, 1960 and was completed on April 30, 1961. Six bimonthly progress reports - entitled "Storage, Servicing, Transfer and Handling of Hydrogen" - were issued on July 15, 1960, September 15, 1960, November 15, 1960, January 17, 1961, March 15, 1961 and May 23, 1961.

In addition to the authors listed on the title page, we acknowledge the major contributions of Prof. R. C. Reid of the Chemical Engineering Department, Massachusetts Institute of Technology, to Sections II and III of this publication.

Technical administration of the contractor's work was under the direction of Captain Raymond A. Tondreau, Project Officer, first with the Servicing and Maintenance Equipment Branch, Aeronautical Accessories Laboratory, Wright Air Development Division and later with the Directorate of Rocket Propulsion and Missiles, Air Force Flight Test Center, Edwards Air Force Base, California.

In order to fulfill the contract requirement specifications, cost and delivery data and sources of supply of certain commercial items obtained from the manufacturers are herein presented. This information is set forth as a guide to the potential user in the selection of commercial items and should not be construed to represent a manufacturer's guarantee. In all instances, it is expected that the user will obtain from the manufacturers the necessary confirmation pertaining to the specifications, cost, and delivery of his product.

No attempt has been made to include all commercial sources for a given item; rather, the intent has been to acquaint the potential user with representative sources. This fact is not to be construed as a preferential endorsement by Arthur D. Little, Inc., of the products of the manufacturers listed.

The service experience of commercial items is set forth to indicate the state of development in reference to liquid hydrogen applications. Again, the potential user is directed to the individual manufacturer for complete and up-to-date service information.

ABSTRACT

This report documents the results of investigations into six technical areas pertaining to the handling of large quantities of liquid hydrogen. The engineering data developed are reported in six separate sections.

Section I establishes the current availability and specifications for liquid hydrogen pumps and cites the operational experience reported by the major users of these items.

Section II sets forth a tested method for predicting the hydrogen gas required for the pressurized transfer of liquid hydrogen.

Section III recounts the known facts relating to the safety and reliability of hydrogen gas cylinders as used in typical operations for the pressurized transfer of liquid hydrogen.

Section IV presents the design specifications and performance characteristics of gravity-fed and boosted pressure-fed vaporizers for liquid hydrogen transfers established as a result of an integrated program of theoretical analysis and tests.

Section V includes an economic comparison of systems using pumps, hydrogen vaporizers and high pressure hydrogen gas bottles to transfer liquid hydrogen. This work represents a refinement or up-dating of that originally presented in Chapter 3 of the "Handbook for Hydrogen Handling Equipment" and WADC Technical Report 59-386.

Section VI presents the results of a further investigation of the single parting line coupling for vacuum-jacketed transfer lines originally reported in WADC TR-59-386. A modified design and its performance characteristics established from tests are included.

PUBLICATION REVIEW

The publication of this report does not constitute approval by the Air Force of the findings or conclusions contained herein. It is published only for the exchange and stimulation of ideas.

FOR THE COMMANDER:

TABLE OF CONTENTS

Page

List of Tables viii

List of Figures ix

I. LIQUID HYDROGEN PUMPS 1

- A. INTRODUCTION 1
- B. CONCLUSIONS 1
- C. LIQUID HYDROGEN TRANSFER PUMPS 1
- D. LIQUID HYDROGEN HIGH-PRESSURE PUMPS 3
- E. REFERENCES 3

II. PRESSURIZED TRANSFER OF LIQUID HYDROGEN WITH HYDROGEN GAS 16

- A. SCOPE 16
- B. INTRODUCTION 16
- C. DESCRIPTION OF PROCESS 16
- D. NOMENCLATURE 18
- E. LIMITING-CASE MODEL 19
- F. EQUIVALENT MASS MODEL 25
- G. REFERENCES 60

III. REQUIREMENTS FOR HYDROGEN GAS STORAGE CYLINDERS USED FOR THE PRESSURIZED TRANSFER OF LIQUID HYDROGEN 61

- A. INTRODUCTION 61
- B. NOMENCLATURE 62
- C. ANALYSIS OF THE BLOWDOWN PROCESS 63

TABLE OF CONTENTS (Continued)

Page

III. REQUIREMENTS FOR HYDROGEN GAS STORAGE CYLINDERS USED FOR THE PRESSURIZED TRANSFER OF LIQUID HYDROGEN (Continued)

- D. EXPERIMENTAL PROCEDURE 65
- E. INSTRUMENTATION 65
- F. RESULTS 67
- G. COMPARISON OF THEORY WITH EXPERIMENTAL DATA 71
- H. TEMPERATURES IN THE NECK OF THE BOTTLE 71
- I. TEMPERATURE GRADIENTS IN THE CYLINDER NECK WALL 71
- J. DEPRESSURIZATIONS OF LARGE GAS STORAGE BOTTLES 73
- K. THERMAL STRESS ANALYSIS 78
- L. BOTTLE NECK STRESSES DURING BLOWDOWN 86
- M. CONCLUSIONS 86
- N. REFERENCES 87

IV. THE TRANSFER OF LIQUID HYDROGEN USING VAPORIZERS 88

- A. SUMMARY 88
- B. NATURAL CONVECTION REGENERATIVE VAPORIZER SYSTEM WITH SUPERHEAT 89
- C. NATURAL-CONVECTION VAPORIZER WITH AN AUXILIARY STORAGE SYSTEM 121

TABLE OF CONTENTS (Continued)

Page

IV. THE TRANSFER OF LIQUID HYDROGEN USING VAPORIZERS (Continued)

D. TEST PROCEDURES AND APPARATUS 134

E. REFERENCES 143

V. ECONOMIC COMPARISON OF VARIOUS MEANS FOR TRANSFERRING LIQUID HYDROGEN 144

A. INTRODUCTION 144

B. BASIS OF COMPARISON 146

C. COMPARISON OF SYSTEMS C_1, C_{1A}, and C_3 146

D. CONCLUSIONS 147

E. REFERENCES 148

VI. DEVELOPMENT OF A COUPLING FOR A VACUUM-JACKETED LINE 150

A. INTRODUCTION 150

B. DESIGN DESCRIPTION 150

C. MANUFACTURING 154

D. TESTS 156

E. CONCLUSION 162

F. REFERENCES 162

LIST OF TABLES

Table No.		Page
1.1	Available Liquid Hydrogen Transfer Pumps	5
1.2	Available Liquid Hydrogen High-Pressure Pumps	13
2.1	Calculated Results Based on "Worst Case" Model For Pressurized Liquid Hydrogen Transfer	23
2.2	Test Results--Pressurized Liquid Hydrogen Transfer Tests	28
2.3	Data for Liquid Hydrogen Transfer Test	47
2.4	Comparison Between Experimental and Calculated Values of Gas Consumption	59
3.1	Temperature Data and Maximum Stress in Bottle Neck During Blowdown	87
4.1	Calculated Design Parameters	129
4.2	Comparison of Measured and Theoretical Pressure Drops	131
4.3	Transfer Test--Experimental vs. Theoretical Results	133

LIST OF FIGURES

Figure No.		Page
1.1	Head-Flow Characteristics of Available Liquid Hydrogen Pumps	2
2.1	"Worst" Case Model for Liquid Hydrogen Transfer	20
2.2	Gas-Requirement Limits for Pressurized Transfer of Liquid Hydrogen	26
2.3	Measured Gas Consumption for Pressurized Transfer of Liquid Hydrogen	27
2.4	Temperature-Enthalpy Diagram Showing Isobar which Results in Zero Correction Mass	32
2.5	Enthalpy-Temperature Plot for Hydrogen	33
2.6	Effect of Ullage Temperature and Pressure on Corrected Mass	34
2.7	Heat Transfer Coefficients for Natural Convection on Cooled Vertical or Horizontal Surfaces--Hydrogen Gas	40
2.8	Integrated Heat Capacity for Stainless Steel	50
2.9	Relationship Between T_s and T_w from Equation (26)	51
2.10	Heat Capacity of Stainless Steel	52
2.11	Relationship Between Wall Temperature and Time	53
3.1	Thermocouple Locations on Gas Storage Cylinder	66
3.2	Experimental Variations of Pressure and Temperature, Run 7	68
3.3	Experimental Variations of Pressure and Temperature, Run 8	69
3.4	Experimental Variations of Pressure and Temperature, Run 9	70

LIST OF FIGURES (Continued)

Figure No.		Page
3.5	Heat Transfer Coefficients in Bottle Neck During Blowdown	72
3.6	Neck Wall Temperatures for Various Thicknesses in Run 7	74
3.7	Neck Wall Temperature at Various Times in Run 7	75
3.8	Gas Temperatures for Large Bottle Blowdowns	77
3.9	Average Neck Wall Temperatures for Large Bottle Blowdowns	79
3.10	Temperature Difference Between Inner and Outer Neck Wall for Case A	80
4.1	Schematic Diagram of Regenerative Vaporizer System	90
4.2	Vaporizer Temperature Rise Characteristics	95
4.3	Influence of Several Variables on Vaporizer Exit Temperature	96
4.4	Vaporizer Pressure Drop Characteristics	102
4.5	Maximum Theoretical Transfer Capabilities--Regenerative System	104
4.6	Vaporizer Operating Characteristics	106
4.7	Basic Natural-Convection Vaporizer Unit	108
4.8	Transfer System Operating Conditions	109
4.9	Vaporizer Valve Characteristics	111
4.10	Vaporizer Heat Transfer Characteristics	113

LIST OF FIGURES (Continued)

Figure No.		Page
4.11	Typical System Operating Characteristics	115
4.12	Comparison of Experimental and Theoretical Pressurizing Gas Requirements	117
4.13	System Pressure Rise Characteristics	120
4.14	Schematic Diagram of an Externally Pressurized Transfer System	122
4.15	Vaporizer Temperature Rise Characteristics	124
4.16	Vaporizer Pressure Drop Characteristics	127
4.17	Maximum Theoretical Transfer Capabilities Externally Pressurized System	128
4.18	Vaporizer Heat Transfer Characteristics	132
4.19	Vaporizer Tube Configurations	135
4.20	Schematic Diagram of Vaporizer Test Apparatus	136
4.21	Schematic Diagram of Transfer System with Regenerative Vaporizer	139
4.22	Schematic Diagram of Transfer System with Auxiliary Fed Vaporizer	142
5.1	Liquid Transfer Systems	145
5.2	Cost Comparison of Vaporizer Systems	149
6.1	Development Coupling for Vacuum-Jacketed Liquid Hydrogen Transfer Line	151
6.2	Warm and Cold Flanges of Liquid Hydrogen Transfer Line Coupling	153
6.3	Coupling Test Apparatus	157
6.4	Supply Dewar for Coupling Test	159

I. LIQUID HYDROGEN PUMPS

A. INTRODUCTION

The state of the art of liquid hydrogen pump design was reviewed and the characteristics of a number of commercially available pumps were presented in the original handbook.(1)* This report gives the latest (April 1961) information supplied by manufacturers and field users of liquid hydrogen pumping equipment.

B. CONCLUSIONS

The manufacturers of liquid hydrogen pumps for ground service have broadened their lines to some extent, improved previous designs, and tested more recent prototype designs,(2) and a few new sources have become available - a natural evolution in response to a modest demand. Pumps that were at the design stage when the initial survey was made have been built and tested. Development work has centered on devising better bearings(3) and seals,(4) which elements still limit the period of reliable operation. A great deal of effort has been directed toward the development of airborne pumps. Much of this work will lead to better ground support equipment.

At the present time, the common method for transferring liquid hydrogen in ground facilities is by pressurization rather than by pumping; consequently, very little operating experience on pumps in field service is available.

C. LIQUID HYDROGEN TRANSFER PUMPS

Table 1.1 presents a current listing of commercially available liquid-hydrogen transfer pumps. Figure 1.1 illustrates the range of flow rates and heads covered by this equipment. It is intended that Table 1.1 include all pumps known to be available, but some may have been unknowingly omitted. It should be noted that some of the pumps listed are primarily intended for airborne service.

In addition to those firms mentioned in Table 1.1, two others have directed their efforts to the development of airborne pumps but should be considered potential suppliers of pumps for ground support activities. These firms are: Rocketdyne Division of North American Aviation, Inc., and Pratt & Whitney Aircraft Division of United Aircraft Corp. The Linde Company, which reported in 1958 that it had hydrogen transfer pumps available, has indicated that

---

*See paragraph E. Separate lists of references are given at the end of each section of this report.

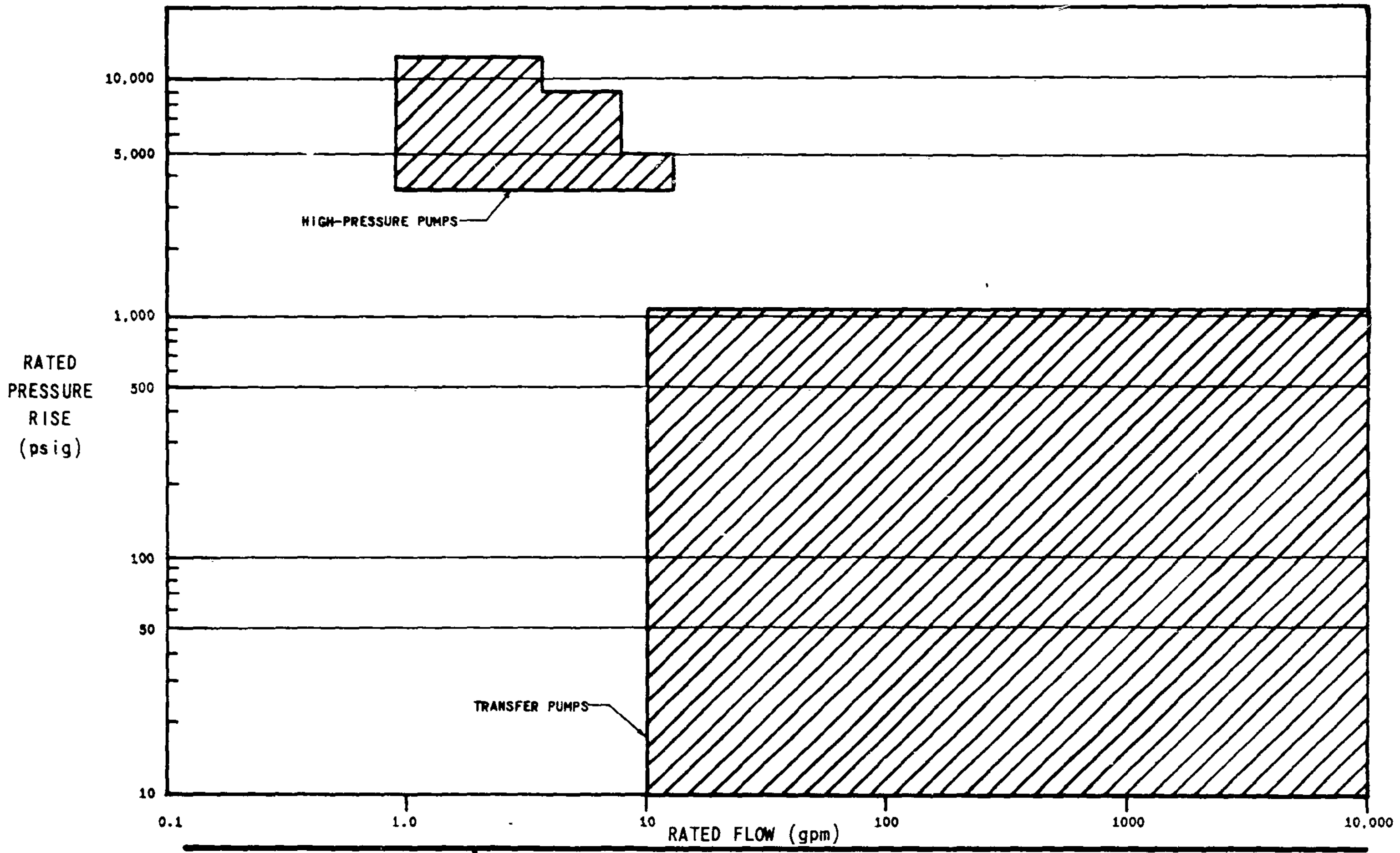

FIGURE 1.1 Head-Flow Characteristics of Available Liquid Hydrogen Pumps

it is now concentrating its efforts on high-pressure pumps to the exclusion of transfer pumps. Most manufacturers indicated that they intend to continue doing design and development work on their pumps and to continue to broaden their lines and improve their products.

D. LIQUID HYDROGEN HIGH-PRESSURE PUMPS

High-pressure pumps are presently available from three companies: Herrick L. Johnston, Inc., Linde Co., and Pesco Products. Again, this list may not be complete. Table 1.2 indicates the characteristics of these high-pressure pumps, and Figure 1.1 indicates the general range of flow rate and head rise that they cover. As may be seen from these exhibits, pumps are available for flow rates from 0.8 gpm to 12 gpm and for discharge pressures from 3500 psig to a maximum of 13,000 psig.

The present design of the single-plunger pumps incorporates the following features:(5, 6) The plunger is sealed by piston rings or chevron seals that, while not forming an absolute seal, limit the blow-by to a tolerably low quantity. The plunger is guided by two close-fitting, self-lubricated guide bushings, which also act as an additional flow restriction. In addition to the plunger seal there is an outboard plunger packing with floating-ring packings similar to the type commonly used on compressor or chevron packings made of Teflon. The floating-ring packings are made from a filled Teflon material. Heat leak into the pump is often reduced to a minimum by passing the pump discharge flow through an annulus in the plunger housing, so that most of the heat leak and friction heat is absorbed in this flow and not by the suction fluid. Limited reports from the field indicate that pumps incorporating the above features have given satisfactory service and require only minor routine maintenance.

E. REFERENCES

1. Handbook for Hydrogen Handling Equipment, WADC Technical Report 59 751 (February 1960).

2. Caine, G., Schafer, L., and Burgeson, D , "Pumping of Liquid Hydrogen," Proc. 1958 Cryogenic Engineering Conf., pp 241-254.

3. Martin, K. B., Jacobs, R. B., and Hardy, R. J., "Operation of Bearings and Pumps at Low Temperatures," Proc. 1957 Cryogenic Engineering Conf., pp 209-217.

4. Wisander, D. W., and Johnson, R. L., "Wear and Friction of Carbon Seal Materials in Cryogenic Liquids," Proc. 1960 Cryogenic Engineering Conf., pp 210-218.

5. Gottzmann, C. F., and Holcombe, A. H., "High Pressure Pumping Equipment for Cryogenic Liquids," Proc. 1958 Cryogenic Engineering Conf., pp 231-240.

6. Gottzmann, C. F., "High-Pressure Liquid-Hydrogen and -Helium Pumps," Proc. 1959 Cryogenic Engineering Conf., pp 289-298.

TABLE 1.1

AVAILABLE LIQUID HYDROGEN TRANSFER PUMPS

Aerojet-General Liquid Hydrogen Pumps
(Courtesy of Aerojet-General Corporation)

Model Number	-	-	-	-	0-219100
Type	Centrifugal	Centrifugal	Centrifugal	Centrifugal	Mixed Flow
Rated Flow	70 gpm	100 gpm	100 gpm	5640 gpm	7800 gpm
Rated Pressure Rise	375 psi	100 psi	1100 psi	1060 psi	800 psi
Efficiency	-	45%	-	-	68%
Speed	30,000 rpm	17,500 rpm	-	27,000 rpm	21,500 rpm
Type of Drive	-	-	-	-	Turbine
Drive Horsepower	-	-	-	-	4500 HP
Mounting	-	-	-	-	Any attitude
Type of Seals	-	-	-	-	Labyrinth
Type of Bearings	-	-	-	-	Commercial Ball and Roller
Design Life	-	-	-	-	100 hr
Status	-	-	-	-	Design, Development
Delivery	-	-	-	-	3 months

TABLE 1.1 (Continued)

AiResearch Liquid Hydrogen Pumps
(Courtesy of AiResearch Manufacturing Co.)

Model Number	549880	549866	549886	549844	549864
Type	Centrifugal	Centrifugal	Centrifugal	Centrifugal	Centrifugal
Rated Flow	80 gpm	200 gpm	1000 gpm	1780 gpm	8000 gpm
Rated Pressure Rise	160 psi	300 psi	978 psi	12 psi	1500 psi
Efficiency	72%	75%	74%	75%	75%
Speed	10, 500 rpm	26, 500 rpm	60, 000 rpm	19, 000 rpm	40, 000 rpm
Type of Drive	Electric Motor	Turbine	Turbine	Turbine	Turbine
Mounting	Optional	Optional	Optional	Optional	Optional
Type of Seals	Carbon Face Seals	Carbon Face Seals	Carbon Face Seals	Carbon Face Seals	Carbon Face Seals
Type of Bearings	Ball	Ball	Ball	Ball	Ball
Design Life	100 hr	100 hr	100 hr	100 hr	100 hr
Status	Prototype	Design	Design	Design	Design

TABLE 1.1 (Continued)

J. C. Carter Liquid Hydrogen Pumps (Courtesy of J. C. Carter Co.)

Model Number	6198 L	6498 L
Type	Centrifugal	Centrifugal
Rated Flow	30 gpm	150 gpm
Rated Pressure Rise	125 psi	250 psi
Speed	10, 000 rpm	7200 rpm
Type of Drive	Hydraulic Motor	Electric Motor
Drive Horsepower	-	50 HP
Mounting	Optional	Vertical Submerged
Type of Seals	Carter Cryo-Seal	None
Type of Bearings	Ball	Journal
Status	Production	Development
Approximate Price	$2500	$15, 000
Delivery	90 days	4 months
Remarks	This pump is in service	

TABLE 1.1 (Continued)

Pesco Products Liquid Hydrogen Pumps
(Courtesy of Pesco Products)

Model Number	X043466-010	X143465-010	XA143465-010
Type	Centrifugal	Centrifugal	Centrifugal
Rated Flow	80 gpm	80 gpm	180 gpm
Rated Head Rise	20 psi	20 psi	80 psi
Efficiency	60%	60%	60%
Speed	12,000 rpm	12,000 rpm	24,000 rpm
Type of Drive	Hydraulic Motor	Submerged Electric Motor	Submerged Electric Motor
Drive Horsepower	1.5 HP	1.5 HP	14 HP
Mounting	Vertical	Vertical	Vertical
Type of Seals	Face	None	None
Type of Bearings	Ball	Ball	Ball
Design Life	1000 hr	1000 hr	1000 hr
Status	Production	Production	Production
Approximate Price	$2000	$2000	$2000

TABLE 1.1 (Continued)

Pesco Products Liquid Hydrogen Pumps
(Courtesy of Pesco Products)

Model Number	X043533-010	X043456-010	X044015-010	X043991-010
Type	Centrifugal	Centrifugal	Centrifugal	Centrifugal
Rated Flow	400 gpm	500 gpm	1260 gpm	1500 gpm
Rated Head Rise	28 psi	46 psi	19 psi	254 psi
Efficiency	60%	65%	65%	70%
Speed	6000 rpm	6000 rpm	8000 rpm	15,000 rpm
Type of Drive	Hydraulic Motor	Hydraulic Motor	Hot Gas Turbine	Electric Motor
Drive Horsepower	11 HP	21 HP	21 HP	318 HP
Mounting	Horizontal	Horizontal	Vertical	Horizontal
Type of Seals	Face	Face	Face	Face
Type of Bearings	Ball	Ball	Ball	Ball
Design Life	500 hr	500 hr	500 hr	500-1000 hr
Status	Production	Production	Production	Development
Approximate Price	$4000	$5500	-	$18,000

TABLE I.1 (Continued)

Turbocraft Liquid Hydrogen Pumps
(Courtesy of Turbocraft, Inc.)

Model Number	2 x 6 x 12	1 x 2 x 6 (2 Stg.)	1 x 2 x 6 (2 Stg.)	2 x 4 x 12 (1 Stg.)
Type	Centrifugal	Centrifugal	Centrifugal	Centrifugal
Rated Flow	5-70 gpm	250 gpm	250 gpm	500 gpm
Rated Pressure Rise	1.5-300 psi	100 psi	200 psi	100 psi
Speed	7200 rpm	13,650 rpm	17,500 rpm	8400 rpm
Type of Drive	Hydraulic Motor thru Timing Belt Speed Increaser	-	-	-
Drive Horsepower	-	25 HP	50 HP	55 HP
Mounting	Vertical	-	-	-
Type of Seals	All-metal Bellows Shaft Seal	-	-	-
Status	Production	Production	-	-
Approximate Price*	$5000	$4700	$4700	$3200
Delivery	10 weeks	-	-	-

*Prices shown are tentative and do not include speed-increasing gear or motor.

TABLE 1.1 (Continued)

Turbocraft Liquid Hydrogen Pumps
(Courtesy of Turbocraft, Inc.)

Model Number	2 x 4 x 12 (2 Stg.)	2 x 4 x 12 (1 Stg.)	2 x 4 x 12 (2 Stg.)	6 x 8 x 14 (1 Stg.)
Type	Centrifugal	Centrifugal	Centrifugal	Centrifugal
Rated Flow	500 gpm	1000 gpm	1000 gpm	5000 gpm
Rated Pressure Rise	200 psi	100 psi	200 psi	100 psi
Speed	8400 rpm	8850 rpm	9000 rpm	10,000 rpm
Type of Drive	-	-	-	-
Drive Horsepower	105 HP	85 HP	170 HP	500 HP
Mounting	-	-	-	-
Type of Seals	-	-	-	-
Status	-	-	-	-
Approximate Price*	$5200	$3200	$5200	$4800
Delivery	-	-	-	-

*Prices shown are tentative and do not include speed-increasing gear or motor.

TABLE 1.1 (Continued)

Turbocraft Liquid Hydrogen Pumps
(Courtesy of Turbocraft, Inc.)

Model Number	6 x 8 x 14 (2 Stg.)	6 x 8 x 16 (1 Stg.)	6 x 8 x 16 (2 Stg.)
Type	Centrifugal	Centrifugal	Centrifugal
Rated Flow	5000 gpm	10,000 gpm	10,000 gpm
Rated Pressure Rise	200 psi	100 psi	200 psi
Speed	10,000 rpm	10,000 rpm	10,000 rpm
Type of Drive	-	-	-
Drive Horsepower	920 HP	800 HP	1500 HP
Mounting	-	-	-
Type of Seals	-	-	-
Status	-	-	-
Approximate Price*	$6700	$4800	$6700
Delivery	-	-	-

*Prices shown are tentative and do not include speed-increasing gear or motor.

TABLE 1.2

AVAILABLE LIQUID HYDROGEN HIGH-PRESSURE PUMPS

Herrick L. Johnston Liquid Hydrogen Pumps
(Courtesy of Herrick L. Johnston, Inc.)

Type	Double-acting reciprocating
Rated Flow	5 gpm
Discharge Pressure	0-5000 psi
Efficiency	76%
Speed	280 rpm
Type of Drive	Electric motor through Scotch yoke
Mounting	Horizontal
Type of Seals	Multiple Teflon chevrons with special backing ring used for both plunger-cylinder seal and plunger-packing seal. Plunger guided by carbon sleeves.
Status	Production
Approximate Price	$20,000*
Delivery	5 months
Remarks	Similar pumps in service on liquid O_2 and liquid N_2. Has been tested using liquid H_2.

*Includes pump, frame, motor, vacuum-jacketed dewar, and manual control panel. Automatic controls available at extra cost.

TABLE 1.2 (Continued)

Linde Co. Liquid Hydrogen Pump Vaporizer Units
(Courtesy of Linde Co.)

Model Number[a]	HP-8H Series	HP-20H Series	HP-60H Series
Type	Immersed single-acting Positive Displacement Reciprocating	Same	Same
Rated Flow[b]	0.8-3.6 gpm (5,500-25,000 SCF/hr)	1.7-7.1 gpm (12,000-48,500 SCF/hr)	2.9-12 gpm (20,000-82,000 SCF/hr)
Discharge Pressure	3500-13,500 psi	3500-9000 psi	3500-5000 psi
Efficiency (Volumetric)	60-90%	60-90%	60-90%
Speed	1200 or 1800 rpm	1200 or 1800 rpm	1200 or 1800 rpm
Type of Drive	Electric motor through a gear drive and cross-head-crank mechanism	Same	Same
Drive Horsepower	5-50 HP	7-1/2 - 60 HP	15-60 HP
Mounting	Vertically in sump	Same	Same
Type of Seals	Segmental rings, Teflon O-rings, longitudinal springs and piston rings	Same	Same
Type of Bearings	Teflon-impregnated porous bronze guide bushings on piston	Same	Same
Design Life	500 maintenance-free hours under normal conditions	Same	Same
Status	Production	Production	Production
Approximate Price Range[c]	$35,000-$40,000	$45,000-$50,000	$55,000-$65,000
Delivery[c]	5-6 months	5-6 months	5-6 months
Remarks	Similar units in nitrogen service	3 units in hydrogen service	5 units in hydrogen service

a. These units may be adapted to a range of flows and pressures. Figures indicate range.

b. Depends upon motor selected and discharge pressure required. Standard conditions are 70°F and 30 inches Hg.

c. Prices and delivery are for a complete skid-mounted pump-vaporizer unit, including skid, frame, pump, motor, drive mechanism, vacuum-insulated sump, atmospheric forced air vaporizer with motor, manual control panel, valves, gages, and switches. Optional equipment available at extra cost includes automatic control monitoring system, electric vaporizer (as substitute for standard atmospheric type) and immersed sump-mounted forepump.

TABLE 1.2 (Continued)

Pesco Products Liquid Hydrogen Pumps
(Courtesy of Pesco Products)

Type	Variable-displacement multiple-piston reciprocating
Rated Flow	1-5 gpm
Discharge Pressure	4000 psi
Efficiency	65%
Speed	3000 rpm
Type of Drive	Electric or hydraulic motor
Drive Horsepower	18 HP
Mounting	Horizontal or vertical
Type of Bearings	Journal
Design Life	300 hr
Status	Development
Approximate Price	$8000

II. PRESSURIZED TRANSFER OF LIQUID HYDROGEN WITH HYDROGEN GAS

A. SCOPE

This section presents a method for estimating the amount of hydrogen gas necessary to pressurize the ullage space in a liquid hydrogen storage tank and to maintain constant ullage-gas pressure as the liquid is transferred.

B. INTRODUCTION

Liquid hydrogen is often used in batch processes. Batch transfer is conveniently accomplished by allowing warm, high-pressure hydrogen gas to pressurize the ullage in a liquid hydrogen tank; this gas pressure "head" is then employed to expel the liquid. Such a system is simple in concept and application and is efficient, as little or no heat energy is transferred to the expelled liquid. The principal liability of such a system stems from the necessity of providing the high-pressure gas storage supply external to the liquid storage tank and of building a liquid storage tank that can withstand the pressures needed for the transfer operation.

It is difficult to estimate the amount of hydrogen gas required to pressurize the ullage; the amount obviously depends upon the rate of heat transfer from the gas to the colder walls and liquid as well as upon the tank volume and pressure. In addition, since the saturation temperature of the hydrogen gas at high pressures is higher than the temperature of the bulk tank liquid, some gas will condense. To calculate accurately the total amount of hydrogen gas required, the amount of gas which condenses and the ullage gas temperature must be known throughout the process. The complexities of the operation make a rigorous analytical approach impossible.

C. DESCRIPTION OF PROCESS

Before some appropriate analytical models are described, it will be helpful to describe qualitatively some of the more important steps in the process.

Usually, liquid hydrogen is stored in a well-insulated tank and vented to a constant pressure. The temperature of the bulk liquid is constant; for example, if the pressure is atmospheric, it is about 20.4°K.

At the onset of pressurization, the vent is closed and warm hydrogen gas is allowed to flow into the tank. To minimize heat transfer between gas and liquid, it is customary to use some type of diffuser to prevent the gas from directly jetting into the liquid.

During pressurization, the gas cools by contact with the walls and liquid; both forced and natural convection heat transfer occur. The surface of the liquid is maintained in a saturated state at the system pressure; i.e., as the pressure increases, the temperature of the surface increases in accordance with the hydrogen vapor-pressure/temperature relationship.(1) Heat transfer into the liquid occurs by molecular and eddy conduction.

When pressurization is completed, and there is imposed a time interval when no liquid is expelled and the pressure is held constant, then gas flow occurs only to compensate for further gas cooling and condensation. The cooling of the gas in contact with the walls occurs predominantly by a natural convection mechanism. The interaction of the gas and liquid is complex; gas is believed to flow down the walls and across the liquid surface. Depending upon conditions, some liquid may be evaporated or some gas condensed.

When liquid transfer is initiated, gas flows into the ullage to maintain a constant pressure. Heat energy is transferred in a manner similar to that described above during pressurization. The liquid is in all probability slightly agitated, but, in the absence of any large disturbances such as whirlpools, the temperature of the surface remains essentially constant and equal to the saturation temperature corresponding to the system pressure. The bulk liquid temperature remains very close to the original liquid temperature.

To predict within engineering accuracy the pressurizing-hydrogen gas requirements for the process just described, one may mentally simplify the process so that the various steps may be adequately described by quantitative relations. Two models that are useful in predicting gas requirements for hydrogen systems have been developed:

The first is termed the limiting-case model. This facilitates a limited analysis that circumvents the heat and mass transfer problems by considering extreme cases where these transfer processes proceed at either infinite or infinitesimal rates; it also permits definition of the gas requirements limits and reveals fundamental differences between the pressurized transfer of liquid hydrogen and liquid oxygen or liquid nitrogen.

The second analytical procedure for predicting gas requirements makes use of an equivalent-mass model. To date this model has been successfully applied to estimate pressurizing gas requirements for liquid hydrogen, nitrogen and oxygen transfer systems ranging in size from 3 to 28,000 gallons(2) within an uncertainty of about 15%.

D. NOMENCLATURE

A = area

b = intercept at $T = 0$ of isobar on enthalpy-temperature plot

C_p = specific heat at constant pressure

e = specific internal energy

g = acceleration due to gravity

h = specific enthalpy

h = heat transfer coefficient

J = energy conversion factor

k = thermal conductivity

k' = constant in Lorenz equation

L = characteristic length

m = mass of gas

M = mass of vessel wall

n = constant in Lorenz equation

p = pressure

Q = total heat flow

q = rate of heat flow

r = constant

R = gas constant

T = temperature

V = volume

v = specific volume

W = work

x = liquid film thickness

Z = compressibility factor

β = coefficient of compressibility

μ = viscosity

ρ = density

θ = time

Superscripts

(prime) indicates conditions after transfer

Subscripts

a - ambient condition
b - transfer vessel
bl - bulk liquid
c - receiver
f - property of film, arithmetic mean between ullage condition and saturation condition
i - input gas
L - liquid
O - original condition, as before pressurization
s - property of ullage gas
sv - saturated vapor
1 - condition before transfer
2 - condition after transfer

E. LIMITING-CASE MODEL

1. Maximum Gas Requirement

In this extreme case, complete mixing occurs between gas and liquid. The two phases are always in thermal equilibrium. This condition might be characteristic of a very slow transfer process where some sort of agitation causes excessive mixing. In no actual transfer case could this condition be obtained. In any event, this type of process produces a maximum requirement for pressurizing gas. For the simple case where the initial ullage is negligible and all the liquid is transferred, gas requirements for this model can be easily determined.

Consider the conditions before and after transfer for the system indicated in Figure 2.1. The following assumptions can be made without losing the essential features of the case: an infinitely large source of gas; no heat transfer from the environment to the system composed of the fluid finally in tanks "b" and

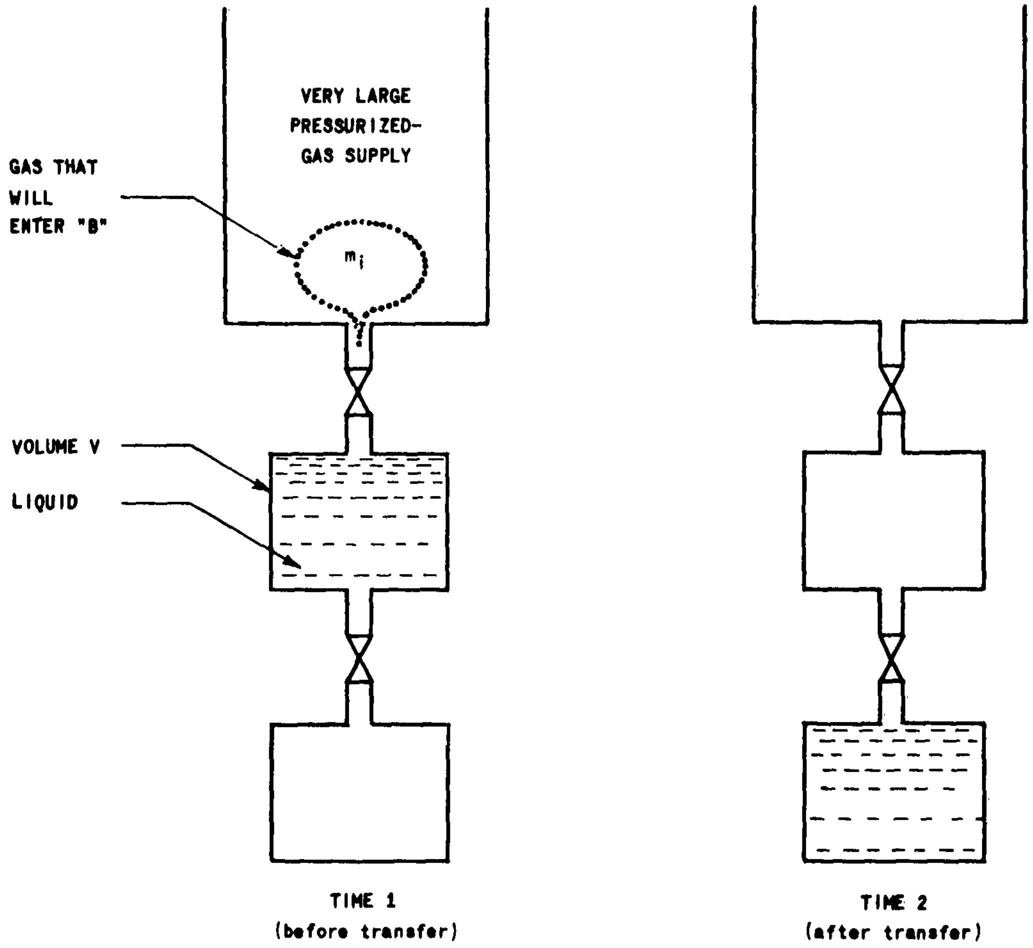
VERY LARGE PRESSURIZED-GAS SUPPLY
GAS THAT WILL ENTER "B"
m_i
VOLUME V
LIQUID
TIME 1
(before transfer)
TIME 2
(after transfer)

FIGURE 2.1	"WORST" Case Model for Liquid Hydrogen Transfer

"c"; liquid in "b" pressurized to the final pressure and the transfer taking place with the pressure remaining constant in both "b" and "c." According to these assumptions, tanks "a," "b" and "c" will have the following contents at times "1" and "2":

	Time 1	Time 2
Tank "a"	High-pressure gas at ambient temperature	High-pressure gas at ambient temperature
Tank "b"	Saturated liquid at initial pressure	Saturated vapor at final pressure
Tank "c"	Empty	Saturated liquid at final pressure

Conservation of energy requires that

$$m_{b_2}e_{b_2} + m_{c_2}e_{c_2} - m_i e_a - m_{b_1}e_{b_1} = \frac{1}{J}\left(p_a v_a m_i - p_2 v_{c_2} m_{c_2}\right), \qquad (1)$$

where m = mass, lb

e = internal energy, Btu/lb

p = pressure, lb/sq ft

v = specific volume, cu ft/lb

J = energy constant (778 ft-lb/Btu)

Subscripts refer to tank volumes and time (before and after transfer). Conservation of mass yields

$$m_{b_2} + m_{c_2} = m_i + m_{b_1} \qquad (2)$$

Rewriting eq. (1) as

$$m_{b_2}e_{b_2} - m_{b_1}e_{b_1} + m_{c_2}h_{c_2} - m_i h_a = 0$$

(where h = enthalpy in Btu/lb), and combining with eq. (2) to eliminate m_{c_2},

$$\frac{m_i}{m_{b_1}} = \frac{m_{b_2}(e_{b_2} - h_{c_2})}{m_{b_1}(h_a - h_{c_2})} + \frac{h_{c_2} - e_{b_1}}{h_a - h_{c_2}} \tag{3}$$

By definition,

$$\frac{m_{b_2}}{m_i} = \frac{m_{b_2}/m_{b_1}}{m_i/m_{b_1}} \tag{4}$$

while from eq. (2),

$$\frac{m_{b_1} - m_{c_2}}{m_{b_1}} = \frac{m_{b_2}}{m_{b_1}} - \frac{m_i}{m_{b_1}} \tag{5}$$

Further,

$$\frac{m_{b_2}}{m_{b_1}} = \frac{\rho_{g_2}}{\rho_{f_1}} \tag{6}$$

where ρ_{g_2} is saturated vapor density at time "2" and ρ_{f_1} is liquid density at time "1."

With the foregoing assumptions, all properties are defined by initial and final pressures. Our present interest is in the case where the liquid in "b" is initially at one atmosphere. With liquid hydrogen, the pertinent properties(3) and the calculated ratios m_i/m_{b_1}, m_{b_2}/m_i, and $(m_{b_1} - m_{c_2})/m_{b_1}$ are tabulated for several pressures in Table 2.1.

The ratio of input-gas mass, m_i, to liquid volume (V) initially in "b" is given by

$$\frac{m_i}{V} = \rho_{f_1} \frac{m_i}{m_{b_1}};$$

TABLE 2.1

CALCULATED RESULTS BASED ON "WORST CASE" MODEL FOR PRESSURIZED LIQUID HYDROGEN TRANSFER

p_2 (psia)	ρ_{g_2} (lb/cu ft)	m_{b_2}/m_{b_1}	$e_{b_2} - e_{b_1}$ (Btu/lb)	$h_{c_2} - e_{b_1}$ (Btu/lb)	$h_a - h_{c_2}$ (Btu/lb)	m_i/m_{b_1}	m_{b_2}/m_i	$(m_{b_1} - m_{c_2})/m_{b_1}$	m_i/V (lb/cu ft)
15	0.085	0.0198	156	1.0	1689	0.00242	8.19	0.017	0.0106
20	0.110	0.0254	153	5.3	1685	0.00545	4.66	0.020	0.0240
25	0.135	0.0307	151	9.5	1680	0.00812	3.78	0.023	0.0357
35	0.180	0.0413	144	17.0	1673	0.01372	3.01	0.028	0.0604
50	0.268	0.0588	138	26.5	1663	0.02085	2.82	0.038	0.0918
75	0.383	0.0892	124	40.3	1650	0.0311	2.87	0.058	0.1370
100	0.520	0.1250	108	52.8	1637	0.0405	3.08	0.085	0.1782
125	0.700	0.161	89	65.5	1624	0.0492	3.27	0.112	0.216
150	0.897	0.204	59	78.0	1612	0.0558	3.65	0.148	0.246

Notes:

h_a = 1800 Btu/lb (corresponds to ambient of 75°F)

e_{b_1} = e_{f_1} = 110 Btu/lb

ρ_{f_1} = 4.40 lb/cu ft

and this quantity is also presented in Table 2.1. The ratio m_i/m_{b_1} indicates the mass of gas required to displace a given mass of liquid. m_{b_2}/m_i shows the ratio of gas finally in "b" to the input gas, while $(m_{b_1} - m_{c_2})/m_{b_1}$ is the amount of liquid lost during the process expressed as a fraction of the initial amount of liquid. A comparison of these ratios calculated for liquid hydrogen and liquid oxygen being pressure-transferred at 100 psia shows that for the so-called worst case, the behavior of the two fluids is indeed basically different.

	Liquid Hydrogen	Liquid Oxygen
m_i/m_{b_1}	0.0405	0.124
m_{b_2}/m_i	3.08	0.202
$(m_{b_1} - m_{c_2})/m_{b_1}$	0.085	-0.099

m_{b_2}/m_i is considerably greater than unity for liquid hydrogen, in sharp contrast with liquid oxygen. Since, for liquid hydrogen, more gas remains in "b" after transfer than was fed into the tank from "a," some liquid must be vaporized during the process. This is further illustrated by the fact that $(m_{b_1} - m_{c_2})/m_{b_1}$ is positive in the case of liquid hydrogen. With liquid oxygen, as indicated by the negative value of this quantity, some of the input gas will condense. This variation in process characteristics is, of course, due to the differences in properties of the two gas-liquid systems.

2. Minimum Requirements

Pressurized transfer would require a minimum amount of gas if no heat (or mass) were transferred from the gas to the liquid. If the initial ullage is negligible, the temperature of ullage gas during and after transfer will be the ambient temperature, and the density, ρ_s, will be

$$\rho_s = \frac{P_2}{RT_a}$$

For complete displacement of liquid,

$$\frac{m_i}{V} = \rho_s = \frac{p_2}{RT_a}$$

The minimum gas requirement for this case is plotted in Figure 2.2. Also plotted is the maximum requirement (as indicated by the worst case). As is evident from the figure, the theoretical maximum requirement is roughly two to five times the minimum, depending on pressure. The establishment of actual requirements between these limits will necessitate analysis of the heat- and mass-transfer processes occurring between liquid and vapor.

3. Comparison With Experiments

The results of some typical transfer runs reported in reference 4 are plotted in Figure 2.3 with the maximum and minimum curves of Figure 2.2 repeated for comparison. For ready reference, Table 2.2 (extracted from reference 4) lists the conditions of these tests. Details of these tests and an interpretation of the results are given in the original source.

F. EQUIVALENT MASS MODEL

1. Derivation of Equations

A system is chosen to include the ullage gas and is bounded by the tank wall and the liquid hydrogen surface. Then for any time interval, $d\theta$,

$$dQ - dW = d(m_s e_s) + h_L\, dm_L - h_i dm_i \qquad (1)$$

Eq. (1) cannot be integrated directly for the pressurization or transfer process. The rate of heat transfer and enthalpy of the condensed liquid vary greatly during the pressurization period, but quickly reach a near-steady state value at the completion of the pressure transient. To avoid the necessity of considering such transients, assume that pressurization is accomplished instantaneously and that the enthalpy of the condensed gas, h_L, is evaluated at the film temperature corresponding to the final system pressure. This film temperature is taken to be the arithmetic mean of the final surface temperature (i.e., saturation temperature at final pressure) and original bulk-liquid temperature. With these assumptions, eq. (1) may be integrated to give eq. (2).

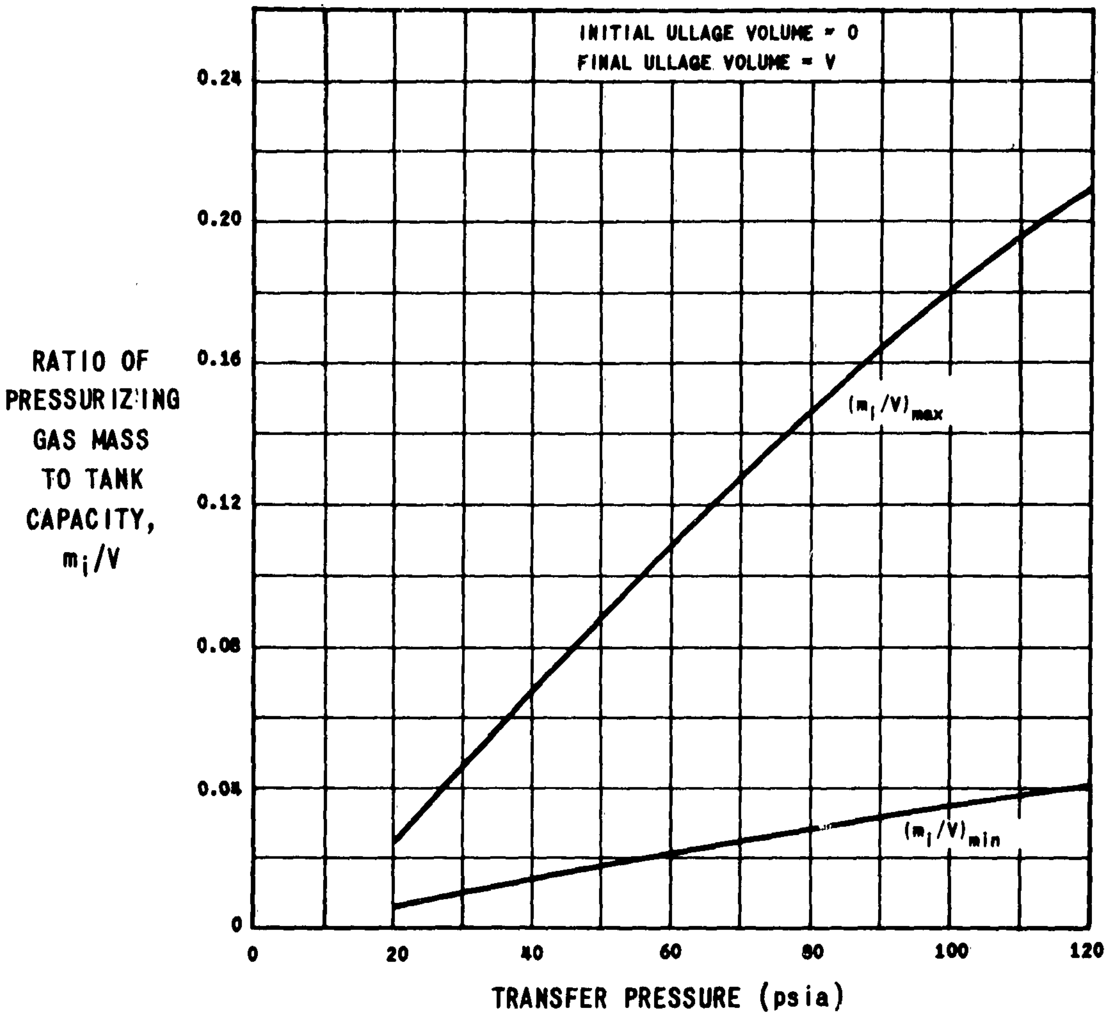

FIGURE 2.2 Gas-Requirement Limits for Pressurized Transfer of Liquid Hydrogen

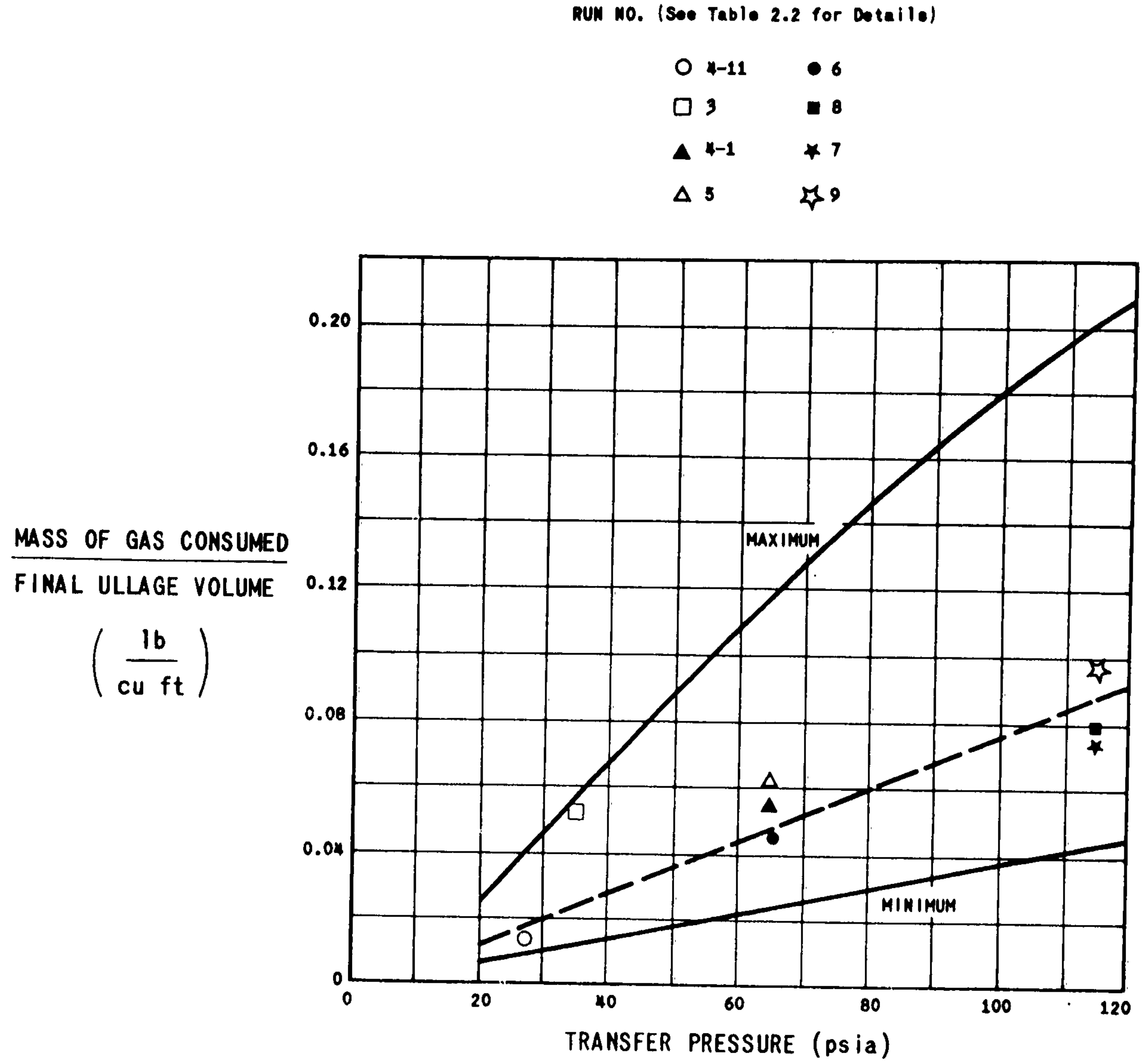

FIGURE 2.3 Measured Gas Consumption for Pressurized Transfer of Liquid Hydrogen

TABLE 2.2

TEST RESULTS--PRESSURIZED LIQUID HYDROGEN TRANSFER TESTS

	Run Number							
	4-11	3	4-1	5	6	8	7	9
Dewar Pressure, psia	27.5	35.0	65.0	65.0	65.0	115.0	115.0	115.0
Initial Ullage Volume, cu ft	52.3	2.01	2.14	2.54	34.3	11.1	18.6	10.6
Final Ullage Volume, cu ft	70.5	66.7	52.3	79.5	60.8	52.3	63.3	37.3
Total Gas Input Consumed (m_i), lb	0.99	3.47	2.85	4.89	2.69	4.08	4.63	3.59
Mass of Initial Ullage Gas, lb	4.37	0.17	0.18	0.21	2.87	0.93	1.56	0.88
Mass of Final Ullage Gas, lb	3.20	2.09	3.31	4.42	3.97	4.66	5.25	3.39
Pressure-Hold Gas Input, lb	0.05	0.31	1.21	0.94	1.27	1.52	-	1.37
Ullage Gas Condensed During Run, lb	2.16	1.55	-0.28	0.67	1.59	0.35	0.94	1.08
Total Gas Input/Final Ullage Volume, lb/cu ft	0.0140	0.0520	0.0545	0.0615	0.0442	0.0780	0.0733	0.0962
Pressurize-Hold Gas Input/ Initial Ullage Volume, lb/cu ft	0.001	0.152	0.564	0.368	0.037	0.137	-	0.130
Total Time, sec	420	1220	400	450	410	368	340	560
Transfer Time, sec	150	950	40	135	140	65	130	48
Average Discharge Flow Rate, gpm	54	31	562	256	85	284	154	250

$$Q - W = m_s e_s - m_{s_o} - m_{s_o} e_{s_o} + \bar{h}_L m_L - \bar{h}_i m_i \tag{2}$$

By material balance,

$$m_i - m_L = m_s - m_{s_o} \tag{3}$$

Combining eqs. (2) and (3) to eliminate the inflow gas m_i, and rearranging,

$$\frac{-Q + W}{\bar{h}_i - \bar{h}_L} = m_L + m_s\left(\frac{\bar{h}_i - e_s}{\bar{h}_i - \bar{h}_L}\right) - m_{s_o}\left(\frac{\bar{h}_i - e_{s_o}}{\bar{h}_i - \bar{h}_L}\right) \tag{4}$$

To obtain the desired equation, a quantity $-\frac{pV_s}{\bar{h}_i - \bar{h}_L}$ is added and subtracted in eq. (4) to yield,

$$m_{co,eq} = m_L + m_s\left(\frac{\bar{h}_i - e_s}{\bar{h}_i - \bar{h}_L}\right) - \frac{pV_s}{\bar{h}_i - \bar{h}_L} - m_{s_o}\left(\frac{\bar{h}_i - e_{s_o}}{\bar{h}_i - \bar{h}_L}\right) \tag{5}$$

where the term

$$m_{co,eq} = \frac{-Q + W - pV_s}{\bar{h}_i - \bar{h}_L} \tag{6}$$

The term $m_{co,eq}$ is defined as the equivalent condensed mass and has a physical significance such that it would equal the total condensed mass in the process if all heat and work interactions resulted in the cooling and condensing of a mass equal to $m_{co,eq}$ while the remainder of the ullage gas were left at the system pressure and entering stagnation temperature, T_a. It may be calculated from heat transfer rates, initial and final tank ullage volumes, and enthalpy data for the feed gas.

The ullage mass at the system pressure and temperature T_a is referred to as the equivalent ullage mass and is calculated from ullage pressure and volume data as,

$$m_{ul,eq} = pV_s/Z_s\ RT_a \tag{7}$$

These equivalent masses are limiting values; the $m_{co,eq}$ represents the maximum amount of gas that could be condensed, and as such is always larger than the true condensed mass. Conversely, the $m_{ul,eq}$ represents the minimum final value for the ullage gas and is always less than the true ullage mass. An approximation might be made that the sum of these hypothetical equivalent masses equals the true input mass, m_i. Actually, it may be shown (see below) that this approximation is only valid at a single ullage pressure level; at other pressures, a correction is necessary. Accordingly, it is postulated that the input mass m_i may be calculated as follows:

$$m_i = m_{co,eq} + m_{ul,eq} + m^* \tag{8}$$

The term m^* is the corrected mass referred to above and is defined in terms of a "correction" temperature T^*:

$$m^* = pV_s/RZ_sT^* \tag{9}$$

2. Discussion of Corrected Mass

If one subtracts eq. (5) from eq. (8), replaces m_i by its equivalent from eq. (3) and simplifies,

$$m^* + m_{ul,eq} = m_s\left(\frac{e_s - \bar{h}_L}{\bar{h}_i - \bar{h}_L}\right) + \frac{pV_s}{\bar{h}_i - \bar{h}_L} - m_{s_o}\left(\frac{e_{s_o} - \bar{h}_L}{\bar{h}_i - \bar{h}_L}\right) \tag{10}$$

If the masses are replaced by eqs. (7) and (9), with m_s analogously expressed as pV_s/Z_sRT_s, one obtains

$$\frac{T_s}{T_a} + \frac{T_s}{T^*} = \frac{\bar{h}_s - \bar{h}_L}{\bar{h}_i - \bar{h}_L} - \left(\frac{m_{s_o}}{m_s}\right)\left(\frac{e_{s_o} - \bar{h}_L}{\bar{h}_i - \bar{h}_L}\right) \tag{11}$$

The second term on the right side of eq. (11) may be neglected without the introduction of a significant error.

A small value of m^* would correspond to a large value of T^* by eq. (9); in the limiting case when m^* is zero, T^* is infinite and eq. (11) may be written,

$$\frac{T_s}{T_a} = \frac{\bar{h}_s - \bar{h}_L}{\bar{h}_i - \bar{h}_L}; \quad m^* = 0 \tag{12}$$

This special case has a simple geometrical interpretation. On an enthalpy-temperature diagram the points T_s, h_s form the locus of points describing the cooling of the ullage gas. By the model proposed, these points would fall on an isobar corresponding to the system pressure. If this isobar were extrapolated to the absolute zero temperature axis, eq. (12) would indicate that the enthalpy intercept would equal $\bar{h}_L$. Figure 2.4 shows such a case. In this diagram, the section of the isobar corresponding to the system pressure is idealized as a straight line in the region of interest. It is obvious that for any other isobar, either higher or lower than the one shown, it is impossible for the enthalpy intercept at $T = 0$ to equal $\bar{h}_L$. In one other way Figure 2.4 is misleading. Actually, one does not want the extrapolated value of enthalpy at $T = 0$ to be equal to the enthalpy of the saturated liquid at the system pressure as shown, but rather it should equal $\bar{h}_L$, which is defined as the enthalpy of saturated liquid at the arithmetic mean temperature between bulk liquid and liquid saturated at the system pressure. In the figure it is assumed that the bulk tank liquid is identical to the liquid saturated at pressure.

3. Corrected Mass for Liquid Hydrogen Systems

Figure 2.5 shows an enthalpy-temperature plot for hydrogen. The 1- and 10-atmosphere isobars are shown, and it may be noted that above 150°K there is essentially no effect of pressure on enthalpy. In most hydrogen pressurization systems the input hydrogen gas is about 50 to 100°F, and during the process the ullage gas may cool to temperatures in the range of -200°F. Thus, T_a varies from about 100°F to -200°F. Over this range the heat capacity at constant pressure varies slightly (as shown by the slight curvature in the isobar of Figure 2.5), but within engineering accuracy, the enthalpy-temperature relationship may be expressed as follows:

$$h_s = 3.20\ T_s + 80 \qquad (13)$$

From what has been discussed previously, therefore, the corrected mass should be negligible for that pressure level where the film enthalpy, $\bar{h}_L$, is 80 Btu/lb. The bulk liquid enthalpy at one atmosphere is very nearly equal to 80 Btu/lb. Thus, for all practical purposes, the corrected mass is zero for the fictitious case wherein a liquid hydrogen tank at one atmosphere is pressurized "to one atmosphere." For higher pressures, the corrected mass is not zero. Figure 2.6 has been drawn to show the effect of ullage temperature and pressure on the ratio $m^*/m_{ul,eq}$. Several facts are deduced from this plot. In all cases of interest, m^* is less than 10% of $m_{ul,eq}$ and so, even if m^* were completely neglected, the final error introduced would not exceed 2-3%. Also, m^* is not a strong function of the ullage temperature T_s. This fact is of importance, since T_s must be estimated to calculate T^* (thus m^*) from eq. (11). As a simple rule, it is suggested that T_s be approximated by T_v where,

$$T_v = 1/2\ (T_a + T_s) \qquad (14)$$

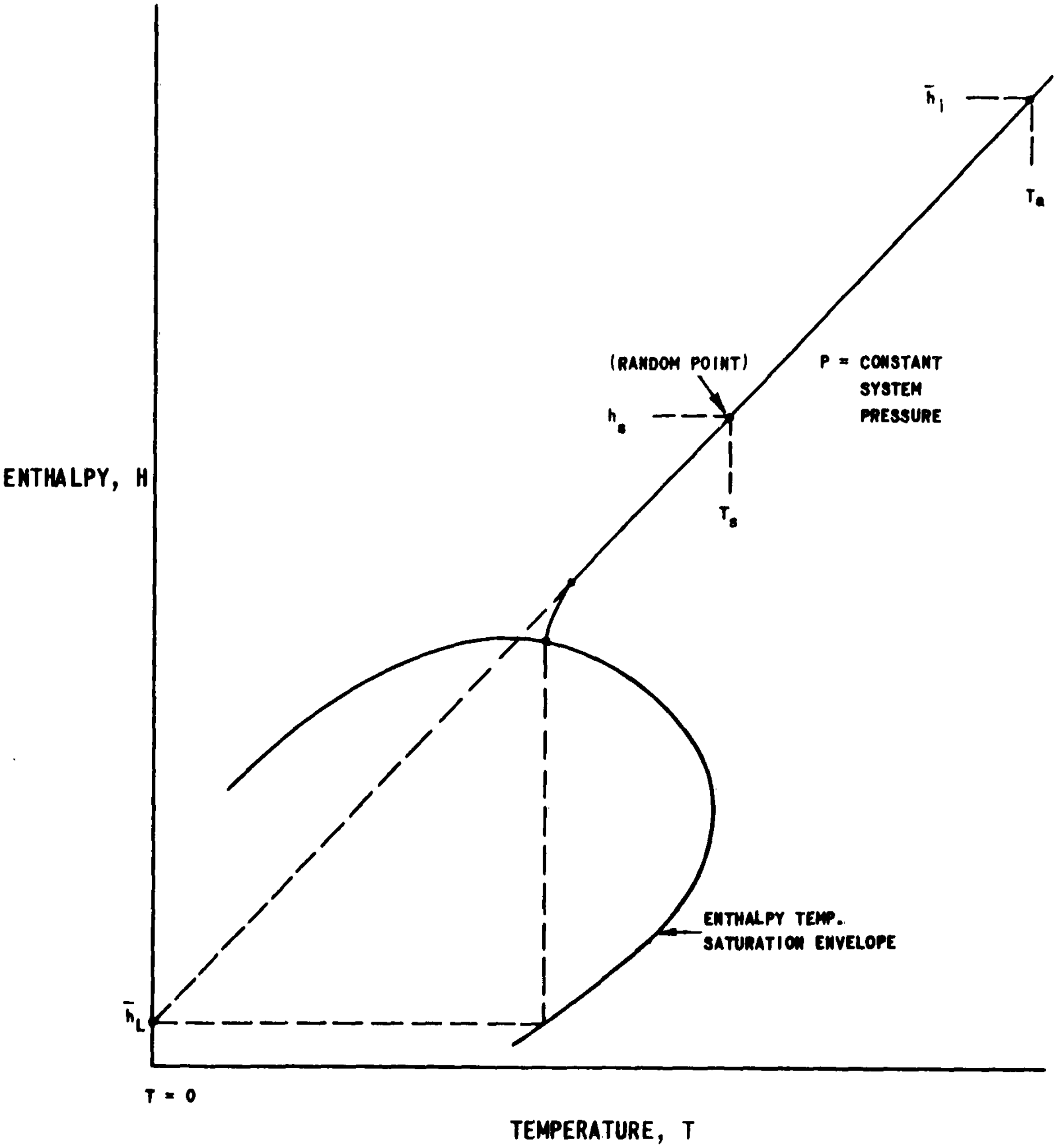
$\bar{h}_I$
T_a
(RANDOM POINT)
P = CONSTANT SYSTEM PRESSURE
h_s
T_s
ENTHALPY, H
ENTHALPY TEMP. SATURATION ENVELOPE
$\bar{h}_L$
T = 0
TEMPERATURE, T

FIGURE 2.4 Temperature-Enthalpy Diagram Showing Isobar Which Results in Zero Correction Mass

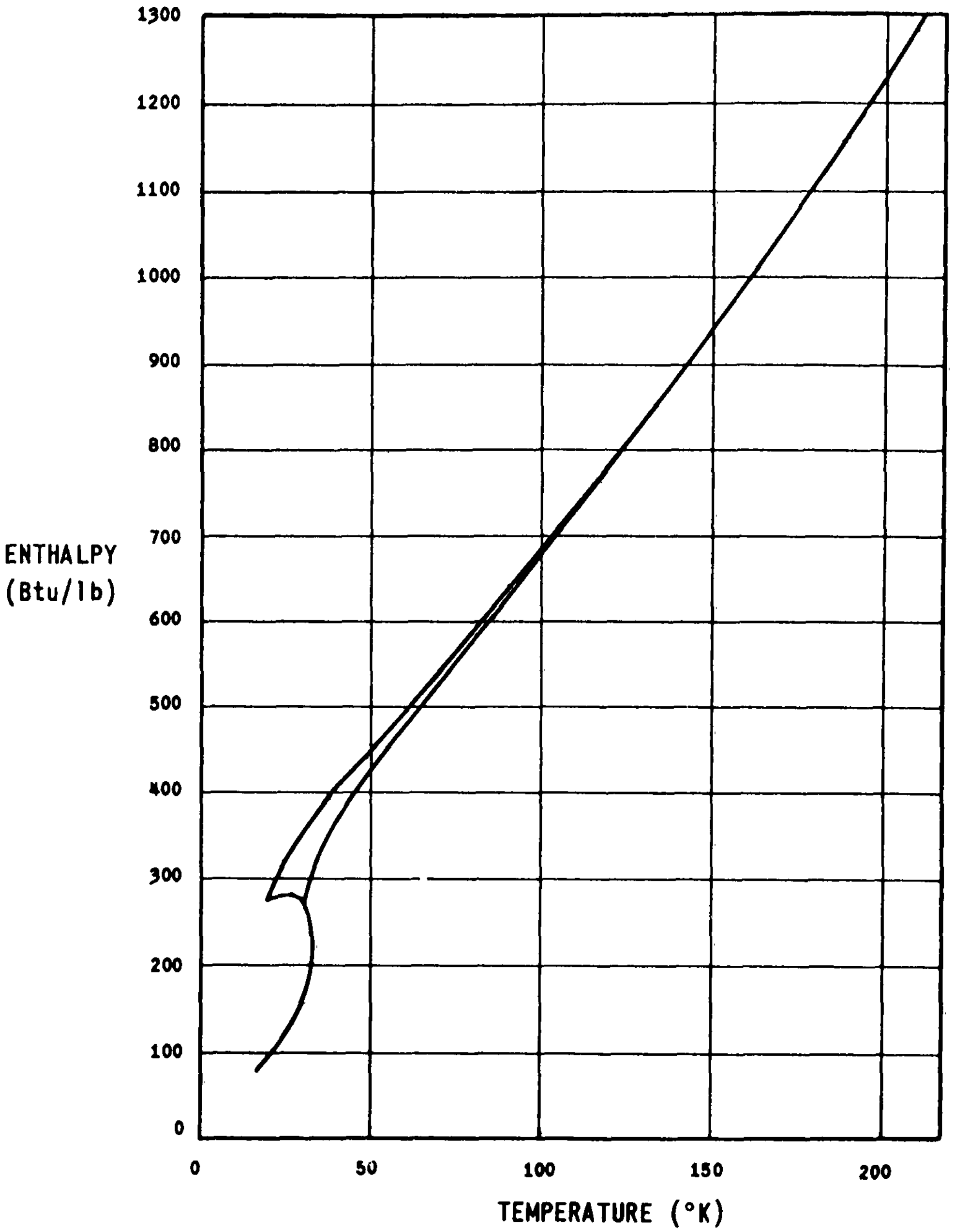

FIGURE 2.5 Enthalpy-Temperature Plot for Hydrogen

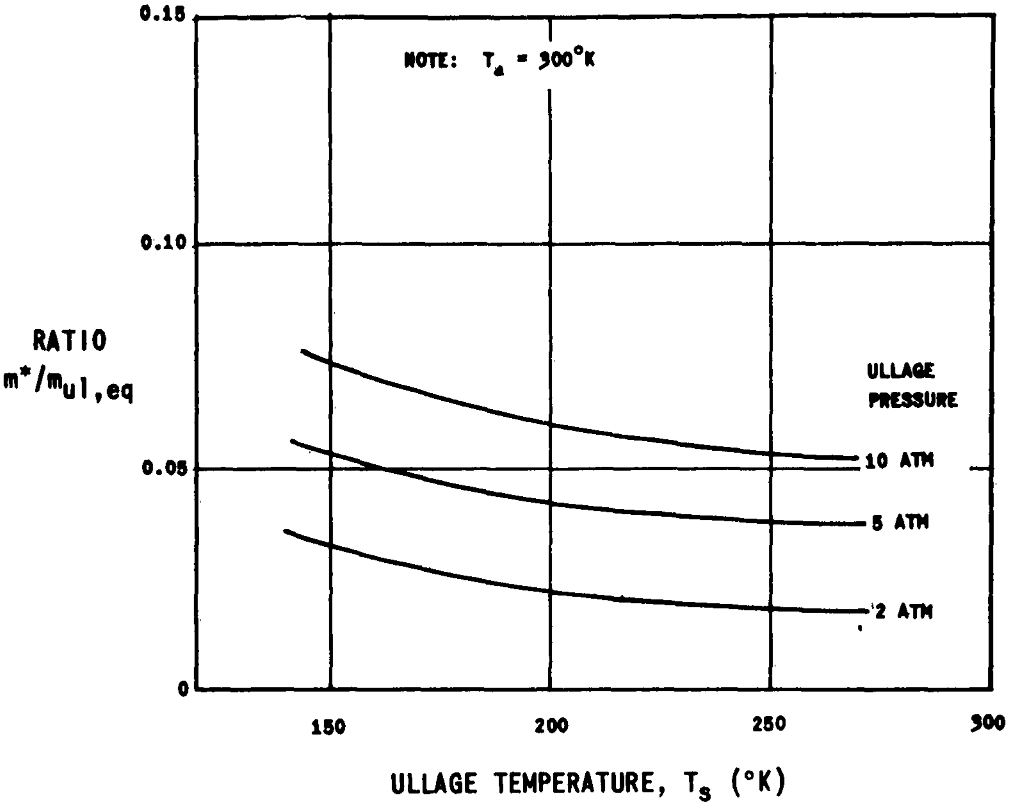

FIGURE 2.6 Effect of Ullage Temperature and Pressure on Corrected Mass

For example, if T_a = 300°K and the tank were pressurized to 10 atm (at which pressure the saturation temperature is about 32°K), then $T_v = 1/2\ (332) = 166°K$. If the true value of T_s is, say, 200°K, then only 1 or 2% error in m* is anticipated. Other similarly simple rules as eq. (13) would be equally acceptable.

4. Final Equation and Summary

From eq. (11), if the second term is neglected, by multiplying both sides by pV_s/R, assuming the compressibility factors to be unity, and substituting T_v and the corresponding h_v for T_s, h_s by eq. (13),

$$m^* + m_{ul,eq} = \frac{(h_v - \bar{h}_L)}{(\bar{h}_i - \bar{h}_L)} \frac{(pV_s)}{RT_v} \tag{15}$$

In summary, for either a pressurization or transfer test, the amount of input pressurizing gas may be estimated as follows:

(1) Calculate $m_{co,eq}$ from eq. (6)

(2) Calculate $m^* + m_{ul,eq}$ from eq. (15)

(3) Add 1 and 2 to obtain the total mass of pressurizing gas

As a final note, it might be thought that the somewhat awkward procedure outlined in eq. (15) to estimate $m^* + m_{ul,eq}$ ought to be eliminated and T_s be estimated from experience or other means. A good estimate of T_s will certainly lead to a good value for true ullage mass, but no estimate of the gas that condenses will be included. The calculation of $m^* + m_{ul,eq}$ yields an artificial number that is meaningless unless combined with the value of $m_{co,eq}$ as indicated by the equivalent mass model described earlier.

5. Heat Transfer to Tank Walls

An estimate of the rate of heat transfer from the warm ullage gas to the cold walls is necessary to calculate the equivalent condensed mass by eq. (6). During periods of high gas flow rates, heat transfer occurs by forced convection. When a constant pressure is held on the tank or when the gas flow rate is low, a natural convection mechanism is more important. A heat transfer model suggested here circumvents many of the problems introduced by the separate consideration of forced and natural convection mechanism. It is assumed in this model that the predominant mode of heat transfer is natural convection.

a. Description of Model

A tank of liquid hydrogen has an initial ullage volume, V_{s_0}. The tank has thin metal walls and is well insulated, so that negligible heat transfer occurs between the wall and environment during any portion of the process. Initially, the walls of the tank are at T_{bl}, the temperature of the bulk liquid, below the surface of the liquid, and at $\bar{T}_w$ above the liquid surface. The gas temperature of the ullage is initially T_s, and the initial pressure is p_{s_0}. Pressurization from p_{s_0} to the final pressure, p_s, is assumed to occur instantaneously and adiabatically to result in an ullage gas of temperature T_s. From an energy balance, T_s may thus be calculated. From this time on the gas is assumed to cool by contact with the wall and liquid by natural convection. At any given time, the total heat flow to the walls may thus be estimated.

b. Pressurization Step

From a First Law balance on the system V_{s_0}, since no heat or work effects are present,

$$d(m_s e_s) - \bar{h}_i \, dm_i = 0 \tag{16}$$

Assuming $\bar{h}_i$ constant and noting that $dm_s = dm_i$, and as

$$m_s = pV_s / Z_s R T_s \tag{17}$$

then,

$$(T_s/T_{s_0})(p_{s_0}/p_s)(Z_s/Z_{s_0}) = (\bar{h}_i - e_s)/(\bar{h}_i - e_{s_0}) \tag{18}$$

Eq. (18) may be solved for T_s, since both e_s and Z_s are single-valued functions of T_s at a given p_s. There is, however, some question concerning the numerical value of $\bar{h}_i$. Consider two extreme cases:

(1) Hydrogen gas in the external storage bottles heats up to T_a after expansion cooling in the bottles. This condition occurs when there is a large heat exchange surface in the lines from the gas storage supply to the liquid hydrogen tank. For such a condition, $\bar{h}_i$ would equal the specific hydrogen gas enthalpy at T_a and would vary only very slightly as the bottle pressure dropped.

(2) Hydrogen gas from the external bottles flows adiabatically to the liquid storage tank. This condition occurs when there is a high flow rate or short gas line length. In this condition, $\bar{h}_i$ would vary as the bottle temperature and pressure dropped; the largest change in $\bar{h}_i$ would be experienced when the supply gas underwent an isentropic expansion.

The values of T_s calculated from (1) or (2) differ, but by a surprisingly small amount; for simplicity, case (1) has been assumed in this report.

After the adiabatic temperature after pressurization has been estimated from eq. (18), the gas is assumed to cool by contact with the walls and liquid. Wall heat transfer is discussed below and liquid heat transfer in a later section.

c. Wall Heat Transfer Equations

Heat is transferred from gas to wall by a natural convection mechanism.

$$Q_w = \int_0^\theta h\, A_w\, (T_s - T_w)\, d\theta \tag{19}$$

Without liquid transfer A_w is constant, but h, T_s, and T_w are presumably functions of time. There is, however, a relationship between T_s and T_w after the assumed pressurization.

The ullage hydrogen gas enclosed by walls and liquid is chosen as the system; heat interactions are allowed. Let the pressure on the system remain constant at p_s while gas enthalpy, $\bar{h}_i$, and pressure, p_s, are added.

Referring to eq. (1) the term dQ may be broken into $(dQ_w + dQ_L)$, where dQ_w indicates heat transfer to the walls and dQ_L indicates the heat transfer to the liquid. Mass m_L will enter with enthalpy $\bar{h}_i$, cool to some lower value, h, by contact with the walls, and transfer energy equivalent to $(h - \bar{h}_L)$ to the liquid before condensing and leaving the defined system. The intermediate enthalpy, h, is not known, but the assumption is made that, within engineering accuracy, the heat interaction with the wall $m_L(\bar{h}_i - h)$ is balanced by an identical amount of heat interchange between the residual gas and liquid. The net result of this compensating assumption is that

$$dQ_L = -(\bar{h}_i - \bar{h}_L)\, dm_L \tag{20}$$

Eq. (1) then becomes

$$dQ_w - dW = d(m_s e_s) - \bar{h}_i \, dm_s \tag{21}$$

By expressing $e_s = h_s - pv_s$ and approximating the enthalpy of hydrogen gas (at p_s) as a linear function of temperature,

$$h_s = C_p T_s + b \tag{22}$$

Assuming the compressibility factor to be constant, eqs. (17), (21) and (22) yield

$$dQ_w - dW = (b - \bar{h}_i) \, dm_s = \frac{(b - \bar{h}_i)}{RZ_s} p_s V_{s_o} \, d\,(1/T_s) \tag{23}$$

Since

$$dQ_w = -M_w C_{p_w} dT_w \tag{24}$$

eqs. (23) and (24) may be equated; for non-liquid transfer cases, dW = 0, and

$$C_{pw} dT_w = \frac{(\bar{h}_i - b)\,(p_s V_{s_o})}{Z_s RM_w} d\,(1/T_s) \tag{25}$$

Integrating,

$$\int C_{pw} dT_w = \frac{k}{T_s} + C \tag{26}$$

where $k = (\bar{h}_i - b)\,(p_s V_{s_o})/(Z_s RM_w)$

C = constant of integration

Eq. (26) expresses a functional relationship between T_W and T_S. It has been checked with data taken in several cryogenic transfer systems operated at Arthur D. Little, Inc.,(1, 5, 6) and excellent agreement has been obtained. The constant C may be determined from initial conditions, specifically the adiabatic temperature from eq. (18) and the known initial wall temperature T_{W_O}.

Considerable experimental work has indicated that the average heat transfer coefficient after a pressure transient, while the gas is cooling, is essentially constant.(2) This fact greatly simplifies the solution of eq. (19); a justification of this fact is presented below.

d. Wall Heat Transfer Coefficients

Liquid hydrogen storage tanks are usually cylindrical. As the walls vary from horizontal to vertical, convective heat transfer coefficients would be expected to vary from point to point. Usually, predictions of natural convection coefficients are made with some variation of the Lorenz equation(7)

$$\frac{hL}{k} = k' \left[\left(L^3 \rho^2 \frac{g\beta}{\mu^2} \Delta T \right) \left(C_p \mu / k \right) \right]^n \qquad (27)$$

Values of the constants k' and n have been recommended for laminar and turbulent flow for horizontal and vertical surfaces. Most values of n are between 0.25 and 0.33. This narrow range of n means that the geometrical length factor L is not of great importance; in fact, if n = 0.33, L has no effect on h. The effect of ΔT and hydrogen properties on h may be directly computed once k' and n are chosen. Large variations in all physical properties except thermal conductivity k and ΔT are not proportionately reflected in h, since n is so much less than unity.

The flow for most ullage cooling processes is highly turbulent; recommended values of n and k' are 0.33 and 0.13 for vertical surfaces and 0.33 and 0.14 for horizontally-cooled plates facing down.(7) Figure 2.7 has been drawn for hydrogen showing h as a function of $\rho_g^2 \Delta T$ for various film temperatures. It may be used to estimate wall heat transfer coefficients for constant-pressure, constant-volume cooling of hydrogen gas. A range of h is encountered during cooling; an average value suffices, however, since small errors in h affect only Q_w and are not proportionately reflected in the calculation of the equivalent condensed mass.

Actually, the true value of h is more nearly constant than would be evident from Figure 2.7, since at large values of ΔT, the film temperature is high, but as ΔT decreases the film temperature also drops. These effects compensate to some degree, yielding a nearly constant h.

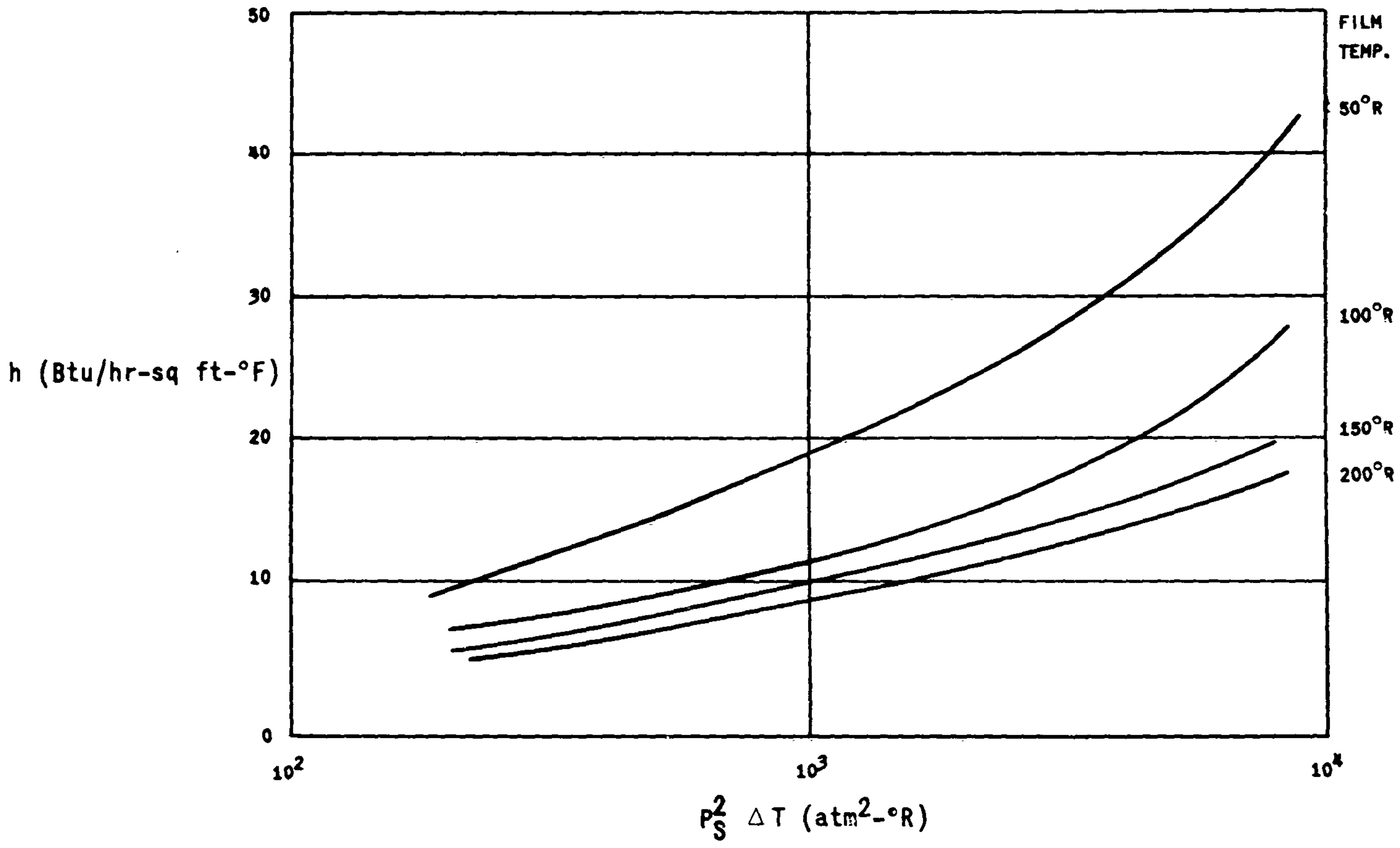

FIGURE 2.7 Heat Transfer Coefficients for Natural Convection on Cooled Vertical or Horizontal Surfaces--Hydrogen Gas

e. Solution of Equation (19)

The wall heat transfer coefficient is assumed independent of time and is estimated from Figure 2.7 or an equivalent plot. The wall area is constant, and the gas and wall temperatures are related by eq. (26). The temperature of the wall is determined as a function of time as follows:

From eqs. (19) and (24):

$$M_w C_{pw} dT_w = hA_w (T_s - T_w) d\theta \tag{28}$$

Rearranging,

$$\int \frac{M_w C_{pw} dT_w}{hA_w (T_s - T_w)} = \int d\theta \tag{29}$$

$$\frac{M_w}{hA_w} \int_{T_{w_o}}^{T_w} \frac{C_{pw} dT_w}{T_s - T_w} = \theta \tag{30}$$

f. Summary of Wall Heat Transfer Estimation

Eq. (19) must be integrated, usually graphically. A_w and h are assumed constant. T_s is related to T_w by eq. (26), and T_w to θ by eq. (30). Q_w may thus be calculated as a function of time. A detailed sample calculation will be presented later.

6. Heat Transfer to Liquid Hydrogen

a. Semi-Infinite Slab Theory

Usually the initial temperature of the bulk liquid hydrogen corresponds to saturation at atmospheric pressure. When the tank is pressurized with hydrogen gas, the bulk liquid temperature is affected only slightly, although heat is transferred very rapidly across the liquid interface. The top layers of liquid have been shown(2) to attain a temperature equal to that corresponding to the saturation temperature of the hydrogen at the existing ullage pressure. It is believed, however, that the ability of the main body of liquid to interchange heat energy is limited by the low thermal conductivity of liquid hydrogen. Without gross turbulence, heat energy cannot rapidly move past the phase boundary.

Temperature measurements have been made in and near the liquid surface during pressurization of cryogenic storage tanks of nitrogen and oxygen.(1) The temperature-depth gradients were found to be smaller than would be predicted if the bulk liquid were treated as a semi-infinite slab whose surfaces were increased instantaneously from the bulk temperature to the saturation temperature at p_S. This discrepancy results from an increase in heat flux due to convective heat transfer in parallel with conductive transfer. Convective transfer can arise from gas impingement on the liquid surface, and from liquid turbulence due to geysering. A gas diffuser will reduce the impingement problem.

b. Film Theory

Since the infinite-slab theory yields low values of heat energy interchange between gas and liquid, a new model is proposed by which this interchange may be more closely approximated. This model is referred to as the film model. The original liquid surface is assumed to remain at the bulk liquid hydrogen temperature, independent of time. The rate of heat transfer is assumed to be limited by conduction through the film of liquid that is condensed on the original liquid surface. It is further postulated that this liquid film results only from gas condensing and transferring heat equal to the enthalpy difference between entering gas and liquid at the film temperature.

If the liquid hydrogen film has a thickness x through which heat flows, then,

$$q_L = dQ_L/d\theta = r\, k_f\, A_L \frac{(T_{sv} - T_{bl})}{x} \tag{31}$$

but

$$Q_L = m_L\, (\bar{h}_i - \bar{h}_L) \tag{32}$$

The condensed mass may be expressed in terms of x as

$$m_L = \rho_f\, A_L\, x \tag{33}$$

thus,

$$\frac{dQ_L}{d\theta} = \rho_f A_L (\bar{h}_i - \bar{h}_L) \frac{dx}{d\theta} = r \frac{k_f A_L}{x} (T_{sv} - T_{bl}) \tag{34}$$

and

$$\int_0^x x\,d\,x = \frac{x^2}{2} = \int_0^\theta rk_f \frac{(T_{sv} - T_{bl})}{(\bar{h}_i - \bar{h}_L)\,\rho_f}\, d\theta \tag{35}$$

Because the equivalent-mass concept assumes all pressure transients to be instantaneous, the integral of $d\theta$ is independent of time; thus,

$$x = \left[\frac{2\,rk_f\,\theta\ (T_{sv} - T_{bl})}{(\bar{h}_i - \bar{h}_L)\ \rho_f}\right]^{1/2} \tag{36}$$

and, from eq. (32),

$$Q_L = A_L \left[2\,\theta\, rk_f\ \rho_f\ (T_{sv} - T_{bl})\,(\bar{h}_i - \bar{h}_L)\right]^{1/2} \tag{37}$$

In the film theory, any convective heat transfer is accounted for if one assumes that all the liquid hydrogen is thoroughly mixed, except for the thin film of condensed liquid on the surface. The proportionality constant r allows for the fact that the theory is only approximate; it has been found to be 4 for all systems investigated.(2) The film theory can allow for variations in fluid properties, pressurization levels, and time. The 'constant' r, while a function of these same parameters, is not strongly affected by changes in them.

7. Gas Consumption for the Transfer Process

In this section the total amount of gas required to transfer liquid hydrogen from a tank held at constant pressure is determined by application of the equivalent mass concept. A similar estimation for the pressurization step has been discussed previously. From the pressurization calculations, the ullage volume, temperature of gas and wall, and pressure are known at the onset of transfer.

To determine the amount of inflow gas during transfer, one must calculate three items if the equivalent mass concept is employed: (a) equivalent ullage mass, (b) heat transfer to the liquid, and (c) heat transfer to the walls. (b) and (c) are used to determine the equivalent condensed mass. The sum of the equivalent condensed and ullage masses is the total inflow mass.

a. Equivalent Ullage Mass

Eq. (15) is applicable, except that V_s is replaced by the volume change in the ullage during transfer.

b. Heat Transfer to Liquid

It would seem reasonable that in most transfer operations a serious disturbance of the liquid occurs at the initiation of transfer. It is thus assumed that at the instant transfer begins, all temperature gradients in the liquid hydrogen are destroyed and the bulk liquid is isothermal at the temperature it was before pressurization. The heat flow into the liquid during the time the temperature gradients are becoming re-established can be estimated by eq. (37), where $r = 4$ and A_L is the average liquid surface area during transfer.

c. Heat Transfer to Walls

The following model is outlined to allow the estimation of heat flow to the walls:

(1) At the end of the pressurization process, the ullage temperature, T_s, ullage pressure, p_s, ullage volume, V_s, wall temperature (exposed), T_w, and mass, M_w, are known from prior calculation.

(2) Transfer to new ullage V_s' is assumed to occur instantaneously at constant p_s.

(3) The transfer operation uncovers a new wall mass ΔM_w, which is assumed to warm up instantaneously to the temperature corresponding to saturation at p_s.

(4) The average ullage gas temperature, T_s', at the end of the "instantaneous" transfer is calculated from an energy balance in which only the heat flow required for item (3) is considered.

(5) Heat transfer between gas and wall is then calculated as a function of time, as discussed previously with eq. (19). In this case, however, two wall regions are considered:

(a) The top region contains the wall mass M_W exposed during pressurization. The wall temperature at the start of item (5) is T_W, as calculated previously for pressurization, and the ullage temperature is T_S' as defined by item (4).

(b) The bottom region contains the wall mass ΔM_W exposed during transfer. Wall and gas temperature at the start of item (5) are T_{SV} and T_S.

The total heat transferred in items (4) and (5) equals the wall heat flux as a function of time of transfer.

Item (5) is the only item that is difficult to calculate. We must first obtain a value of T_S' from item (4). Assume the ullage gas as a system during the instantaneous transfer. A First Law balance that assumes no condensation gives

$$dQ_w - dW = d(m_s e_s) - \bar{h}_i \, dm_i \tag{38}$$

since

$$e_s = h_s - p_s v_s$$

$$dW = p_s \, dV_s$$

$$dm_i = dm_s$$

$$h_s = C_p T_s + b$$

$$m_s = p_s V_s / Z_s RT_s$$

then

$$dQ_w = \frac{C_p p_s}{R} dV_s - (\bar{h}_i - b) \, dm_s \tag{39}$$

But from item (3),

$$Q_w = \Delta M_w \int_{T_{bl}}^{T_{sv}} C_{pw} \, dT_w \tag{40}$$

Combining and integrating, with Z = 1.0,

$$\Delta M_w \int_{T_{bl}}^{T_{sv}} C_{pw} \, dT_w = C_p p_s (V'_s - V_s) - (\bar{h}_i - b) \frac{p_s}{R} \left(\frac{V'_s}{T'_s} - \frac{V_s}{T_s} \right) \tag{41}$$

For any given transfer operation, all the terms in eq. (41) are known except T'_s.

8. Example of Equivalent Mass Concept

An example is presented using actual experimental data from a liquid hydrogen transfer system erected and tested by Arthur D. Little, Inc., in April 1959. The tank was a horizontal, cylindrical container, vacuum insulated; a full description of the system is given in Reference 4. Table 2.3 summarizes the test conditions.

a. Pressurization and Hold Period

(1) Adiabatic Gas Temperature at End of Assumed "Instantaneous Pressurization."

From eq. (18):

T_{s_o} = -423°F = 37°R

p_{s_o} = 14.7 psia

p_s = 65 psia

TABLE 2.3

DATA FOR LIQUID HYDROGEN TRANSFER TEST

Ullage Volume, Initial	2.14 cu ft
Ullage Volume, Final	52.3 cu ft
Ullage Pressure	65 psia
Volume of Liquid Transferred	50.2 cu ft
Time to Pressurize	20 sec
Duration of Hold before Transfer	340 sec
Duration of Transfer Operation	40 sec
Wall Area before Transfer	47 sq ft
Wall Area after Transfer	97 sq ft
Area of Liquid Surface before Transfer	8.0 sq ft
Area of Liquid Surface during Transfer (Average)	22 sq ft
Wall Mass before Transfer	230 lb
Wall Mass after Transfer	480 lb
Temperature of Ullage Gas, Initial	-423°F
Temperature of Ullage Walls, Initial	-423°F
Ambient Temperature	43°F
Enthalpy of Input Hydrogen (65 psia, 43°F)	1700 Btu/lb
Enthalpy of Saturated Vapor at One Atmosphere	283 Btu/lb
Enthalpy of Saturated Liquid at One Atmosphere	88 Btu/lb
Internal Energy of Saturated Vapor at One Atmosphere	250 Btu/lb

$(Z/Z_o) \cong 1$

$\bar{h}_i = 1700$ Btu/lb

$e_{s_o} = 250$

$e_s = f(T_s)$ at $p_s = 65$ psia

Solving for T_s, $T_s = 137°R = -323°F$

(2) Relationship Between Wall and Gas Temperature.

From Eq. (26),

$\bar{h}_i = 1700$ Btu/lb

$b = 80$ Btu/lb; see eq. (13)

$p_s = 65$ psia

$V_{s_o} = 2.14$ cu ft

$Z_s \cong 1$

$R = 767$ ft-lb/lb - °F

$M_w = 230$ lb

$k = (\bar{h}_i - b)(p_s V_{s_o})/ZR\, M_w = 185.0$ Btu - °R/lb

Eq. (26) becomes

$$\int_{37}^{T_w} C_{pw}\, dT_w = 185.00 \left(\frac{1}{T_s} - \frac{1}{137} \right)$$

The walls of the liquid hydrogen tank were stainless steel, and for this material the integrated heat capacity plot is shown in Figure 2.8. With Figure 2.8, eq. (26) may be solved to give a relationship between T_S and T_W; this is shown in Figure 2.9. Since the heat capacity of stainless steel is so small at low temperatures, the wall shows a very large change in temperature for only a small change in gas temperature.

(3) Wall Heat Transfer Coefficient. Heat transfer coefficients may be obtained from Figure 2.7. Over most of the range, h is less than 10 Btu/hr-sq ft-°F. For example, consider the case where $T_W = 95°R$; from Figure 2.9, $T_S = 132°R$, $p_S^2 \Delta T = (19.6)(37) = 7.3 \times 10^2$ atm²-°R, the film temperature is $\frac{95 + 132}{2} = 114°R$ and $h \cong 8$ Btu/hr-sq ft-°R.

As an average, consider h = 8 Btu/hr-sq ft-°R.

(4) Relationship Between Wall Temperature and Time.

From eq. (30),

M_w = 230 lb

h = 8 Btu/hr-sq ft-°R

A_w = 47 sq ft

$(T_s - T_w)$ from Figure 2.9

C_{pw} from Figure 2.10

The left side of eq. (30) was integrated and the results shown in Figure 2.11. Initially the wall temperature increases very rapidly due to a high ΔT and low wall heat capacity. In the test run under consideration, transfer occurred 360 seconds after pressurization was begun. This time interval is sufficient to allow the walls to come essentially into thermal equilibrium with the gas at about 98°R (see Figure 2.9).

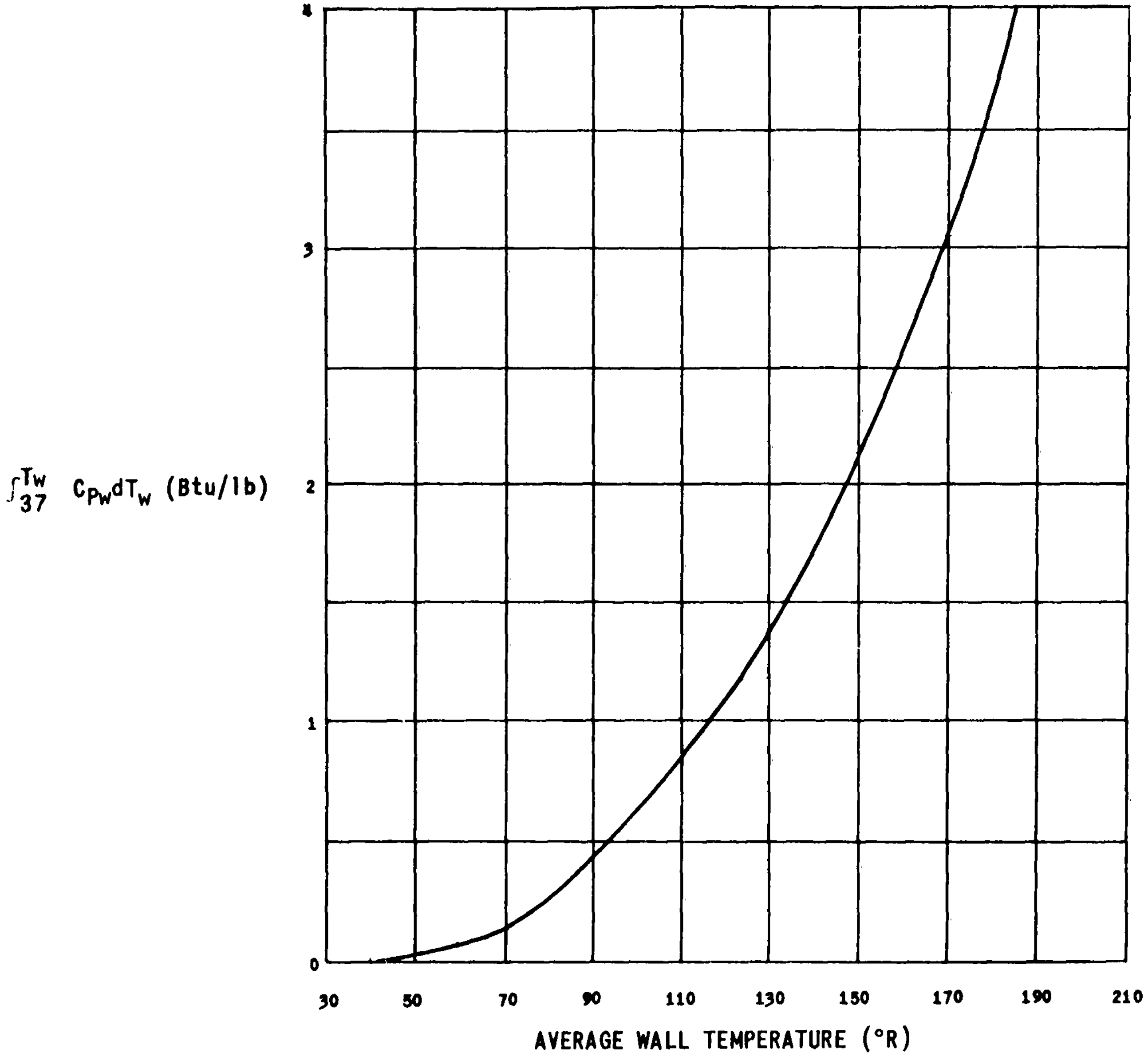

FIGURE 2.8 Integrated Heat Capacity for Stainless Steel

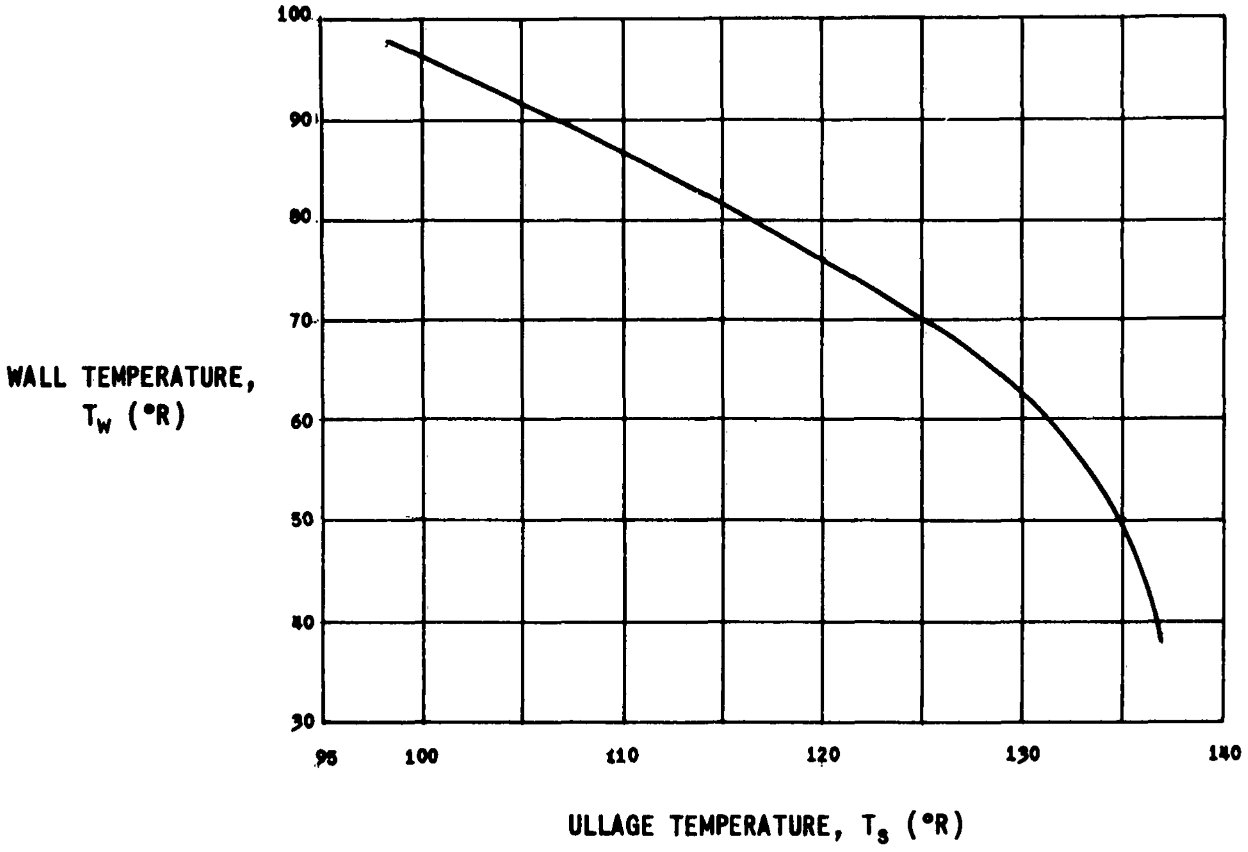

FIGURE 2.9 Relationship Between T_S and T_W from Equation (26)

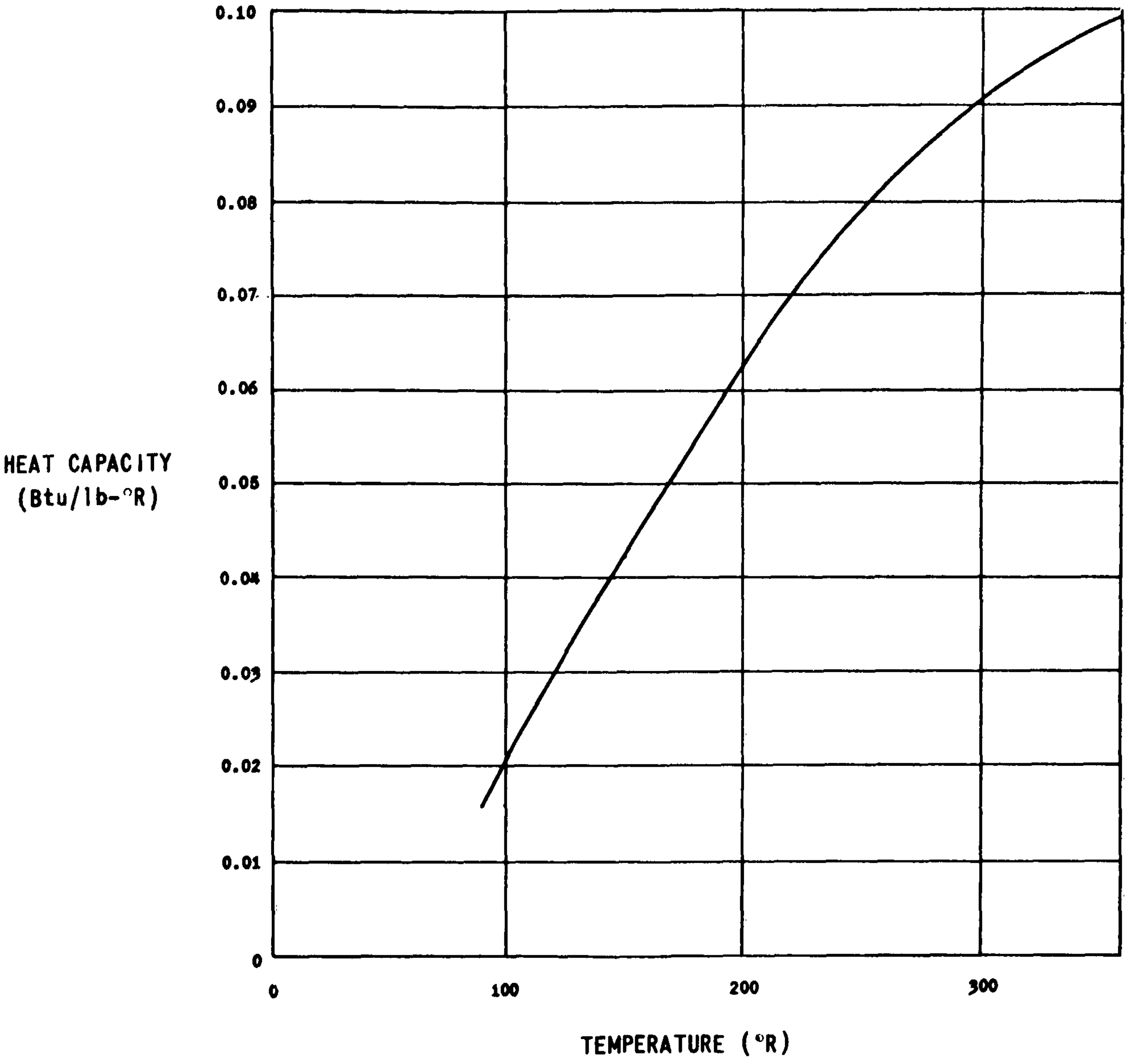

FIGURE 2.10 | Heat Capacity of Stainless Steel

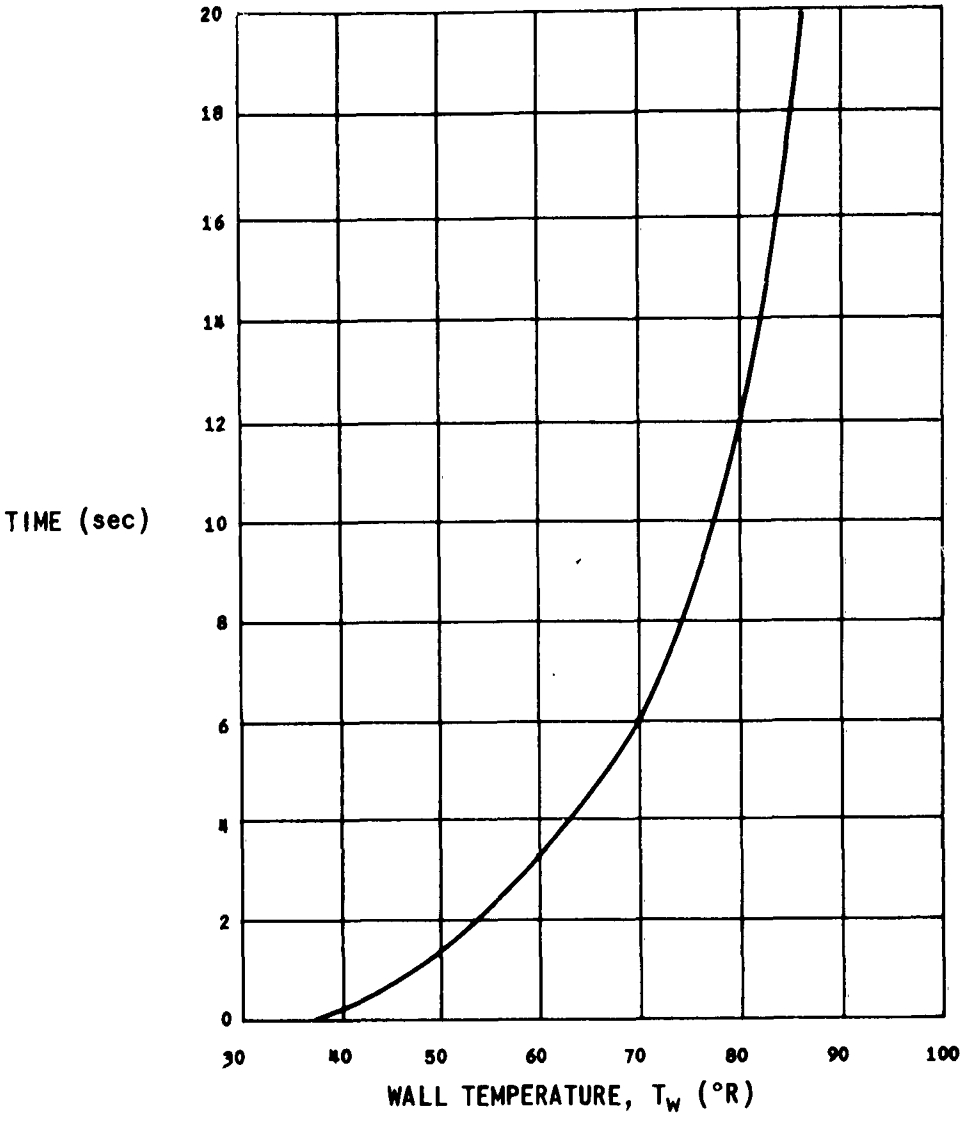

FIGURE 2. 11 Relationship Between Wall Temperature and Time

(5) Heat Transfer to Walls Before Liquid Transfer. Eq. (19) may be used to estimate Q_w, as all the terms are known or have been determined as functions of time. In the present case, however, a simpler method is possible. In the preceding paragraph it was noted that the time interval was sufficient to allow the walls to heat up to the equilibrium temperature of 98°R; thus,

$$Q_w = M_w \int_{37}^{98} C_{pw} \, dT_w$$

From Figure 2.8

$$Q_w = (230)(0.55) = 126 \text{ Btu}$$

(6) Estimation of Heat Flow to Liquid. Heat transfer to the liquid is calculated with eq. (37).

$r = 4$

$\theta = 360 \text{ sec}$

$T_{sv} = 48.3°\text{R at } p_s = 65 \text{ psia}$

$T_{bl} = 37°\text{R}$

$\bar{h}_i = 1700 \text{ Btu/lb}$

$T_{film} = 1/2\,(T_{sv} + T_{bl}) = 42.5°\text{R}$

$\bar{h}_L = 103 \text{ Btu/lb @ } T_{film}$

$k_f = 0.0129 \text{ Btu/hr-sq ft-°R}$

$\rho_f = 4.18 \text{ lb/cu ft}$

$A_L = 8 \text{ sq ft}$

Substituting

$Q_L = 230 \text{ Btu}$

(7) Estimation of Equivalent Condensed Mass Prior to Start of Transfer.

From eq. (6),

$$m_{co,eq} = \frac{-Q + W - p_s V_s}{\bar{h}_i - \bar{h}_L}$$

$$-Q = 126 + 230 = 356 \text{ Btu}$$

$$W = 0$$

$$p_s = 65 \text{ psia}$$

$$V_s = 2.14 \text{ cu ft}$$

$$p_s V_s = 65 \times \frac{2.14}{778} \times 144 = 26 \text{ Btu}$$

$$m_{co,eq} = \frac{(356 - 26)}{(1700 - 103)} = 0.21 \text{ lb}$$

(8) Estimation of Equivalent Ullage Mass Prior to Start of Transfer.

From eq. (15),

$$m^* + m_{ul,eq} = \left(\frac{h_v - \bar{h}_L}{\bar{h}_i - \bar{h}_L}\right)\left(\frac{p_s V_s}{RT_v}\right)$$

$$T_{sv} = 48.3°R \text{ at } 65 \text{ psia}$$

$$T_a = 43°F = 503°R$$

$$T_v = 1/2\,(T_{sv} + T_a) = 276°R$$

$$h_v = 948 \text{ Btu/lb}$$

$$h_L = 103 \text{ Btu/lb}$$

$$m^* + m_{ul,eq} = \left(\frac{948 - 103}{1770 - 103}\right)\left(\frac{65 \times 144 \times 2.14}{767 \times 276}\right)$$

$$= 0.05 \text{ lb}$$

(9) Total Mass Required to Pressurize and Hold Until Start of Transfer.

From eq. (8),

$$m_i = m^* + m_{ul,eq} + m_{co,eq}$$

$$= 0.05 + 0.21 = 0.26 \text{ lb}$$

b. Transfer Period

(1) Estimation of Equivalent Ullage Mass. As above, except using the volume of liquid transferred, 50.2 cu ft,

$$m_{ul,eq} = 1.20 \text{ lb}$$

(2) Estimation of Heat Transfer to Liquid. As above, except in this case the time decreases from 360 to 40 seconds, and the average liquid area increases from 8 to 22 sq ft.

$$Q_L = 210 \text{ Btu}$$

(3) Estimation of Ullage Gas Temperature After Assumed Instantaneous Transfer.

From eq. (41),

$$\Delta M_w = 250 \text{ lb}$$

$$T_{sv} = 48.3°\text{R at 65 psia}$$

$$T_{bl} = 37°\text{R}$$

$$\int_{T_{bl}}^{T_{sv}} C_{pw}\, dT_w = 0.02 \text{ Btu/lb}$$

C_p = 3.20 Btu/lb-°R (average value)

p_s = 65 psia

$R = 767 \frac{\text{ft - lb}}{\text{lb - °R}} = 0.985 \frac{\text{Btu}}{\text{lb - °R}}$

V'_s = 52.3 cu ft

V_s = 2.14 cu ft

h_i = 1700 Btu/lb

b = 80 Btu/lb

T_s = 125°R (from previous calculation)

$$\Delta M_w \int_{T_{bl}}^{T_{sv}} C_{pw}\, dT = \frac{C_p p_s}{R} (V'_s - V_s) - \frac{(\bar{h}_i - b)}{R} p_s \left(\frac{V'_s}{T'_s} - \frac{V_s}{T_s} \right)$$

$$(250)\,(0.02) = \frac{3.20 \times 65 \times 144 \times (52.3 - 2.14)}{767}$$

$$- \frac{(1700 - 80)\; 65 \times 144}{767} \left(\frac{52.3}{T'_s} - \frac{2.14}{125} \right)$$

Solving for T'_s,

T'_s = 450°R

(4) Estimation of Wall Heat Transfer - Top Region. This calculation is carried out exactly as described in the pressurization example, except that the wall temperature at the start is not 37°R but 98°R, the temperature of the walls at the instant transfer began. The ullage temperature, T'_s, at this instant was 450°R as calculated above. Accordingly,

Q_w (top), during transfer = 260 Btu

(5) Estimation of Wall Heat Transfer - Bottom Region. Similar statements apply to the top region, $T'_s = 450°R$, and the wall temperature at the start is the temperature of the saturated vapor at p_s, 48°R. In addition, k in eq. (26) has changed as the ullage volume increases from 2.14 cu ft to 50.2 cu ft, and the wall mass represents only that in the newly exposed region, 480 lb. Upon calculation,

$$Q_w \text{ (bottom), during transfer } = 2000 \text{ Btu}$$

(6) Estimation of Equivalent Condensed Mass During Transfer.

From eq. (6),

$$m_{co,eq} = \frac{-Q + W - p\,(V'_s - V_s)}{\bar{h}_i - \bar{h}_L}$$

$$-Q = 210 + 260 + 2000 = 2470 \text{ Btu}$$

$$W = p_s\,(V'_s - V_s)$$

$$m_{co,eq} = 2470/(1770 - 103) = 1.55 \text{ lb}$$

(7) Estimation of Gas Requirements During Transfer.

$$m_i = m^* + m_{ul,eq} + m_{co,eq}$$

$$= 1.20 + 1.55 = 2.75 \text{ lb } H_2$$

9. Comparison Between Calculated and Experimental Values

From the previous calculations, the predicted gas requirement for pressurization and transfer is 2.75 + 0.26 = 3 lb. The experimentally measured value was 2.9 lb. A total of 15 runs were made in the hydrogen test facility described in Reference 4. The conditions for these runs are tabulated in Table 2.4, as are calculated and experimental hydrogen gas consumptions. In all runs but No. 2, the check is satisfactory; in test run No. 2 there was a leak in the inlet system of undetermined size, which may account for the difference.

TABLE 2.4

COMPARISON BETWEEN EXPERIMENTAL AND CALCULATED VALUES OF GAS CONSUMPTION

Test	Tank Pressure (psia)	Ullage Volume (cu ft)		Gas Consumed (lb)	
		Initial	Final	Calc.	Exp.
1	27.5	52.30	70.5	0.87	0.99
2	65.0	2.14	52.3	2.41	3.47
3	65.0	2.54	79.5	3.00	2.90
4	65.0	34.30	60.8	4.20	4.90
5	115.0	11.10	52.3	2.50	2.60
6	115.0	18.60	63.3	4.30	4.10
7	115.0	10.60	37.3	3.30	3.60
8	65.0	5.40	47.0	2.50	2.40
9	65.0	5.90	43.5	2.50	2.70
10	65.0	7.50	49.5	2.00	1.90
11	65.0	34.00	30.0	3.30	3.80
12	65.0	6.10	75.0	0.70	0.40
13	65.0	7.50	36.8	2.70	2.50
14	65.0	5.90	34.8	2.70	2.50

This method has been applied to calculate gas consumptions for many other cryogenic transfer systems containing nitrogen and oxygen liquid. The systems varied in size from 3 to 28,000 gallons, and pressurization times ran between 4 seconds and 2 minutes. Pressures varied between 20 and 465 psia. Most tests involved pressurization of a cryogenic liquid in a vacuum-insulated storage tank, although in one test series a tank immersed within a second tank of liquid nitrogen was used. The predicted and measured gas consumptions agreed within about 15%. These tests and data are described in Reference 2.

G. REFERENCES

1. Arthur D. Little, Inc., Pressurized Transfer of Cryogenic Liquids, Special Report No. 78 to AFBMD under Contract AF04(645)-34, June 1, 1958.

2. Arthur D. Little, Inc., Gas Requirements in the Pressurization and Transfer of Cryogenic Fluids, ADL Technical Report No. 2 to AFBMD, Contract AF04(647)464, Cambridge, Mass., March 15, 1960.

3. Chelton, D. B. and Mann, D. B., Cryogenic Data Book, U. S. Atomic Energy Commission UCRL-3421, 1956, 116 pp available as WADC Tech. Rpt. 59-8 from Dept. of Commerce, Printing Dept., Washington, D. C.

4. Moore, R. W. et al., "Gas Pressurized Transfer of Liquid Hydrogen," Proc. 1959 Cryogenic Eng. Conf., p. 450.

5. Arthur D. Little, Inc., Rapid High Pressure Transfer of Liquid Oxygen Within a System Immersed in Liquid Nitrogen, Special Report No. 103 to AFBMD under Contract AF04(645)-34, September 1, 1959.

6. Arthur D. Little, Inc., Pressurized Cooldown of Cryogenic Transfer Lines, Special Report No. 106 to AFBMD under Contract AF04(645)-34, October 1, 1959.

7. McAdams, W. H., Heat Transmission, 3rd ed. New York, McGraw-Hill Book Co., 1954.

III. REQUIREMENTS FOR HYDROGEN GAS STORAGE CYLINDERS USED FOR THE PRESSURIZED TRANSFER OF LIQUID HYDROGEN

A. INTRODUCTION

Rapid transfer of liquid hydrogen using hydrogen gas as the pressurizing and transferring medium raises the question of adequacy of design of high-pressure hydrogen storage cylinders made of forged steel. Work was initiated under contracts AF 33(616)-5641 and AF 04(645)-34 to study the heat transfer effects associated with rapid depressurization of storage cylinders and the resultant thermal stresses imposed upon the cylinder. This work was continued under the present contract and is summarized in its entirety below.

In 1957 Reynolds and Kays(1) analyzed the blowdown and charging process in a single gas receiver. The basic equations derived from the first law of thermodynamics related the gas temperature to the residual amount of gas in the receiver for a given blowdown or charging rate. Heat transfer between the walls and the gas was allowed. A few experimental data were taken by depressurizing a small air supply tank. Measured air temperatures agreed well with calculated values for blowdown times of about 20 seconds and initial pressures of 150 psia.

We proposed to conduct analytical and experimental programs simultaneously in an effort to test the proposed method over a much wider pressure range. The results are summarized below. In addition to reporting experimental gas temperatures during the blowdown of a gas cylinder, we will discuss the temperature, radial temperature gradients and tangential stresses in the bottle neck.

The process of rapid cylinder depressurization results in low temperatures in the exit gas. As this gas has a high velocity in the neck of the bottle, heat transfer rates between the gas and neck metal are also high. It is known that low temperatures have a detrimental effect on the structural properties of many metals, particularly on carbon steels. Furthermore, as a result of the temperature gradients in the neck, large tangential stresses are induced. Because many high-pressure gas storage cylinders are made of carbon steel, the temperature gradients in the bottle neck must be estimated if the probability of failure of the bottle is to be ascertained.

The objectives of this work are as follows:

1. To introduce experimental data that will confirm the general method of Reynolds and Kays for estimating gas temperatures during the rapid blowdown of gas cylinders. Data were taken from tests run at initial pressure levels of 2000 psia and with horizontal and vertical bottle configurations. Hydrogen gas was used in some tests, and nitrogen gas was used in others. Blowdown times ranged from 14 seconds to 33 minutes.

2. To present methods for calculating typical neck temperatures and temperature gradients for small laboratory bottles and for very large industrial cylinders.

3. To present a method for calculating stresses in the bottle neck.

4. To discuss the possible hazards resulting from low temperatures and large temperature gradients in the bottle neck that occur during blowdown.

During the course of this work, an article by Potter and Levy(2) appeared in the open literature. Their work expanded somewhat upon the work of Reynolds and Kays, but did not include methods of estimation of forced-convection heat transfer coefficients.

B. NOMENCLATURE

A = heat transfer area of cylinder walls, sq ft

b = radial distance, ft

a = constant in eq. (4), hr^{-1}

C = dimensionless constant in eq. (5)

C_p = heat capacity at constant pressure, Btu/lb-°F

D = diameter of cylinder neck, ft

E = Young's Modulus

G = mass flow rate of gas out of cylinder, lb/hr-sq ft

g = acceleration due to gravity = $32.2 \times (3600)^2$ ft/hr^2

h = heat transfer coefficient between gas and cylinder, Btu/hr-sq ft-°F

k = thermal conductivity, Btu/hr-ft-°F

L = characteristic length, ft

m = mass of gas in cylinder

n = dimensionless constant in eq. (5)

N_{Gr} = dimensionless Grashoff Number

N_{Pr} = dimensionless Prandtl Number

N_{Re} = dimensionless Reynolds Number

P = bottle pressure, lb/sq ft

Q = heat flow, between gas and walls, Btu

r = radius

T = temperature, °F (in the stress analysis, T refers to a temperature above an arbitrary datum)

u = radial displacement

V = cylinder volume, cu ft

x = thickness of metal neck, ft

α = coefficient of thermal expansion, $°F^{-1}$

ρ = density, lb/cu ft

μ = viscosity, lb/ft-hr

θ = time, hr

σ_r = radial stress

σ_t = tangential stress

ν = Poisson's ratio

Subscripts

g - gas

n - neck of cylinder

o - initial conditions

w - wall of cylinder

C. ANALYSIS OF THE BLOWDOWN PROCESS

If the gas within the cylinder is chosen as the system, an energy balance shows that:

$$dQ = m\,C_p\,dT_g - VdP \qquad (1)$$

Ideal gases are assumed. For nitrogen and hydrogen at 2000 psia, this assumption is warranted; for gases for which such an assumption is not warranted, a similar but somewhat unwieldy energy balance may be written from the law of corresponding states, van der Waals' equation, or other applicable equations of state.

The heat flow into the system is determined as:

$$dQ = hA\ (T_w - T_g)\ d\theta \tag{2}$$

Combining eqs. (2) and (3), we obtain:

$$hA\ (T_w - T_g) = mC_p\ (dT_g/d\theta) - V\ (dP/d\theta) \tag{3}$$

Eq. (3) is easily solved by finite difference techniques. Where the depressurization is adiabatic or isothermal or where the flow is constant, eq. (3) can be analytically integrated.(1) In many of our runs the flow was choked, so the experimental pressure-time profile was essentially exponential and of the form:

$$P/P_o = e^{-a\theta} \tag{4}$$

It was, therefore, convenient to arrange eq. (3) in a dimensionless form to facilitate solution on a digital computer. In other runs an experimental data plot of P vs θ was used to obtain $dP/d\theta$.

Heat transfer from the cylinder walls to the gas occurs predominantly by natural convection, and values of h can be estimated from standard turbulent-free convection correlations. This same conclusion was reached by Reynolds and Kays and tested for low pressures and small temperature differences. Thus:

$$\frac{hL}{k} = C\ (N_{Gr} N_{Pr})^n \tag{5}$$

where the following values of C and n are recommended by McAdams(3):

	C	n
Vertical Cylinders	0.13	0.33
Horizontal Cylinders		
Bottom Slice	0.14	0.33
Top Slice	0.27	0.25

It must be noted, however, that in the neck of the bottle, essentially all heat transfer occurs by a forced convection mechanism.

The wall temperature T_W in eq. (3) is a variable, but for most high-pressure gas storage cylinders, the thermal capacity of the wall metal is so large that T_W decreases only slightly during a blowdown. When necessary, an energy balance may be written to include the cylinder walls as a part of the system, to provide a quantitative relationship between wall temperature and time.

D. EXPERIMENTAL PROCEDURE

Experimental depressurization tests were made with a "K"-type laboratory gas cylinder, 9.125 in. OD and 8.56 in. ID. The over-all height was 55 in.. from neck to base, and the volume was rated as 300 SCF (water volume = 1.75 cu ft). The neck ID was about 0.74 in., and the neck wall thickness 0.62 in. The shut-off valve was removed and replaced by a 9/16-in. Minneapolis-Honeywell control valve. The bottle was first charged with either hydrogen or nitrogen gas and then depressurized. The rate of depressurization could be controlled by varying the control valve position.

All tests were carried out with initial pressures of 2000 psia and terminal pressures of 200 psia. The time required for the depressurization was varied between 14 seconds and 33 minutes. In all tests the bottle was enclosed in a weatherproof shelter and insulated with Perlite.

E. INSTRUMENTATION

1. Pressure

The pressure in the bottle was measured on a remote Bourdon tube gage, and still photographs were made during blowdown for a record of the pressure level. Included in the photographs was a clock synchronized to start at the beginning of the test.

2. Gas Temperature

Gas temperatures in the bottle were measured by copper-constantan thermocouples Nos. 10 and 17, as shown in Figure 3.1. The temperatures were read on a Bristol recorder.

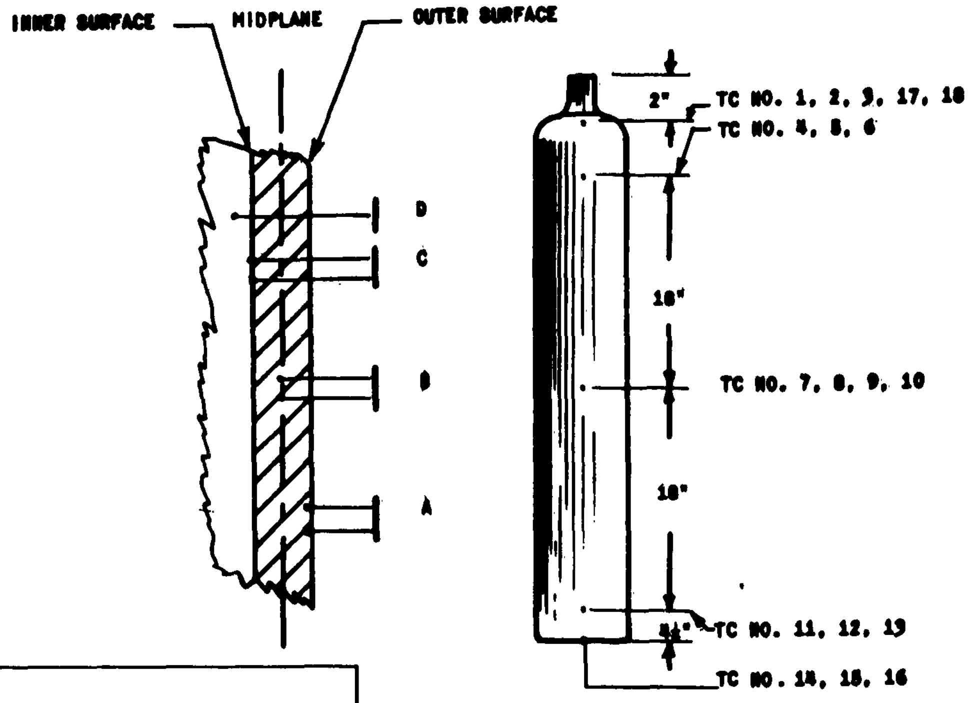
INNER SURFACE
MIDPLANE
OUTER SURFACE
D
C
B
A
2"
TC NO. 1, 2, 3, 17, 18
TC NO. 4, 5, 6
18"
TC NO. 7, 8, 9, 10
18"
4½"
TC NO. 11, 12, 13
TC NO. 14, 15, 16

PENETRATION OF THERMOCOUPLE INTO CYLINDER WALL

PENETRATION	THERMOCOUPLE NO.
A	1, 4, 7, 11, 14
B	2, 5, 8, 12, 15, 18
C	3, 6, 9, 13, 16
D	10, 17

FIGURE 3.1 Thermocouple Locations on Gas Storage Cylinder

3. Wall Temperature

Wall temperatures were measured at four heights and three radial distances, as shown in Figure 3.1. A bottle similar to the one used in the tests was cut in half longitudinally, and the wall thickness was measured for use in drilling the thermocouple holes in the test bottle. Two holes spaced 1/8-in. apart were drilled to the desired depth. Each wire was arc welded in the bottom of the hole, and the holes were filled with an epoxy resin. The couple thus incorporated a portion of the wall metal. Temperatures were read out on the Bristol recorder as noted above.

F. RESULTS

Each test produced data relating the variation of pressure and gas and wall temperatures with time. The principal independent variable was the time for blowdown, although initial gas temperature and type (hydrogen or nitrogen) were also varied.

Smoothed temperature-and-pressure-time traces for three typical runs, Nos. 7, 8 and 9, are shown in Figures 3.2, .3 and .4. These tests were made with hydrogen gas in a horizontal cylinder. The time required to drop the bottle pressure from 2000 to 200 psia was 30, 480 and 14 seconds respectively for these three runs. In Run 9, the rate of depressurization was so high that heat transfer from the walls did not have an appreciable effect on the gas temperature. In Runs 7 and 8, the blowdown time was longer, and sufficient heat transfer took place for the gas temperature to pass the minimum value and begin to increase at the end of the tests.

Average wall temperatures are also shown in these figures. Most of the adjacent wall couples differed by only 1 or 2 degrees; the set located near the bottle neck did, however, indicate radial gradients as high as 10°F. Such gradients are not unexpected, because the gas is beginning to accelerate in this section of the bottle and may attain sufficient velocities to produce high convective coefficients. Radial gradients are much more pronounced in the neck of the cylinder, and a discussion of the stresses they produce is given later.

Energy balances, based on the experimental data, showed the results to be consistent. Heat transfer coefficients calculated from the wall heat flow and temperatures were found to correspond closely to those calculated by eq. (5).

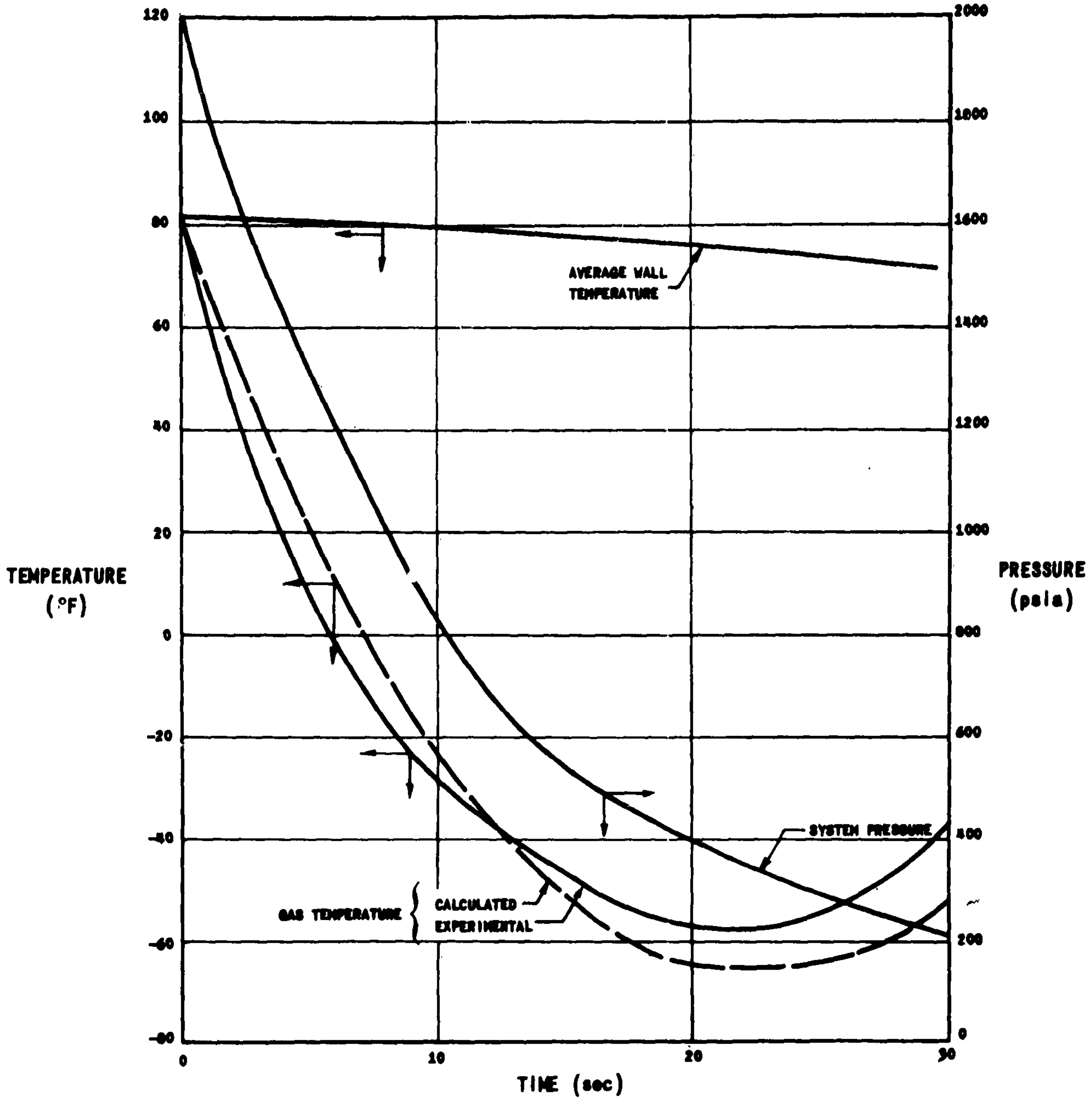

FIGURE 3.2 Experimental Variations of Pressure and Temperature, Run 7

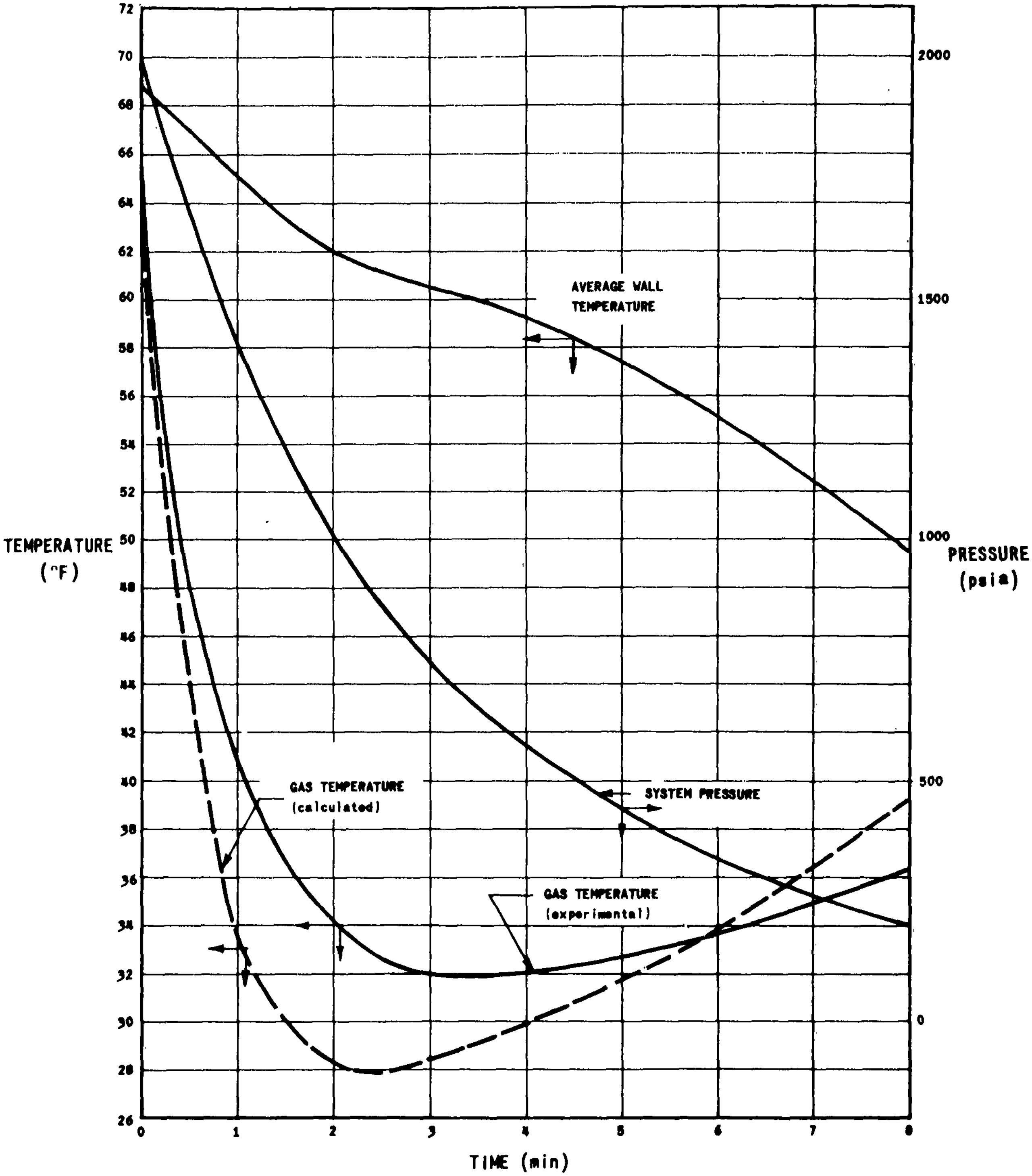

FIGURE 3.3 Experimental Variations of Pressure and Temperature, Run 8

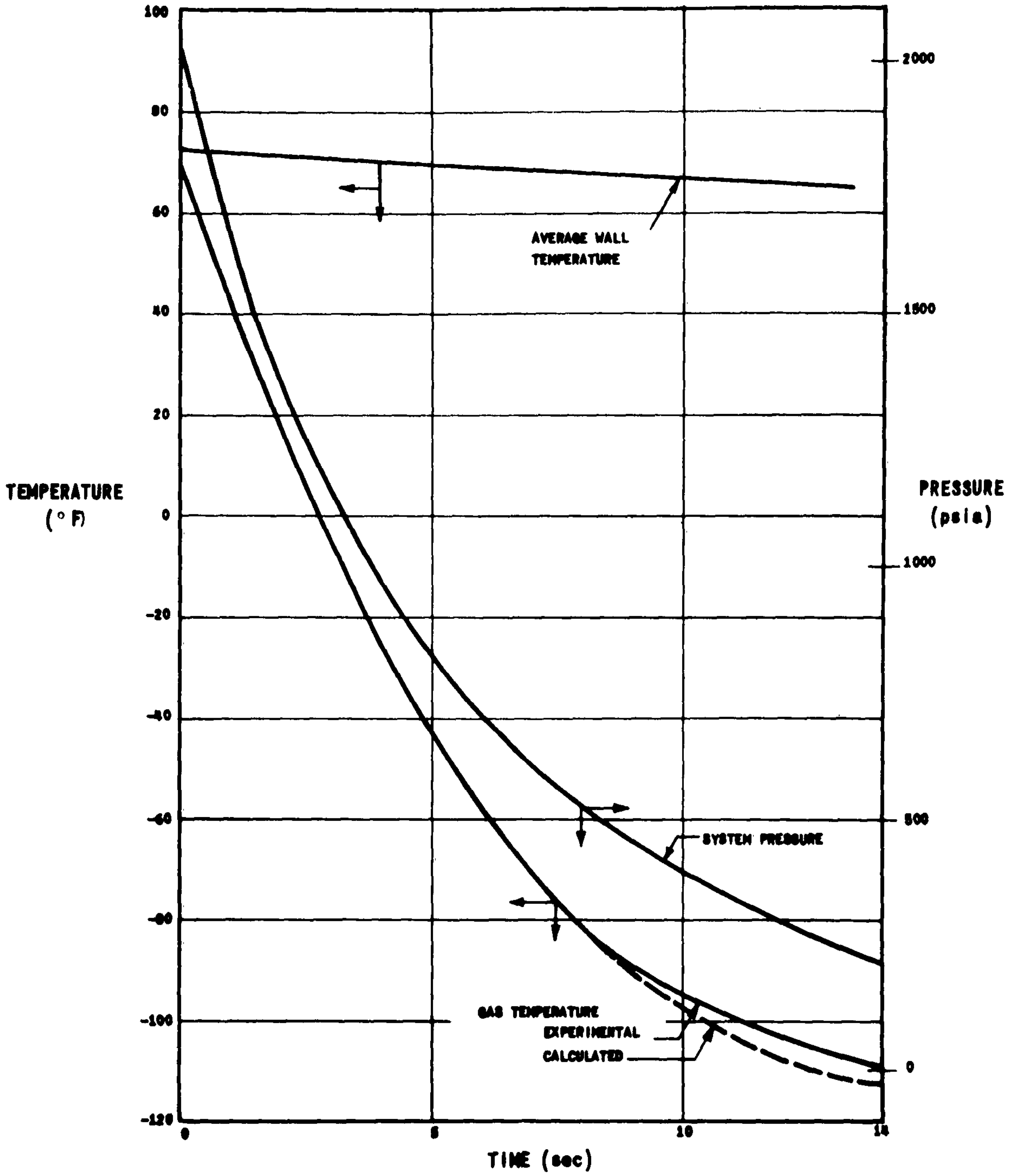

FIGURE 3.4 Experimental Variations of Pressure and Temperature, Run 9

G. COMPARISON OF THEORY WITH EXPERIMENTAL DATA

By use of experimental data to determine the cylinder pressure as a function of time, eq. (3) may be solved by numerical techniques to yield a relation between gas temperature and time. Wall heat transfer coefficients are determined by eq. (5).

Gas temperatures calculated by this method agreed well with experimentally measured temperatures. On Figures 3.2, .3 and .4 the dotted lines indicate the calculated values. For other runs, equally good results were obtained.

H. TEMPERATURES IN THE NECK OF THE BOTTLE

The cold gas flowing at high velocity through the bottle neck rapidly cools the inner fibers of metal. Radial temperature gradients induced in the wall metal as a result of heat transfer may be calculated by the graphical, modified Schmidt method discussed by McAdams.(3) The gas-wall heat transfer coefficient is calculated by the usual forced-convection correlation:

$$\frac{hD}{k} = 0.023\ (N_{Re})^{0.8}\ (N_{Pr})^{0.4} \qquad (6)$$

Both the N_{Re} and the N_{Pr} in the cylinder neck vary during blowdown, because of the rapid decrease in the gas velocity, pressure and temperature with time. The history of these properties is, however, known after eq. (3) has been solved. In other words, from eq. (3) the mass flow rate of gas and its temperature and pressure are defined at each time during blowdown; these properties may be used with eq. (6) to obtain values of h as a function of time. Velocities are high, as are the calculated values of h. Figure 3.5 has been drawn to indicate values of h and the variation of h with time. For Runs 7, 8 and 9, which were discussed earlier, the sharp drop in the heat transfer coefficient with time results from the reduction in flow rate as the pressure upstream of the control valve decreases.

I. TEMPERATURE GRADIENTS IN THE CYLINDER NECK WALL

From the graphical, modified Schmidt method a solution for the transient heat transfer process in the bottle neck is available. The data necessary to allow the delineation of neck wall temperatures with time are: (a) geometry of the bottle (i.e., thickness and diameter of the neck), (b) the history of the cold gas in the neck (i.e., velocity, temperature and pressure of the bulk flow as a function of time), (c) the ambient conditions for an estimate of heat flow into the bottle neck and (d) the properties of the gas and metal at various temperatures and the properties of the gas at various pressures.

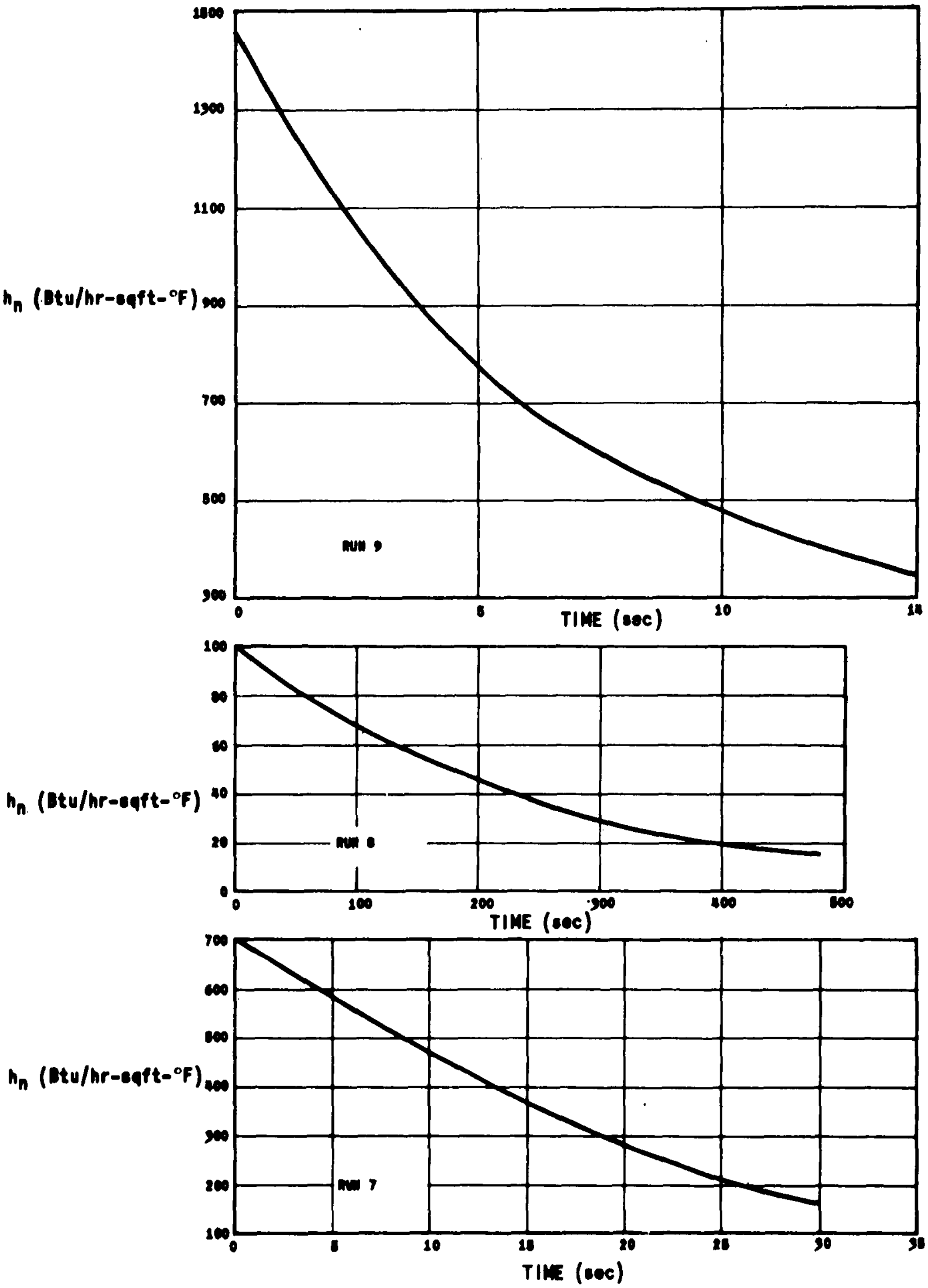

FIGURE 3.5 Heat Transfer Coefficients In Bottle Neck During Blowdown

Figures 3.6 and 3.7 show the result of these calculations for Run 7, which was conducted with a blowdown time of 30 seconds. Figure 3.6 shows the temperature variation at different locations within the wall and for times between 0 and 30 seconds. The gradient does not deviate greatly from being linear; the largest temperature difference between inner and outer walls was calculated to be about 55°; i.e., a maximum gradient of some 70°F/in. exists in the neck wall metal.

Figure 3.7 is a plot of wall temperatures at various times. The top and bottom curves show the calculated temperatures of the inner and outer sides of the wall. The curve marked "A" is a plot of the integrated average wall temperature as determined from Figure 3.6. The curve marked "B" has been calculated on the assumption that no radial gradient exists, i.e., the metal conductivity is to be high. In this case:

$$(\rho x C_p)_n \; dT_n/d\theta = h_n \; (T_g - T_n) \tag{7}$$

In eq. (7), values of the average neck wall temperature, T_n, may be found for various values of time, since the only other variables, h and T_g, are known as functions of time from eqs. (3) and (6). As seen in Figure 3.7, the agreement between the two wall temperature averages is not close; for tests of longer blowdown times, the difference between averages decreases. For example, in Run 8 the agreement is excellent, and there is no appreciable wall temperature gradient at any time during depressurization.

The low temperatures attained by the gas and neck metal during depressurization are somewhat surprising. Figure 3.4 shows that the gas has actually dropped from 70°F to less than -100°F in the 14-second blowdown; the neck wall registered a smaller temperature drop, but the 60-70°F decrease (average wall temperatures) results in a definite decrease in the resistance to brittle fracture. The possibility of brittle fracture may be enhanced if the initial bottle temperature is low. Another problem may be introduced during depressurization. Condensible vapors in the gas may be frozen out at the low gas temperatures and plug the throttling valve on the bottle; the analysis given in this paper would allow the possibility of freezing to be evaluated, but the rate of solid nucleation and crystal growth would probably control the actual rate of valve plugging.

J. DEPRESSURIZATIONS OF LARGE GAS STORAGE BOTTLES

In many instances, gas is stored at high pressure in large cylinders. Lower gas temperatures would be expected to accompany blowdown in the large bottles, because the ratio of the wall heat-transfer area to bottle volume is less than for small bottles. Also, in large storage cylinders, gas would contact the neck metal for relatively long periods of time.

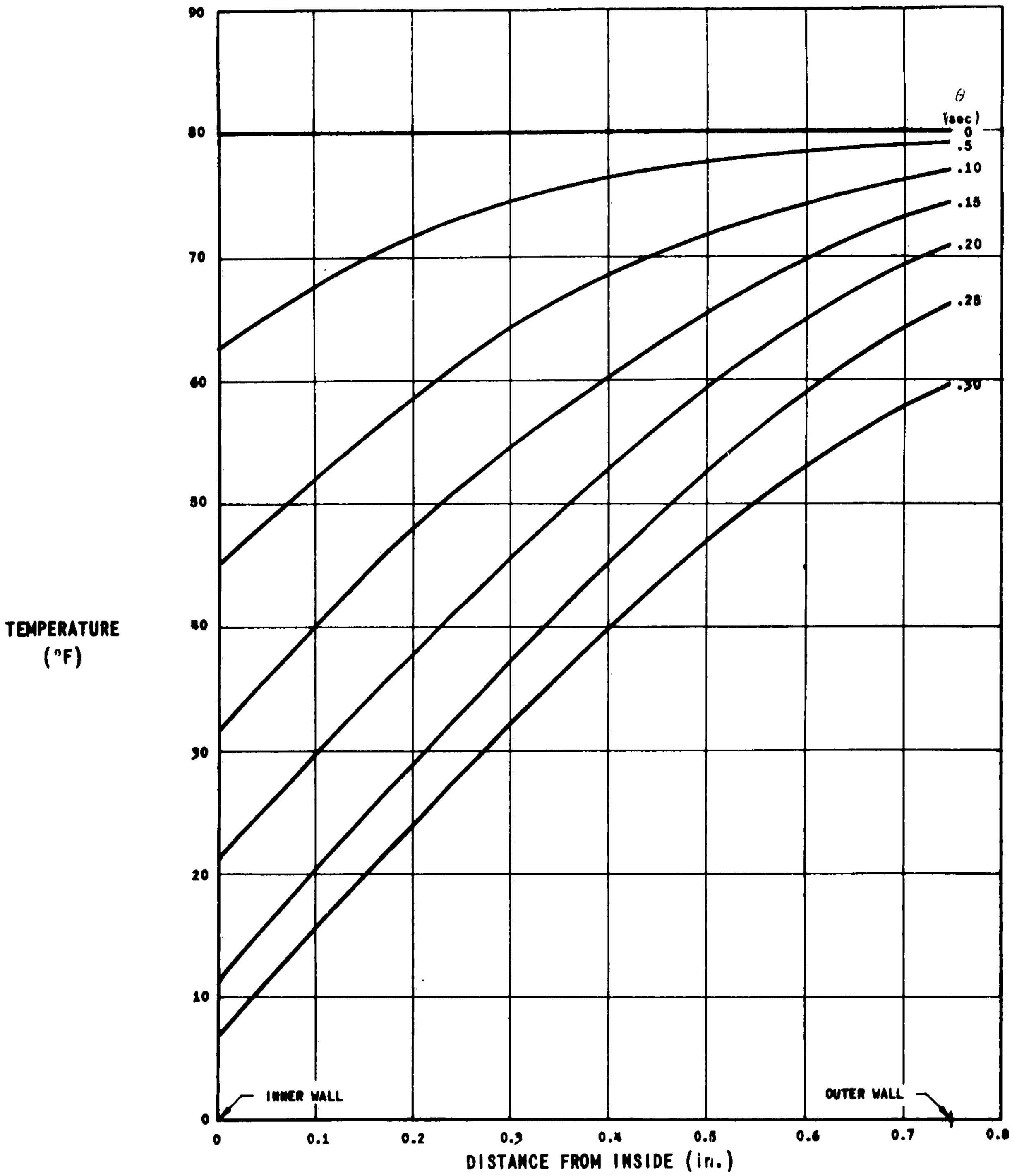

FIGURE 3.6 Neck Wall Temperatures for Various Thicknesses in Run 7

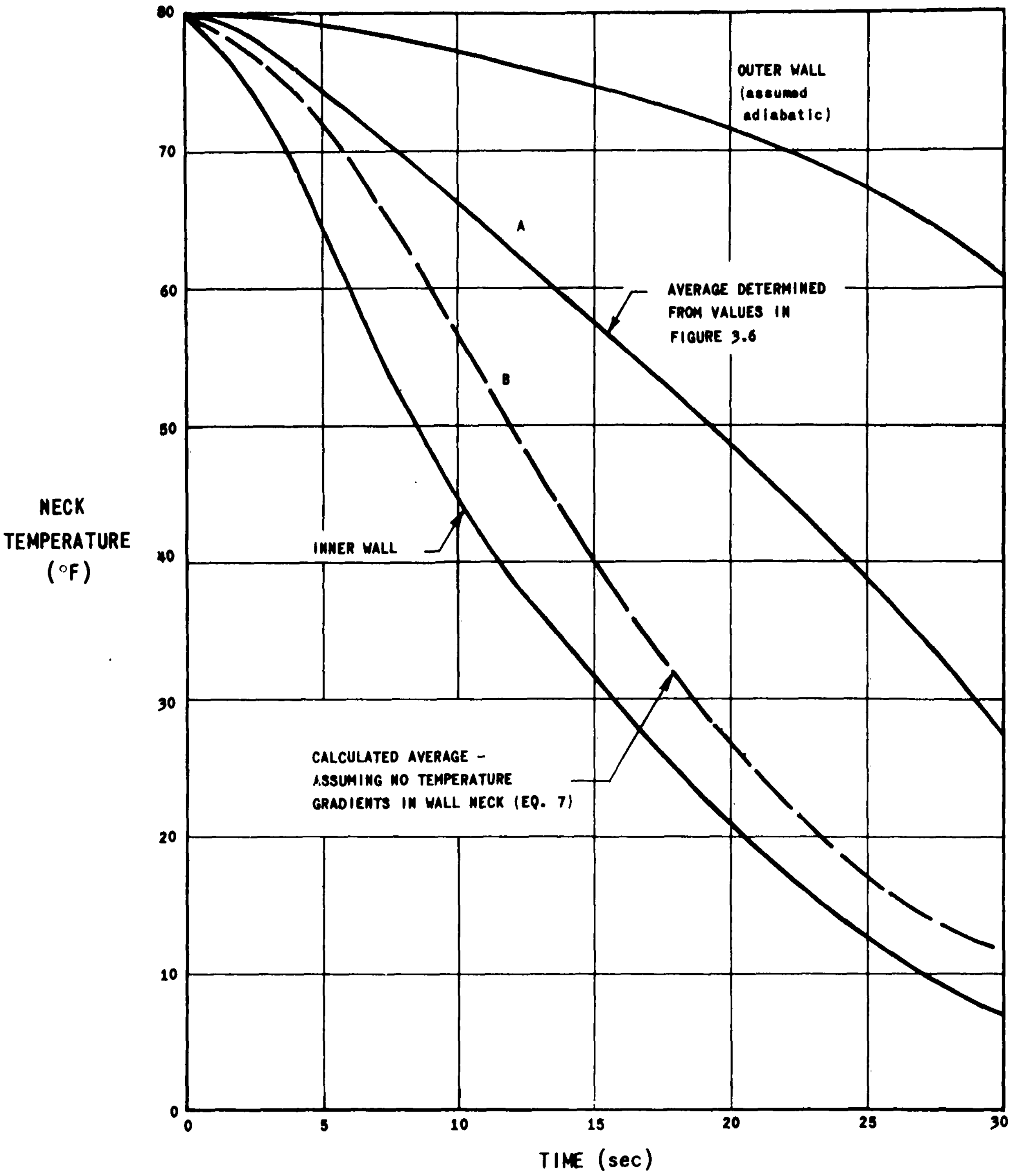

FIGURE 3.7 Neck Wall Temperature at Various Times in Run 7

For very rapid blowdowns, the heat that the bottle wall contributes to the gas is negligible, and the temperature history of the gas is closely approximated by an isentropic path. For longer blowdown times, there is an increasing quantity of heat transfer from the walls to the gas, so the temperature decrease is not as pronounced. The effect of variations in blowdown time on the neck-wall cooling process is not so clearly visualized. For short blowdown times, the lowest gas temperatures and highest forced-convection coefficients are found; however, the cooling process is of short duration. For longer blowdown times, the rate of wall neck cooling decreases, but the time available for cooling increases. Certainly, longer blowdown times result in less severe wall temperature gradients.

To illustrate the effect of blowdown times on large bottles, we will calculate the effects of two extreme conditions of depressurization. An A. O. Smith large, horizontal bottle was chosen as the cylinder. The principal dimensions were:

ID	52 in.
Length	18 ft 3 in.
Wall Thickness	2.08 in.
Volume	311.5 cu ft
Weight	29,000 lb
Neck ID	2.376 in.
Neck Wall Thickness	1.800 in.

These cylinders are typical of many of the large gas storage bottles used by the United States Air Force.

Two blowdown rates were chosen, both assuming a pressure decay as given by eq. (4). For Calculation A, $a = 0.0231\ \text{sec}^{-1}$, which corresponds to a 50% reduction in pressure every 30 seconds. This is equivalent to a sonic flow through a 1.25-in. diameter restriction, a fairly arbitrary selection. Calculation B corresponds to a halving of pressure every 12.5 minutes, i.e., $a = 0.00093\ \text{sec}^{-1}$. An initial gas and bottle temperature of -25°F was chosen, and the initial pressure was 2000 psia. Gas temperatures at various times were calculated from eq. (3) as described earlier, and they are plotted against bottle pressure in Figure 3.8. For comparison, gas temperatures for both runs are shown on the same figure. In Calculation A, depressurization is so rapid that the path approximates an isentropic one, as indicated by the dashed curve. Calculation B is longer; the gas temperature decrease is less and wall heat transfer is important. However, even in this "slow" blowdown, a gas temperature drop of nearly 55°F was calculated.

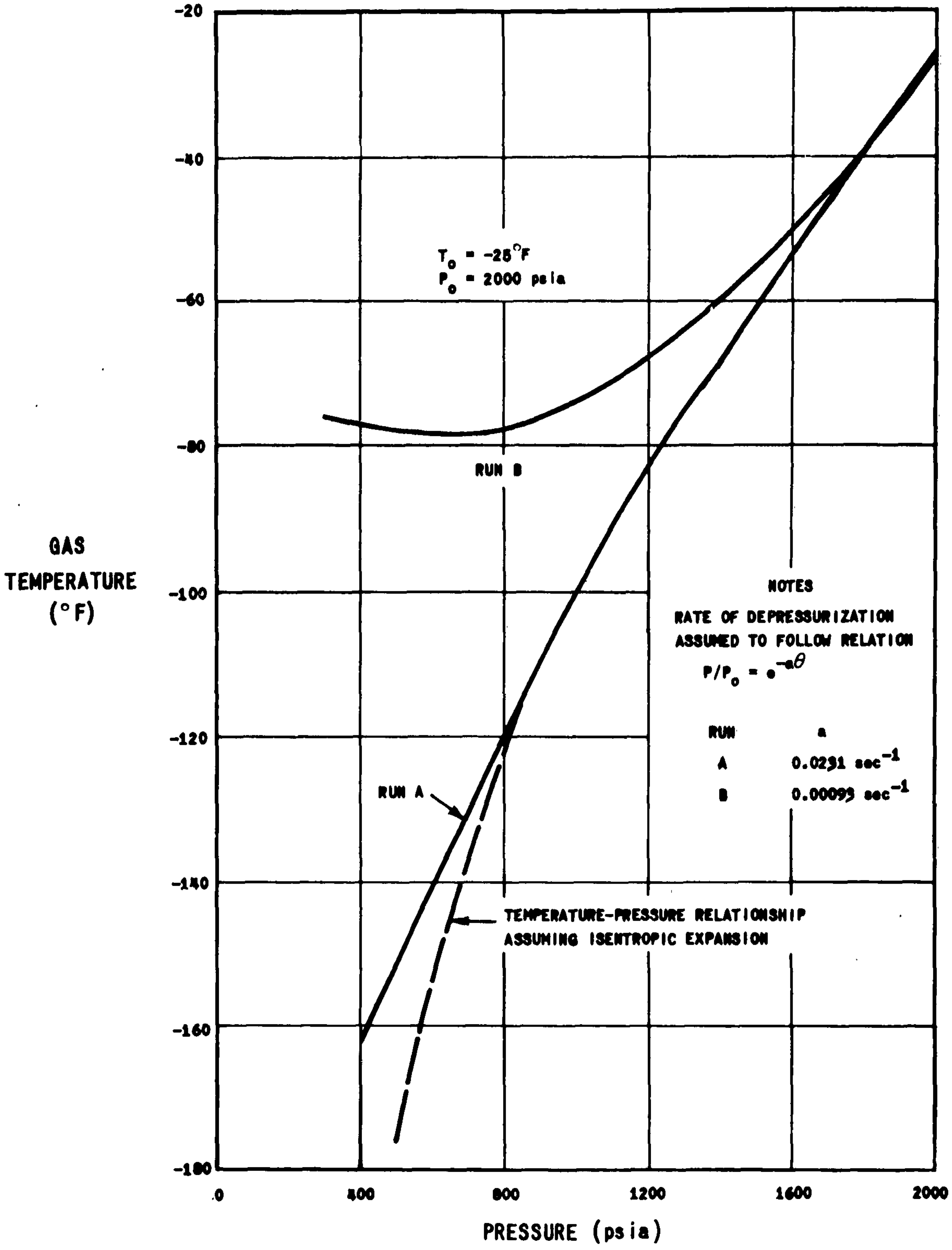

FIGURE 3.8 Gas Temperatures for Large Bottle Blowdowns

Average neck wall temperatures as determined from eq. (7) are shown in Figure 3.9. In Case A, a drop of about 113°F was calculated for the 80-second run. As might have been expected, temperatures for Case B were not nearly as low; nevertheless, carbon steel is susceptible to brittle fracture at the -80°F temperature attained.

Case B was of such a long duration that no appreciable neck-wall radial temperature gradients were established. In Case A, however, large gradients exist. Estimates of wall temperature gradients as a function of time were made for Run A using the Schmidt graphical method,(3) and in Figure 3.10 the difference in temperatures between the inner and outer neck wall metal is shown at different times. As the thickness of metal was about 2.08 in., gradients as high as 113°F were found near the end of the run.

Case A is typical of a very rapid depressurization; the gas temperature may be approximated by an isentropic path, and the neck-wall metal is rapidly cooled with the simultaneous existence of large temperature gradients. Case B is typical of a slow depressurization; the gas and neck wall temperatures decrease and pass through a minimum; no appreciable radial temperature gradient exists in the neck wall. Runs slower than B would show progressively smaller temperature drops until the isothermal path is reached. Runs faster than A would yield gas temperatures as in A but smaller temperature drops in the neck wall due to the shorter time of blowdown. The temperature gradient in the inside fibers of the neck wall would be larger, due to the higher heat-transfer coefficient in the gas phase.

It is probable that a run at a somewhat slower blowdown rate than A but higher than B would result in the lowest average neck wall temperature. The gas temperature would deviate only slightly from an isentropic path, and the increased time of contact between neck wall and cold gas could lead to a lower average neck temperature than either A or B.

From this discussion, it is clear that there is a possibility of rapid cooling of the neck of a high-pressure gas storage cylinder during rapid depressurizations. The induced stresses and the possibility of brittle fracture, as discussed in the next section, should be investigated before any cylinder is put into a service requiring a rapid blowdown of the bottle.

K. THERMAL STRESS ANALYSIS

1. Basic Theory

The present discussion is confined to a plane stress analysis of the bottle wall neck, except where stated to the contrary; Timoshenko(4) has reported the plane strain solution.

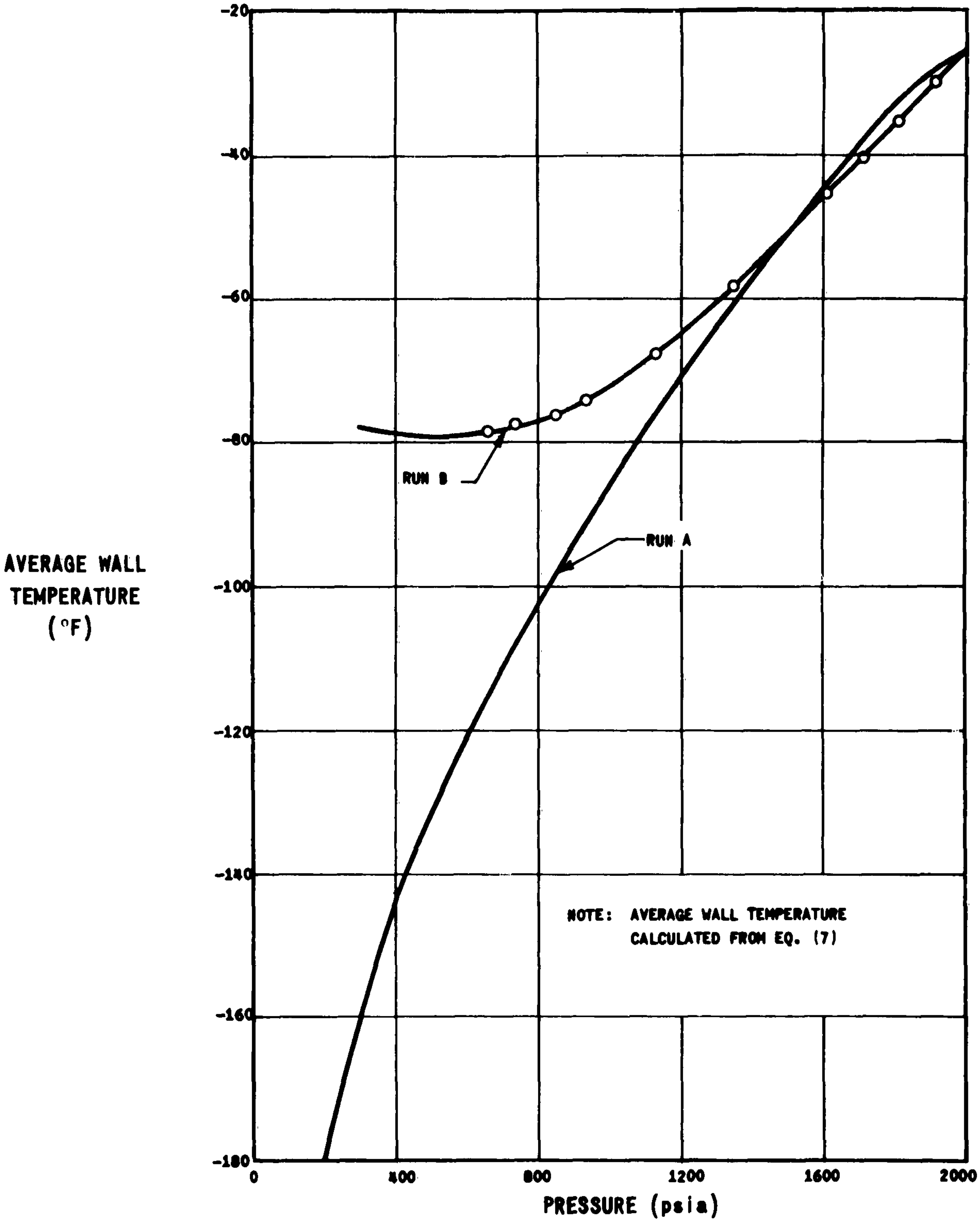

FIGURE 3.9 Average Neck Wall Temperatures for Large Bottle Blowdowns $T_{N_0} = -25°F$

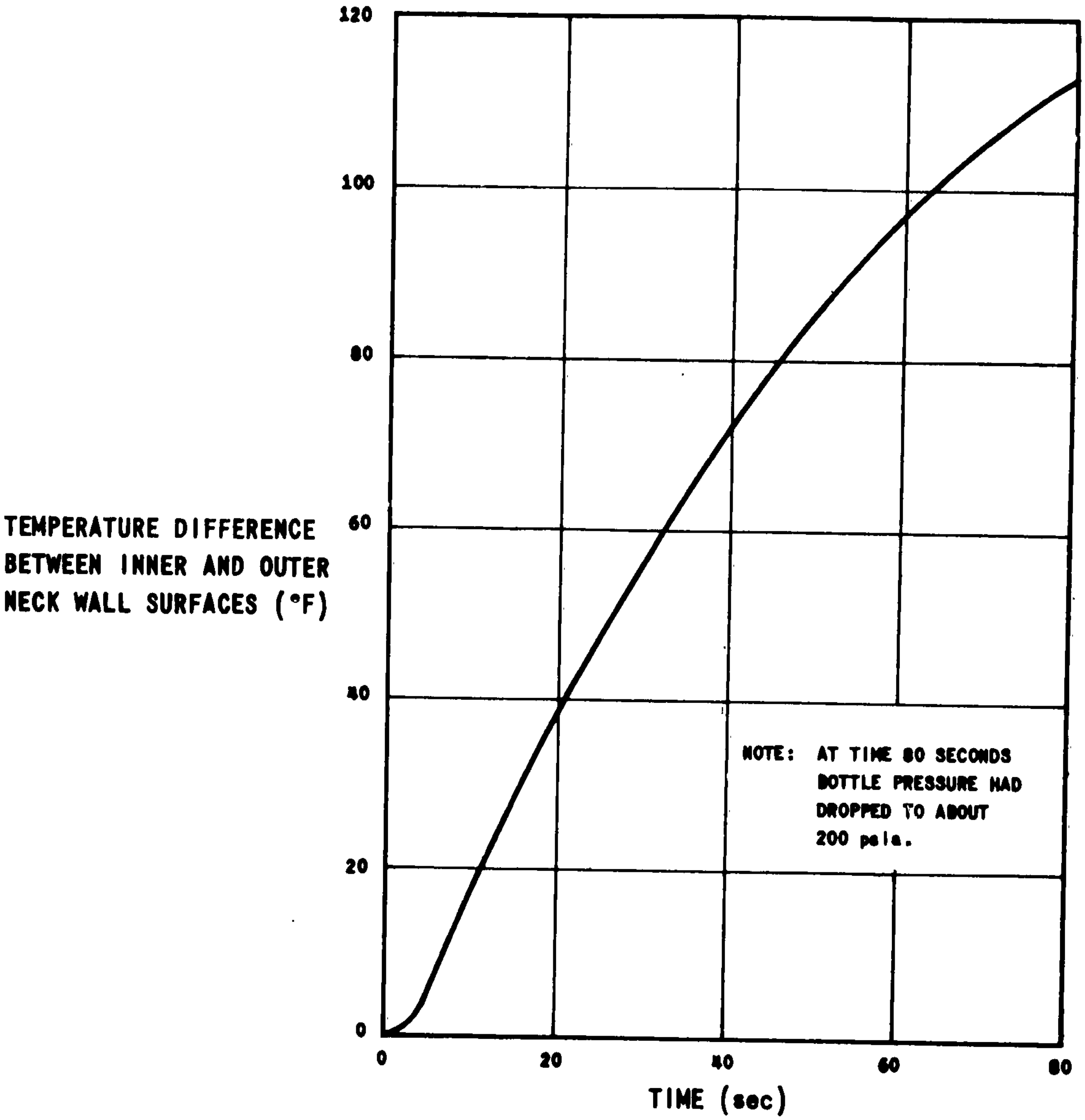

FIGURE 3.10 Temperature Difference Between Inner and Outer Neck Wall for Case A

Let σ_r and σ_t be the radial and tangential stresses in polar coordinates, positive when tensile, and let r be the radial coordinate. Assume that σ_r and σ_t are principal stresses, and that they are independent of all coordinates except r. In the absence of body forces the equilibrium equation is

$$\frac{d}{dr}(\sigma_r r) - \sigma_t = 0 \tag{8}$$

If the third principal stress (the axial stress) is zero, then the statement of Hooke's law is

$$\frac{du}{dr} = \frac{1}{E}(\sigma_r - \nu\sigma_t) + \alpha T \tag{9a}$$

$$\frac{u}{r} = \frac{1}{E}(\sigma_t - \nu\sigma_r) + \alpha T \tag{9b}$$

Upon elimination of u, eqs. (9) reduce to:

$$\frac{d^2}{dr^2}(\sigma_t - \nu\sigma_r) + \frac{1+\nu}{r}(\sigma_t - \sigma_r) + E\alpha\frac{dT}{dr} = 0 \tag{10}$$

Upon substitution for σ_t from eq. (8), eq. (10) becomes:

$$\frac{d^2}{dr^2}(\sigma_r r) + \frac{d\sigma_r}{dr} + E\alpha\frac{dT}{dr} = 0 \tag{11}$$

The general solutions of eqs. (8) and (11) are:

$$\sigma_r = K_1 + \frac{K_2}{r^2} - \frac{E\alpha}{r^2}\int_{r_1}^{r} Tr\,dr \tag{12a}$$

$$\sigma_t = K_1 - \frac{K_2}{r^2} + \frac{E\alpha}{r^2}\int_{r_1}^{r} Tr\,dr - E\alpha T \tag{12b}$$

After substitution for σ_r and σ_t from eqs. (12), eq. (9b) reduces to:

$$u = \frac{r}{E}\left[(1 - \nu)K_1 - (1 + \nu)\frac{K_2}{r^2}\right] + \frac{(1 + \nu)\alpha}{r}\int_{r_1}^{r} Tr\, dr \qquad (13)$$

K_1, K_2 and r_1 are constants of integration.

2. Infinite Plate with Hole--Thermal Transient

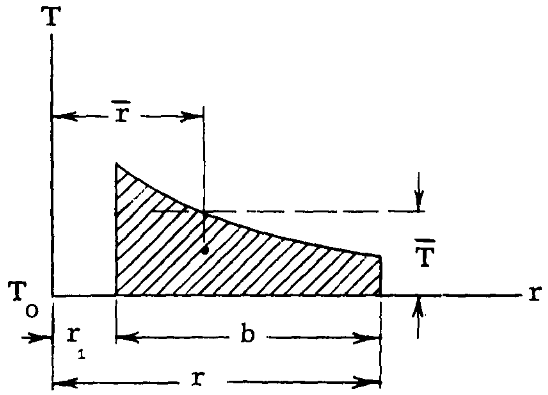

Let an infinite plate with a hole initially be at uniform temperature, T_O, and subsequently let heat flow across the boundary of the hole. Assume either that there is no heat flow across other boundaries of the plate, or that such heat flow, if it does occur, tends to restore the temperature to its initial value.

After heat has begun to flow, the temperature curve might appear as shown above where r_1 is the radius of the hole. The integral appearing in eqs. (12) and (13) is the moment about the T axis of the crosshatched area and could be written

$$\int_{r_1}^{r} Tr\, dr = \bar{T}\, b\, \bar{r}$$

where

$$\int_{r_1}^{r} T\, dr = \bar{T}\, b$$

$$b = (r - r_1)$$

$\overline{T}$ is the arithmetic average temperature in the interval b, and $\overline{r}$ the distance to the center of gravity of the crosshatched area. Eq. (13) can be written:

$$u = \frac{r}{E}\left[(1 - \nu) K_1 - (1 + \nu)\frac{K_2}{r^2}\right] + (1 + \nu)\,\alpha\frac{\overline{T}b\overline{r}}{r} \tag{14}$$

Assume that $\overline{T}b\overline{r}$ approaches a finite limit as r approaches infinity. This is a reasonable assumption, at least for a finite time after the beginning of heat flow. Under this limitation the last term in eq. (14) approaches zero as r approaches infinity.

As limiting conditions, the boundary of the hole is unloaded ($\sigma_r = 0$ when $r = r_1$), and the radial displacement is bounded at infinity (u does not approach infinity as $\overline{r}$ approaches infinity). Eq. (14), then, requires that $K_1 = 0$, and eq. (12a) requires that $K_2 = 0$, since

$$\int_{r_1}^{r} Tr\,dr = 0 \text{ when } r = r_1$$

Eqs. (12) and (13) become:

$$\sigma_r = -E\,\alpha\overline{T}\,\frac{b\overline{r}}{r^2} \tag{15a}$$

$$\sigma_t = E\alpha\left(\overline{T}\,\frac{b\overline{r}}{r^2} - T\right) \tag{15b}$$

$$u = (1 + \nu)\,\alpha\overline{T}\,\frac{b\overline{r}}{r} \tag{15c}$$

Note that at the boundary of the hole ($r = r_1$),

$$\sigma_r = u = 0 \tag{16a}$$

$$\sigma_t = -E\,\alpha\,T_1 \tag{16b}$$

where T_1 is the difference between the temperature at the boundary of the hole and where $\overline{r}$ approaches infinity.

3. Finite Circular Plate with Hole

Let r_1 and r_2 be the inner and outer radii, respectively, and let the surface loads be zero at the two boundaries (σ_r = 0 when $r = r_1$ or r_2). The solutions are:

$$\frac{\sigma_r}{E\alpha} = \frac{(r^2 - r_1^2)}{(r_2^2 - r_1^2)r^2}\int_{r_1}^{r_2} Tr\,dr - \frac{1}{r^2}\int_{r_1}^{r} Tr\,dr \tag{17a}$$

$$\frac{\sigma_t}{E\alpha} = \frac{(r^2 + r_1^2)}{(r_2^2 - r_1^2)r^2}\int_{r_1}^{r_2} Tr\,dr + \frac{1}{r^2}\int_{r_1}^{r} Tr\,dr - T \tag{17b}$$

$$\frac{u}{\alpha r} = \frac{(1 - \nu)r^2 + (1 + \nu)r_1^2}{(r_2^2 - r_1^2)r^2}\int_{r_1}^{r_2} Tr\,dr + \frac{1 + \nu}{r^2}\int_{r_1}^{r} Tr\,dr \tag{17c}$$

To verify eqs. (17) it is necessary merely to see that the expression for σ_r satisfies the boundary conditions and that the equations are obtained from eqs. (12) and (13) with:

$$K_1 = \frac{1}{(r_2^2 - r_1^2)}\int_{r_1}^{r_2} Tr\,dr$$

$$K_2 = \frac{r_1^2}{(r_2^2 - r_1^2)}\int_{r_1}^{r_2} Tr\,dr \tag{18}$$

Let $\bar{T}$ be the average temperature throughout the plate, and $\bar{r}$ the radial coordinate of the center of gravity of the area under the temperature curve (these definitions are similar to those for the infinite plate, except that they are in terms of the fixed interval $(r_2 - r_1)$ instead of the variable interval b. Also, let

$$r_m = \frac{r_1 + r_2}{2} \tag{19}$$

Then,

$$\frac{1}{(r_2^2 - r_1^2)}\int_{r_1}^{r_2} Tr\ dr = \frac{\overline{Tr}}{2r_m} \tag{20}$$

At both boundaries the tangential stress and radial displacement can be written

$$\sigma_t = E\alpha\,(\frac{\overline{Tr}}{r_m} - T) \tag{21a}$$

$$u = \frac{\alpha\overline{Tr}}{r_m}\ r \tag{21b}$$

All terms in eqs. (21) are constants, except T and r. The latter are the temperature and radius of the inner or outer boundary, as the case may be.

4. Thermal Shock

Suppose a cold fluid be introduced into a pipe that, initially, is at a uniform temperature of T_0. The ratio $\bar{r}/r_m$ will always be less than unity, even for thin-wall pipe. The average temperature $\bar{T}$ will be very small for a short time immediately following introduction of the cold liquid, and the tangential stress at the inner surface, as given by eq. (21a), will be approximately

$$\sigma_t = E\,\alpha\,T$$

during this short time. In other words, the thermal stress, $- E\,\alpha T$, corresponding to full restraint is closely approached for a short time. In the case of an infinitely thick cylinder the stress is precisely $- E\,\alpha T$, and this value persists throughout finite time. For a plane strain analysis:

$$\sigma_t = -\,(\frac{E\,\alpha\,T}{1 - \nu}) \tag{22}$$

Eq. (22) is more realistic for the case under consideration. Intuition suggests that eq. (22) would be applicable in cases when the cooled (or heated) region is a boundary layer whose thickness is small compared to the thickness of the body. Eq. (22) also provides an upper bound. These comments are believed to express sound engineering rules. Certainly they are not rigorous mathematical statements, and exceptions probably can be contrived.

L. BOTTLE NECK STRESSES DURING BLOWDOWN

Thermal stresses have been calculated for Run A at 10, 30, 60 and 80 seconds after start of blowdown. This run was the hypothetical case wherein a large bottle was allowed to blow down as shown in Figures 3.8 and 3.9. In each case the maximum stress is the tangential stress at the inner wall. Eq. (21a) was corrected for a plane strain case:

$$\sigma_{t_1} = \frac{E\,\alpha}{1 - \nu}\left(\frac{\overline{Tr}}{r_m} - T_1\right) \qquad (23)$$

was used. $\overline{T}$ and $\overline{r}$ were obtained from the calculated curves for temperature through the bottle neck wall. The subscript "1" refers to the inner surface. Data for this bottle were taken to be:

$E = 30 \times 10^6$ psi

$\nu = 0.3$

$\alpha = 7 \times 10^{-6}$ in./in.-°F

$r_1 = 1.188$ in.

$r_2 = 2.988$ in.

$r_m = 2.088$ in.

M. CONCLUSIONS

The thermal stresses in Table 3.1 indicate that when stresses due to pressure are superimposed on the thermal stresses, the resultant total stresses may well be excessive for certain commonly used structural steel materials when allowance is made for unknown stress concentrations. For the conditions assumed in the above calculations, steel that retains its ductility at low temperature should be used for the material of construction to avoid the problem of low-temperature embrittlement. AISI - 4130X is now used in the manufacture of large gas bottles for the pressurized transfer of cryogenic liquids. For an ambient temperature below 0°F, our calculations indicate that certain blowdown schedules would cause a temperature stress condition in the neck wall of the bottle that could lead to failure of this material because of low-temperature embrittlement. For this reason we believe that a 2% nickel alloy steel, such as AISI - 4340, should be used for such conditions.

TABLE 3.1

TEMPERATURE DATA AND MAXIMUM STRESS IN BOTTLE NECK DURING BLOWDOWN

Time (Sec)	$\bar{T}$ (°F above -25°F)	T_1 (°F above -25°F)	$\bar{T}\frac{\bar{r}}{r_m} - T_1$ (°F)	σt_1 (psi)
10	- 2.9	- 16.0	14.0	4, 200
30	-27.8	- 57.1	36.4	10, 900
60	-48.5	-103.6	62.0	18, 600
80	-63.0	-124.7	69.9	21, 000

No universally accepted method is developed for the selection of materials to meet low-temperature service requirements. The ASME Boiler Construction Code for Unfired Pressure Vessels and ASTM Specifications require that the steel must meet a minimum of 15 ft-lb Charpy, keyhole notch, at minimum service temperature. AISI - 4340 would be acceptable on this basis at temperatures reaching as low as -140°F.

N. REFERENCES

1. Reynolds, W. C., and Kays, W. M., "Blowdown and Charging Processes in a Single Gas Receiver with Heat Transfer," Trans. ASME, Vol. 80, No. 5 (July 1958).

2. Potter, J. H., and Levy, M. J., "The Free Expansion of Dry and Moist Air," Paper No. 60-SA-23, Trans. ASME, Series B, Journal of Engineering for Industry, Vol. 83, No. 1, p. 97 (February 1961).

3. McAdams, W. H., Heat Transmission, McGraw-Hill Book Company, Inc., New York, 3rd Ed. (1954).

4. Timoshenko, S., Strength of Materials, D. van Nostrand, Princeton, N. J. (1955).

IV. THE TRANSFER OF HYDROGEN USING VAPORIZERS

A. SUMMARY

Theoretical analyses were completed to determine the performance of two types of vaporizer systems for transferring liquid hydrogen: 1) a regenerative system, in which a fraction of the liquid in the storage vessel is vaporized and superheated (by exchanging heat with ambient air) and returned to pressurize the ullage volume of the storage vessel, and 2) a system in which liquid stored in an auxiliary storage vessel is vaporized and superheated (also, by exchanging heat with the ambient air) and used to pressurize the ullage volume of the main storage vessel. In addition to the theoretical studies, an experimental program was conducted to support the analyses and to determine the operating characteristics of each system.

The results of the analyses and experiments indicate that either system is feasible for transferring large quantities of liquid hydrogen, and that little difference in vaporizer size, operating characteristics, etc., exists between the two systems. The choice between the systems would primarily be dictated by the economics of the over-all transfer system, as discussed in Section V following.

B. NATURAL CONVECTION REGENERATIVE VAPORIZER SYSTEM WITH SUPERHEAT

1. Introduction

A common method for transferring liquid hydrogen from a storage vessel is to vaporize a fraction of the liquid and to utilize the vaporized fraction to pressurize the ullage volume of the storage vessel. One simple and reliable system that has been used in both stationary and mobile storage units consists of an external vaporizer loop, in which the liquid is vaporized by the natural convection of atmospheric air. In a regenerative system the vaporizer is placed below the storage vessel, and the head of liquid in the tank is used to force the liquid being vaporized through the vaporizer and into the ullage volume. A schematic diagram illustrating a typical self-pressurizing regenerative system is shown in Figure 4.1.

In Reference 1 the operation, costs, and design aspects of a natural convection, regenerative system were discussed for a vaporizer configuration that discharged saturated vapor into the ullage volume. In the following discussion we will consider a vaporizer system that is similar but has the ability to discharge superheated vapor into the ullage volume. In addition, the results of a test program designed to determine experimentally the operating characteristics of a typical regeneratively pressurized transfer system will be presented and the results compared with a theoretical analysis of the transfer process.

2. Nomenclature

A_i = vaporizer tube inside cross sectional area

A = vaporizer tube inside surface area

A_s = outside surface area of finned tubing

C_p = specific heat of hydrogen

D = inside tube diameter

f = friction factor

g = local acceleration of gravity

h_o = tube outside surface coefficient of heat transfer

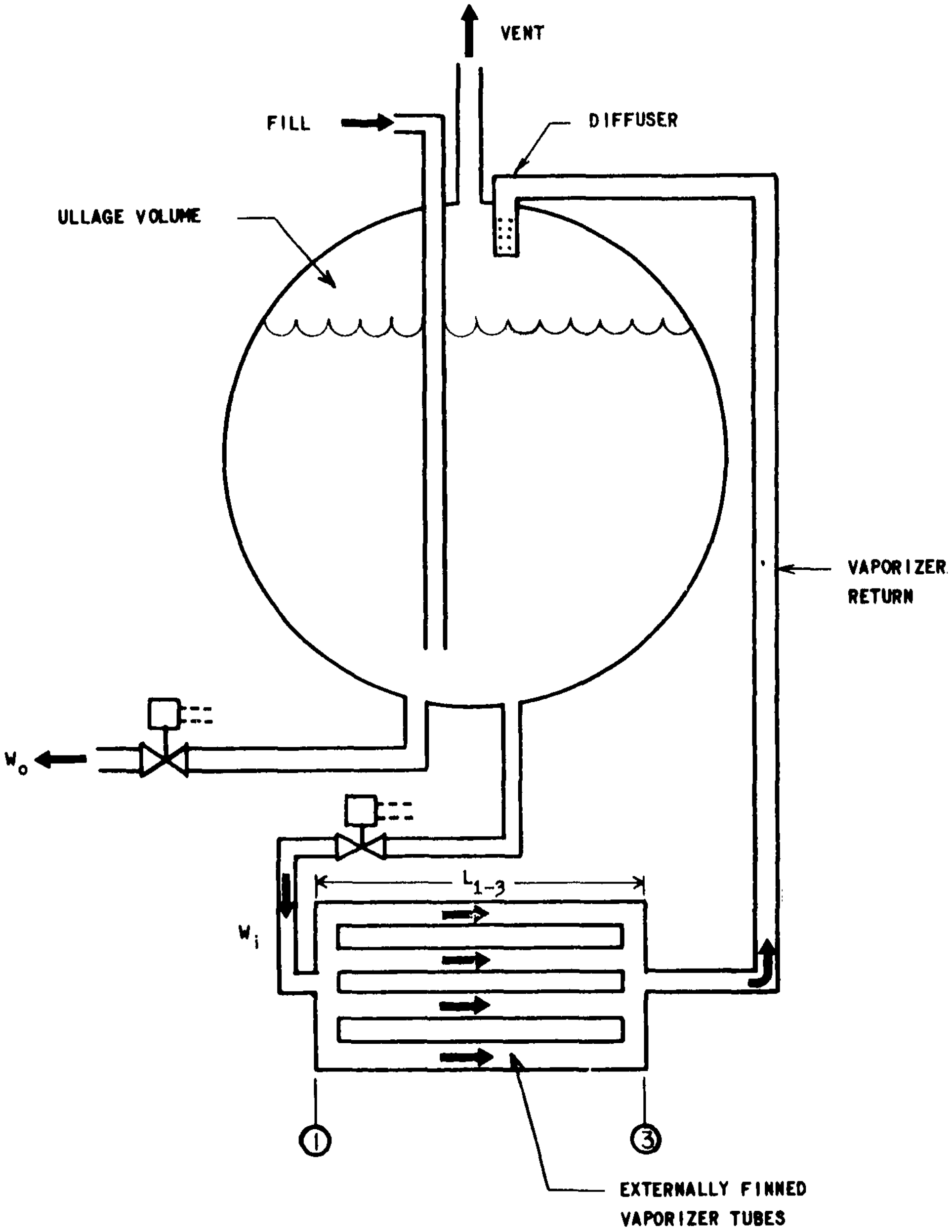
VENT
FILL
DIFFUSER
ULLAGE VOLUME
VAPORIZER RETURN
W_o
W_i
L_{1-3}
①
③
EXTERNALLY FINNED VAPORIZER TUBES

FIGURE 4.1	Schematic Diagram of Regenerative Vaporizer System

Δh = enthalpy change of hydrogen
k = ratio of specific heats
L = tube length
M = Mach number
N = number of vaporizer tubes
P = pressure
q = heat flow
R = gas constant of hydrogen
T_a = ambient air temperature
T = hydrogen temperature
U = over-all coefficient of heat transfer
V = velocity
w = hydrogen mass flow rate
W_o = liquid hydrogen transfer rate
W_i = vaporizer total mass flow rate
x = increment of tube length
ρ = density of hydrogen
τ_w = wall shear stress
η_{FIN} = fin effectiveness

Subscripts

1 - refers to state of hydrogen at the vaporizer inlet
2 - refers to the saturated vapor state of the hydrogen in the vaporizer
3 - refers to the state of the hydrogen at the vaporizer exit
f - saturated liquid
g - saturated vapor
L - liquid
O - stagnation conditions

3. Theoretical Analysis

a. Analytical Model

Consider the flow of liquid "equilibrium" hydrogen in a finned-tube vaporizer whose configuration would be similar to one that would be used in a regeneratively pressurized transfer system. The heat is added to the liquid in the vaporizer by a natural-convection heat transfer process that occurs on the outer finned surfaces of the vaporizer tubes. Since the analytical model is restricted to a regeneratively pressurized system, it is assumed that the vaporizer will have an extremely low pressure drop.

It is desired to obtain analytical expressions for the vaporizer temperature rise and the static pressure drop in the vaporizer as a function of the hydrogen flow rate, vaporizer geometry, the static pressure, etc. A sketch of the model that will be used in the theoretical analysis is shown below.

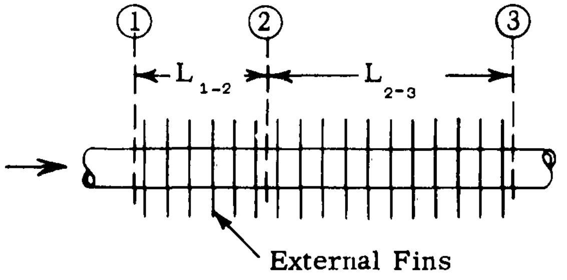

Liquid "equilibrium" hydrogen enters the vaporizer tube at (1). It is assumed that the storage vessel is filled at atmospheric pressure with saturated liquid; therefore, when the vessel is pressurized, the liquid enters at (1) in a sub-cooled state. Between points (1) and (2) sufficient heat is added to the hydrogen from the ambient air to produce saturated vapor. Additional heat is added to the hydrogen between (2) and (3) to produce a stream of superheated gas. This superheated gas is returned to the storage vessel to pressurize it. Two further assumptions are made: 1) the static pressure drop in the vaporizer is small with respect to the average static pressure, i.e., less than 0.5% of the static pressure, and 2) the mass flow through the vaporizer after "cooldown" is maintained constant by a control valve in the vaporizer supply line.

The pressure-enthalpy diagram shown on the following page indicates the thermodynamic state of the hydrogen flowing in the vaporizer. From the diagram it can be seen that the heat transfer processes that occur in the vaporizer are characterized by heat transferred in a subcooled region, by heat transferred in a two-phase flow region, and by heat transfer to a single-phase superheated gas.

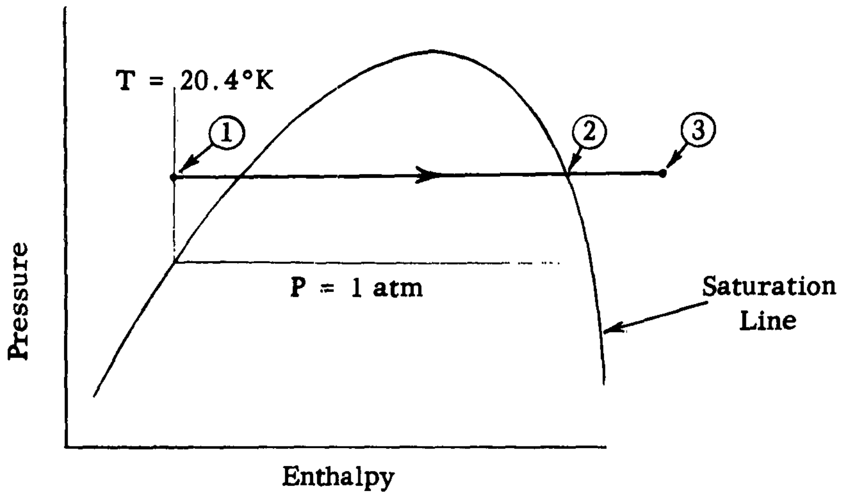

b. Calculation of Vaporizer Temperature Rise

The heat flux between points 1 and 2 is related to the mass flow by the expression

$$q_{1-2} = w \ (\Delta h)_{1-2} \tag{1}$$

By definition

$$A_{1-2} = \pi D \ L_{1-2} \tag{2}$$

From continuity, for steady flow and a constant-area tube,

$$w = \rho A_i V = \frac{\pi}{4} D^2 \ \rho_1 \ V_1 \tag{3}$$

Combining eqs. (1), (2) and (3) yields an expression for the length required to vaporize the entering liquid:

$$L_{1-2} = \frac{\rho_1 \ V_1 \ D \ \Delta h_{1-2}}{4 \ (\bar{q}/A)_{1-2}} \tag{4}$$

Here it is assumed that the heat flux can be represented by a mean value.

A similar expression is obtained for section between 2 and 3, by applying the energy equation and assuming that kinetic energy changes are negligible. For an incremental portion of the tube length the energy equation yields

$$w\,\bar{C}_{p_{2-3}}\,dT = \bar{U}_{2-3}\,\pi\,D\,(T_a - T)\,dx \tag{5}$$

Combining eqs. (3) and (5), and integrating between the proper limits, yields the following expression for the length required to superheat the gas:

$$L_{2-3} = \frac{\rho_1 V_1 D \bar{C}_{p_{2-3}}}{4\,\bar{U}_{2-3}} \ln\left(\frac{T_a - T_2}{T_a - T_3}\right) \tag{6}$$

In eq. (6) $\bar{U}_{2-3}$ and $\bar{C}_{p_{2-3}}$ represent mean values for the over-all coefficient of heat transfer and the specific heat of the hydrogen.

The total length of the vaporizer required to vaporize the entering liquid and raise it to an exit temperature T_3 is therefore

$$L_{1-3} = L_{1-2} + L_{2-3} = \frac{\rho_1 V_1 D\,\Delta h_{1-2}}{4\,(\bar{q}/A)_{1-2}} + \frac{\rho_1 V_1 D \bar{C}_{p_{2-3}}}{4\,\bar{U}_{2-3}} \ln\left(\frac{T_a - T_2}{T_a - T_3}\right) \tag{7}$$

Rearranging eq. (7) and utilizing eq. (3) results in the following expression relating the vaporizer exit temperature to the vaporizer mass flow:

$$T_3 = T_a + (T_2 - T_a)\exp\left[\frac{\bar{U}_{2-3}}{\bar{C}_{p_{2-3}}}\left(\frac{\Delta h_{1-2}}{(\bar{q}/A)_{1-2}} - \frac{4\,L_{1-3}}{D\,w/A_i}\right)\right] \tag{8}$$

The values of the vaporizer exit temperature as a function of the mass flow per unit area calculated from eq. (8) are shown in Figure 4.2. The effects of several variables on the vaporizer temperature are shown in Figure 4.3. It is important to note that the static pressure does not influence the exit temperature significantly.

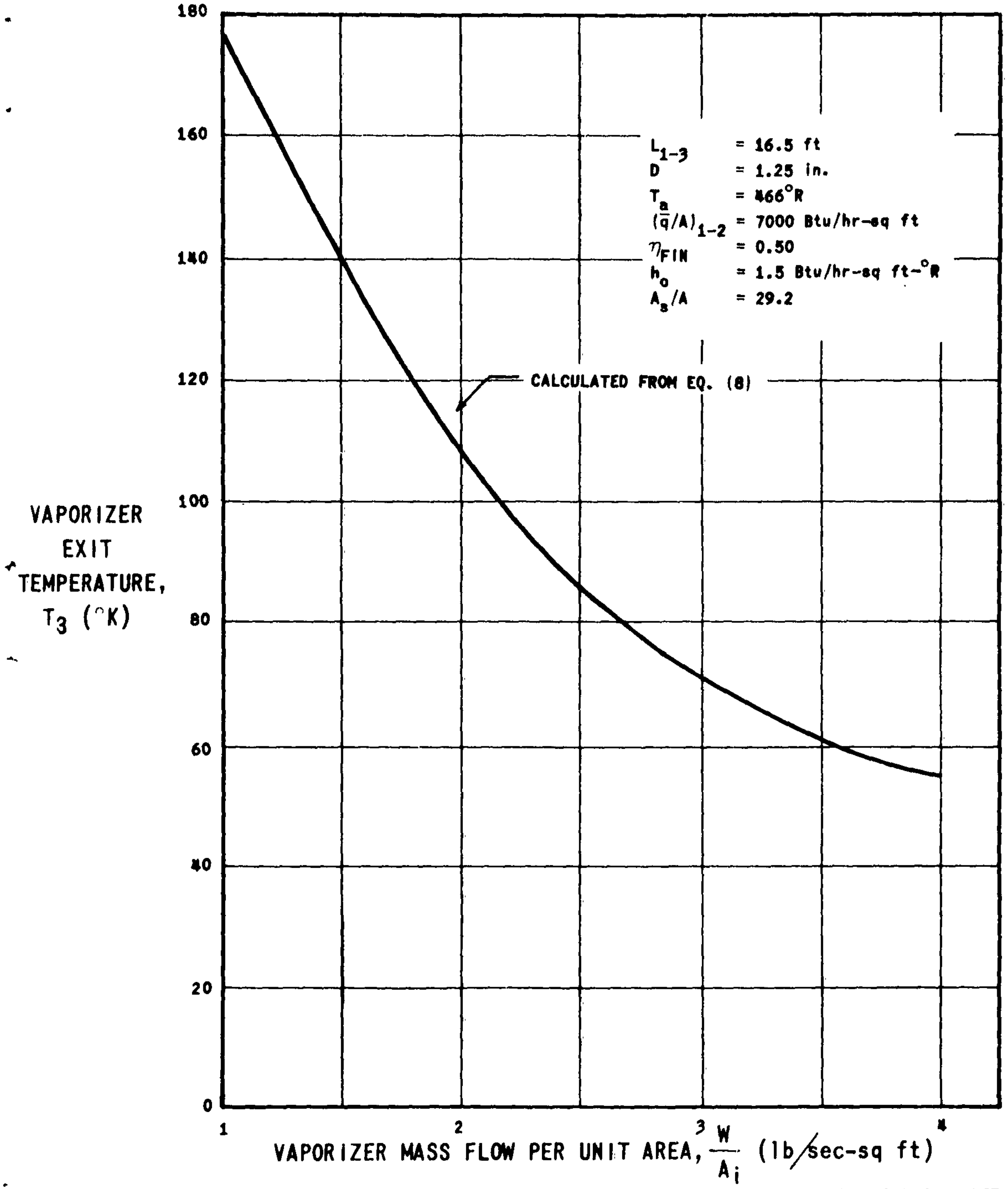

FIGURE 4.2 Vaporizer Temperature Rise Characteristics

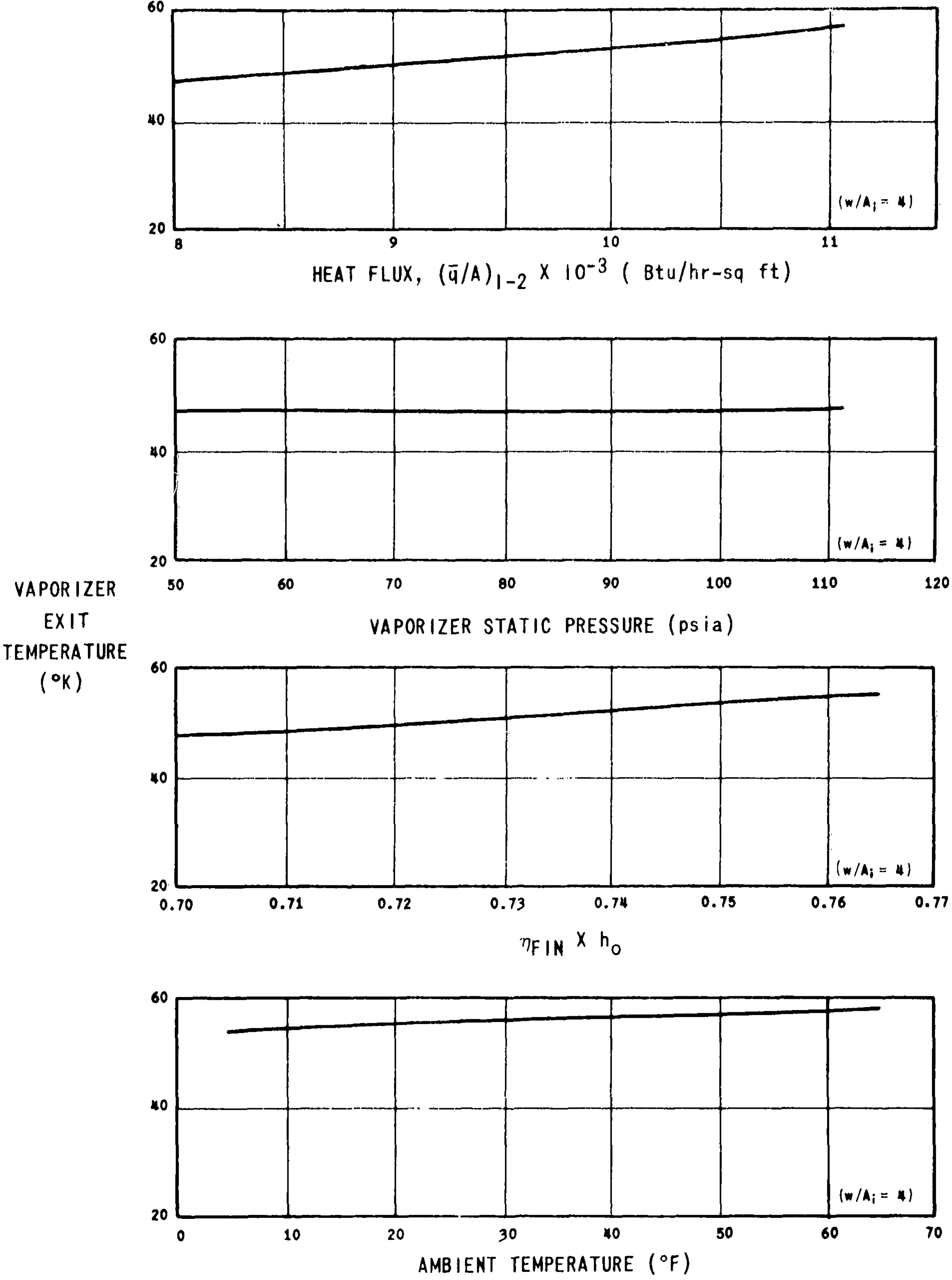

FIGURE 4.3 Influence of Several Variables on Vaporizer Exit Temperature

The following tube geometry and assumptions pertain to the analytical results shown in Figures 4.2 and 4.3:

L_{1-3}	-	vaporizer length	16.5 ft
D	-	vaporizer tube ID	1.25 in.
A_S/A	-	area ratio of surface to inside	29.2
T_a	-	ambient air temperature	466°R
$(\bar{q}/A)_{1-2}$	-	heat flux in subcooled and two-phase flow region	7000 Btu/hr-sq ft
η_{FIN}	-	fin effectiveness of vaporizer	0.50
h_o	-	outside free-convection heat transfer coefficient	1.5 Btu/hr-sq ft-°F
Δh_{1-2}	-	enthalpy change from subcooled liquid to saturated vapor	208 Btu/lb

The above values of $(\bar{q}/A)_{1-2}$, η_{FIN} and h_o were chosen as representative of what one might expect in an externally finned vaporizer. Reference 1 gives a detailed discussion of the heat transfer characteristics of hydrogen in the boiling regime.

c. Calculation of Vaporizer Pressure Drop

In this calculation it is assumed that the pressure drop in the vaporizer from states (1) to (2) is determined by the two-phase flow pressure drop. The pressure drop in the two-phase flow region has been analyzed in Reference 1 and is given by:

$$\Delta P_{1-2} = 4 f \frac{L_{1-2}}{D} \frac{\rho_1}{\rho_2} \frac{\rho_1 V_1^2}{2g} + \left(\frac{\rho_1}{\rho_2} - 1 \right) \frac{\rho_1 V_1^2}{g} \tag{9}$$

The pressure drop in the superheated region (2-3) will now be derived for a steady mass flow with heat addition and friction in a constant-area tube. Consider the control volume shown on the following page. For steady flow, constant molecular weight and constant specific heat, the static pressure variation as a function of tube length and total temperature can be written as shown in eq. (10) (see Reference 2).

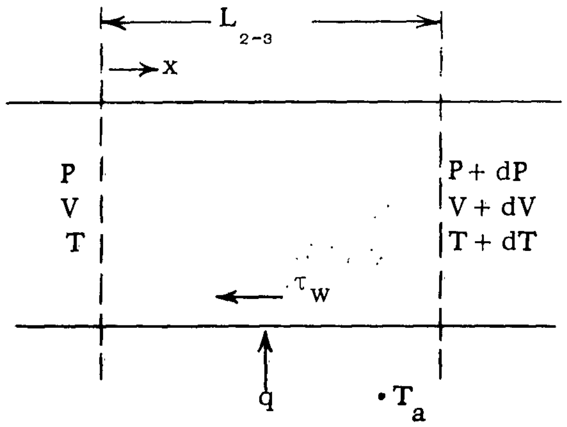

$$\frac{dP}{P} = -kM^2 \left(\frac{1 + \frac{k-1}{2} M^2}{1 - M^2} \right) \left(\frac{d\,T_o}{T_o} \right) - \frac{kM^2}{2} \left(\frac{1 + (k-1)\,M^2}{1 - M^2} \right) \left(\frac{4f\,dx}{D} \right) \qquad (10)$$

where the Mach number, friction factor, and total temperature are defined as

$$M \equiv \frac{V}{\sqrt{kg\ RT}} \qquad (11)$$

$$f \equiv \frac{\tau_w}{\rho V^2/2g} \qquad (12)$$

$$T_o \equiv T\left(1 + \frac{k-1}{2} M^2\right) \qquad (13)$$

For low Mach numbers ($M \leq 0.1$) the total temperature is approximately equal to the static temperature, and the terms in brackets in eq. (10) assume a value of approximately one. With the restriction that the local Mach number never exceeds 0.1, eqs. (10) and (13) can be combined to yield the following expression:

$$\frac{dP}{P} = -kM^2 \left(\frac{dT}{T}\right) - \frac{kM^2}{2} \left(\frac{4\,f\,dx}{D}\right) \qquad (14)$$

As stated earlier, the energy equation is

$$w \bar{C}_{p_{2-3}} \; dT = \bar{U}_{2-3} \; \pi D \; (T_a - T) \; dx \tag{5}$$

By definition

$$\alpha \equiv \frac{\bar{U}_{2-3} \; \pi D}{w \; \bar{C}_{p_{2-3}}} \tag{15}$$

Integrating eq. (5) and using eq. (15) yields an expression for the temperature variation as a function of tube length:

$$T = T_a + (T - T_2) \; e^{-\alpha x} \tag{16}$$

Also, by use of integral relationships it can be shown that

$$M^2 = \left(\frac{P_{o_2}}{P_o}\right)^2 \left(\frac{T_o}{T_{o_2}}\right) \left(\frac{1 + \frac{k-1}{2} M^2}{1 + \frac{k-1}{2} M_2^2}\right) M_2^2 \tag{17}$$

Eq. (17) becomes the following expression if the Mach numbers are low:

$$M^2 = \left(\frac{P_2}{P}\right)^2 \left(\frac{T}{T_2}\right) M_2^2 \tag{18}$$

When eqs. (5), (10), (15), (16) and (18) are combined, the following differential equation is obtained for the static pressure change as a function of tube length:

$$\frac{P\,dP}{P_2^2} = -kM_2^2 \left(\frac{T_a}{T_2}\right) \left[\left(\frac{T_a - T_2}{T_a}\right)\left(\alpha - \frac{4f}{2D}\right) e^{-\alpha x} \; dx + \frac{4f\,dx}{2D}\right] \tag{19}$$

Integrating eq. (19) between the limits

$$x = 0,\ P = P_2 \text{ and } x = L_{2-3},\ P = P_3$$

yields

$$\frac{P_3^2}{P_2^2} = 1 - 2\,kM_2^2 \left(\frac{T_a}{T_2}\right)\left[\left(\frac{T_a - T_2}{T_a}\right)\left(1 - \frac{2f}{\alpha D}\right)(1 - e^{-\alpha L_{2-3}}) + \frac{2f\,L_{2-3}}{D}\right] \qquad (20)$$

Using the definition of Mach number, the continuity equation (eq. 3) and the following equation of state

$$\rho_2 = \frac{P_2}{R\,T_2} \qquad (21)$$

an expression for M_2^2 is obtained

$$M_2^2 = \frac{(w/A_i)^2\ R\ T_2}{P_2^2\ k\ g} \qquad (22)$$

Combining eqs. (20) and (22), one obtains a general expression that can be used to calculate the static pressure change in a tube for low Mach numbers:

$$\frac{P_3^2}{P_2^2} = \frac{1 - 2\,(w/A_i)^2\ R\,T_a}{P_2^2\,g}\left[\left(\frac{T_a - T_2}{T_a}\right)\left(1 - \frac{2f}{\alpha D}\right)\left(1 - e^{-\alpha L_{2-3}}\right) + \frac{2f\,L_{2-3}}{D}\right] \qquad (23)$$

Note that if $\Delta P_{2-3} = P_2 - P_3$, and if one assumes that $\frac{\Delta P_{2-3}}{P_2} <<< 1.0$, eq. (23) becomes the expression shown below. (Second-order terms in Δ are neglected.)

$$\Delta P_{2-3} = (w/A_i)^2\,\frac{R\,T_a}{g\,P_2}\left[\left(\frac{T_a - T_2}{T_a}\right)\left(1 - \frac{2f}{\alpha D}\right)\left(1 - e^{-\alpha L_{2-3}}\right) + \frac{2f\,L_{2-3}}{D}\right] \qquad (23a)$$

The above expression can now be used to calculate the pressure drop in the superheat region of the vaporizer for a tube design in which the pressure drop is a small fraction of the average static pressure. It should be re-emphasized that the above equation was derived for a gas with constant specific heat, and one that obeyed the perfect gas law. These assumptions will introduce some inaccuracies in the calculated pressure drop; however, we believe that eqs. (23) and (23a) can be used for preliminary design purposes with a fair degree of confidence. For a final design it is suggested that a margin of safety be used in applying the calculated results.

The tube length between points 2 and 3 is obtained from (6).

$$L_{2-3} = \frac{(w/A_i)\, D\, \bar{C}_{p_{2-3}}}{4\, \bar{U}_{2-3}} \ln\left(\frac{T_a - T_2}{T_a - T_3}\right) \qquad (6a)$$

From eq. (9) one obtains the ΔP_{1-2} for a given pressure, heat flux and mass flow. Then, for a given length of vaporizer, an over-all coefficient of heat transfer, ambient temperature, etc., a numerical calculation using eqs. (6a) and (23a) yields the pressure drop between points 2 and 3. The total pressure drop in the tube from entrance to exit is the sum of ΔP_{1-2} and ΔP_{2-3}. The results of a calculation of the pressure-drop characteristics of the vaporizer configuration, described in the preceding section, are shown in Figure 4.4 for static pressures of 25, 50 and 100 psi.

d. Transfer Capabilities of a Regenerative Vaporizer System with Superheat

In Reference 1 a relationship was derived that related the transfer flow rate to the mass flow of pressurizing gas entering the ullage space, assuming that no heat transfer occurs between the ullage boundaries and the pressurizing gas. In addition, experimental results were presented for the quantity of external pressurizing gas (at room temperature) required to effect typical transfers; these results indicated that heat transfer did indeed occur and that the minimum pressurization gas requirements calculated from the "no heat-transfer model" were not applicable. However, one can reason that at lower pressurizing gas temperatures the calculated pressurizing gas requirements using the "no heat-transfer model" would become more accurate, because of the decrease in driving force for heat transfer between the pressurizing gas and the liquid surface. A basic vaporizer system will be designed assuming a "no heat-transfer model" and using the previous analytical results for the vaporizer temperature rise and pressure drop characteristics. The analytical estimates of the pressurizing gas requirements will be compared with the experimental results of a number of tests with a similar vaporizer system in a following section.

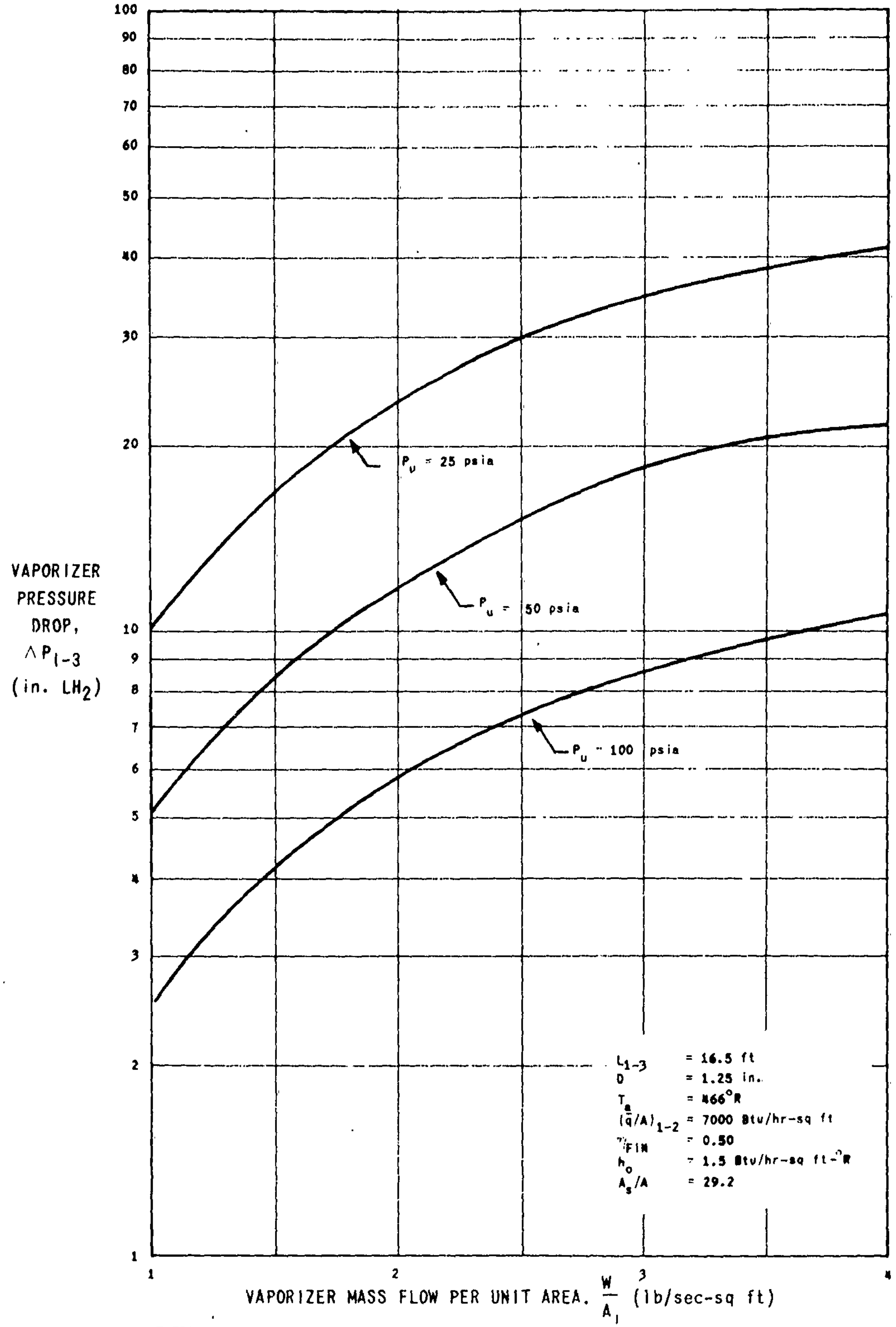

FIGURE 4.4 Vaporizer Pressure Drop Characteristics

The minimum pressurizing gas requirement for the system illustrated in Figure 4.1 is related to the transfer flow by the following expression:

$$\frac{W_i}{W_o} = \frac{1}{\frac{\rho_L}{\rho_T} - 1} \tag{24}$$

where ρ_L is the liquid density being transferred and ρ_T is the density of the vapor entering the ullage space from the vaporizer. If no heat is added and the pressure drop is small in the return line between the vaporizer exit and the ullage space, the density of the vapor entering the ullage volume will be equal to the vaporizer exit density. The ratio of liquid transfer rate to pressurizing gas flow is shown in Figure 4.5 as a function of the ullage pressure and pressurizing gas temperature. From Figure 4.5 it is seen that for a given ullage pressure and vaporizer flow rate, an increase in the vaporizer exit temperature increases the liquid transfer rate. Also, the capability of the vaporizer is increased as the transfer ullage pressure is decreased. However, in a transfer system the ullage pressure is fixed by the impedance in the transfer line and receiving vessel, and by the transfer flow rate.

Using the information presented in Figures 4.2 and 4.4, which relate the pressure drop and temperature rise characteristics of a specific vaporizer configuration to the mass flow rate in a vaporizer tube, and the transfer capabilities presented in Figure 4.5, one can design a "basic" vaporizer system that pressurizes an ullage volume with superheated gas. Manifolding a number of finned vaporizer tubes in parallel results in a system that could effect transfers at a given rate and pressure consistent with the capability curves shown in Figure 4.5.

4. Design of a Basic Vaporizer System with Superheat

Consider a regenerative vaporizer system similar to that illustrated in Figure 4.1. Liquid flows into the vaporizer by virtue of the liquid head in the storage vessel. A flow control valve is used in the vaporizer inlet to modulate the vaporizer flow for "off-design" operation. Assume the following tube geometry for design purposes:

L_{1-3} = 16.5 feet

D = 1.25 inches

A_S/A = 29.2

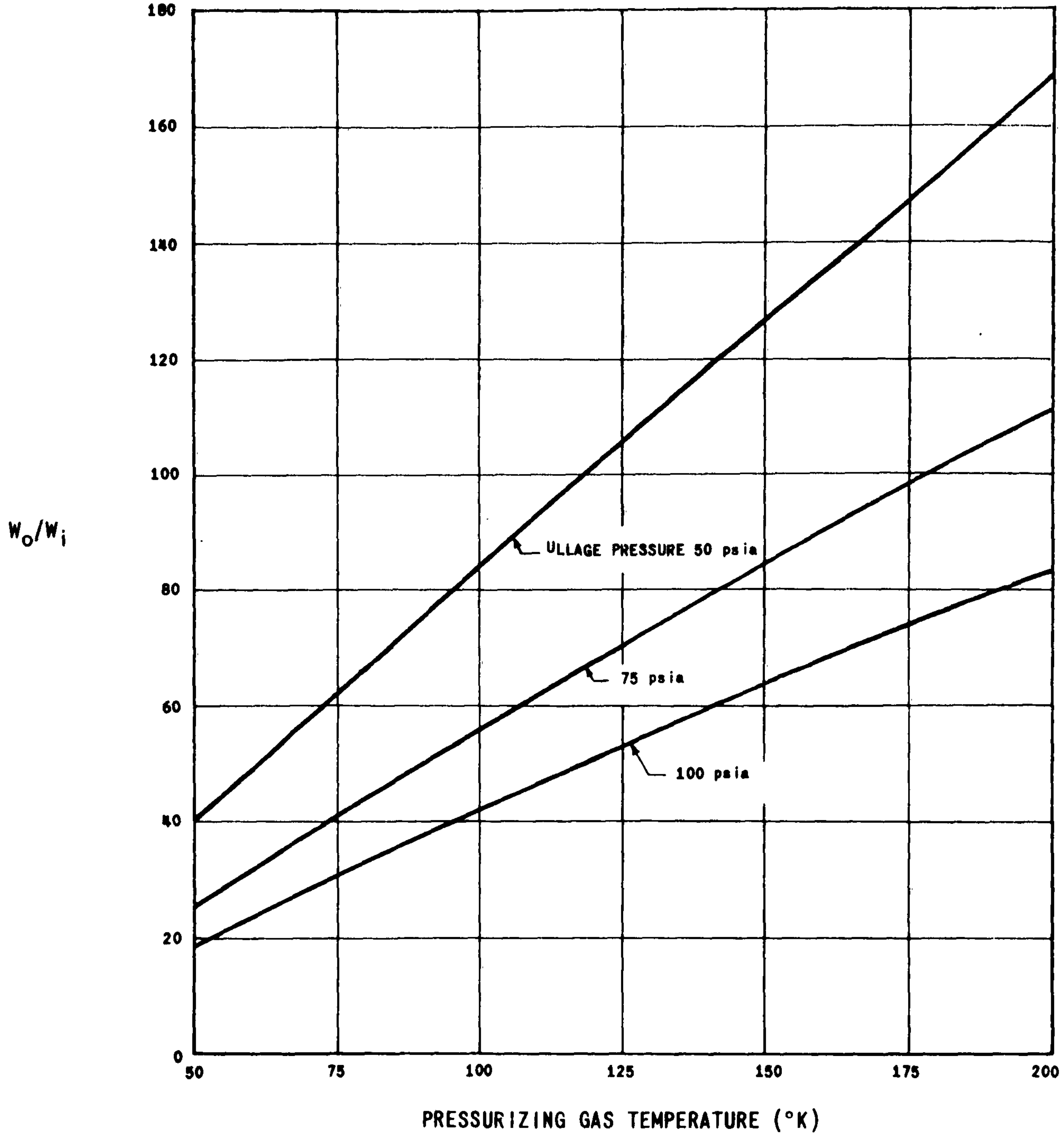

FIGURE 4.5 Maximum Theoretical Transfer Capabilities-- Regenerative System

To obtain this surface-to-inside area ratio, a tube with a linear fin spacing of 40 fins per foot and a rectangular fin 4-1/4 x 4-1/4 inches are required. Inexpensive, commercial finned tubing having the above dimensions is readily available as a stock item.

From the analytical results presented in Figures 4.2, 4.4 and 4.5 (for an identical vaporizer tube) an operating map of a single tube can be established for assumed values of ambient temperature, heat flux, etc. A map for this single tube is shown in Figure 4.6. The liquid transfer rate is shown plotted as a function of the pressure drop in the vaporizer for various ullage pressures. From Figure 4.6 it is seen that each curve has a maximum capability and that the vaporizer pressure drop associated with this maximum capability is a function of the ullage pressure.

If it is assumed that a reasonable maximum design operating pressure for a typical system would be approximately 100 psi, the maximum transfer rate per vaporizer tube (W_0/N) is shown in Figure 4.6 to be 82 gpm. A six-tube vaporizer with the tubes mounted in parallel would thus have a theoretical capability of 492 gpm. Allowing for frost buildup, etc., one could reasonably expect that under any conditions, the transfer rate would be approximately 450 gpm. For this rate the pressure drop in the vaporizer would have to be maintained at approximately six inches of liquid hydrogen by a control valve located in the vaporizer inlet line.

The inlet line size is governed by the vaporizer flow. For the basic six-tube vaporizer described, a two-inch vaporizer feed line would limit the pressure drop to less than five inches of LH_2 in a 20-foot section. There may be some question of the advisability in insulating the liquid feed line to the vaporizer, since it would increase the effective vaporizer area. However, to minimize the problems associated with the distribution of partially vaporized liquid in the vaporizer tubes, and to minimize the hazards of liquid air formation around the moving parts of the vaprozier control valve, it is suggested that the feed line be insulated.

The return line to the ullage space should be sized to have a pressure drop of the same order of magnitude as the vaporizer feed line. Since the density changes between the vaporizer inlet and outlet by a factor of 42, the ratio of feed to return line diameters for equal pressure drop would be

$$\sqrt[5]{\rho_L/\rho_T} = 2.1$$

A four-inch diameter return line would thus be appropriate for this design.

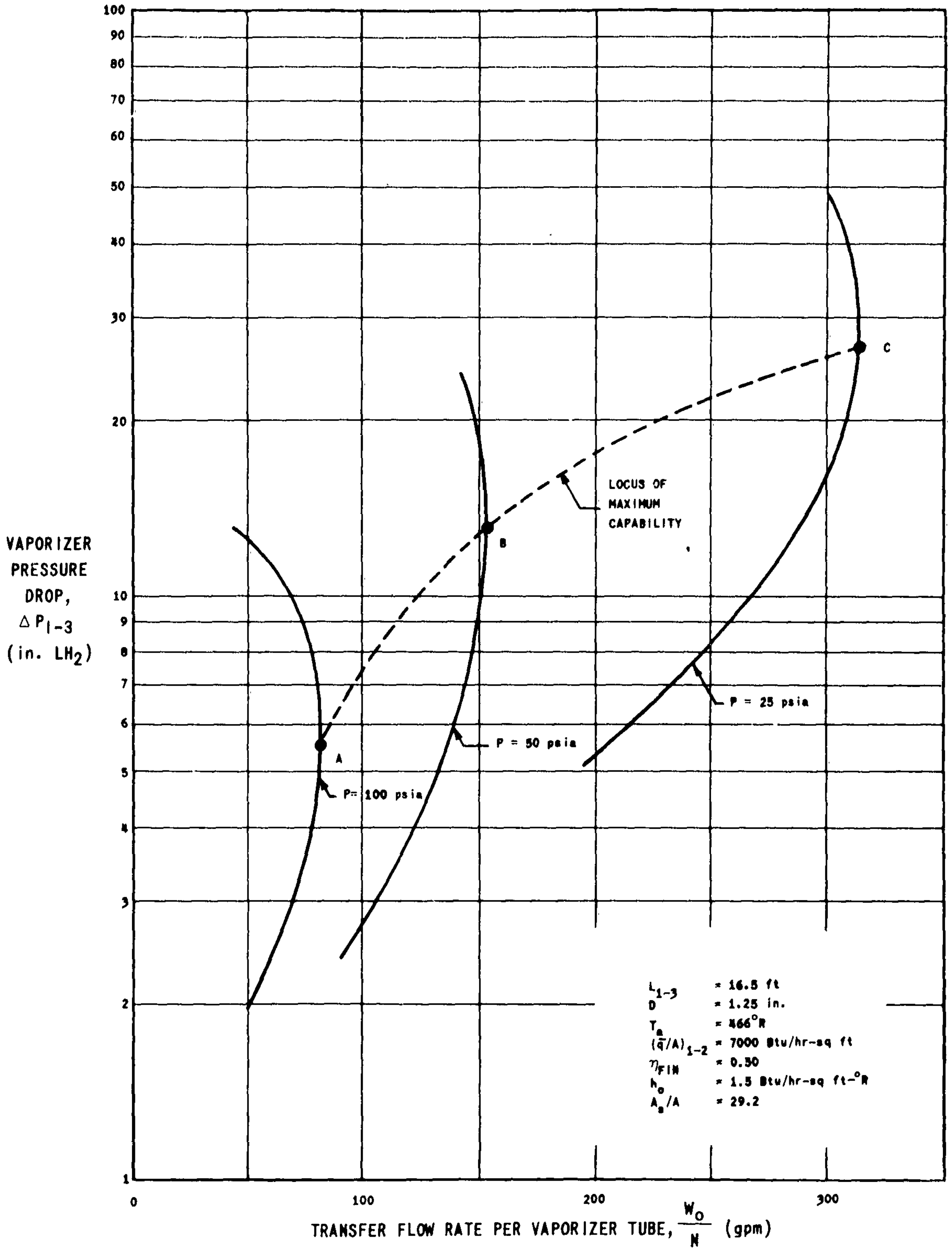

FIGURE 4.6 Vaporizer Operating Characteristics

The vaporizer configuration shown in Figure 4.7 might be considered a basic unit, with a transfer capability of 450 gpm, for the regeneratively pressurized system described. A multiple stack of these basic vaporizer units could be used to effect transfers at higher transfer rates.

It is of interest to predict the off-design performance of this basic vaporizer and to discuss the control aspects of the unit incorporated in a typical transfer system. Assume that the impedance of the transfer line is variable and that it is desired to obtain a maximum capability at various ullage pressures. Following the locus of the maximum capability points A, B, and C in Figure 4.6, the following off-design conditions are obtained for a six-tube vaporizer unit:

Storage Vessel Ullage Pressure	Maximum Transfer Rate	Required Vaporizer Pressure Drop
100 psia	492 gpm	5.5 inches LH_2 (design)
50	914	13.0
25	1885	27.0

Note that the transfer capability increases by a factor of three as the transfer pressure is decreased to 25 psi.

The control of a transfer system will depend upon the characteristics of the transfer system, i.e., the vaporizer control and the transfer line control. To illustrate the control of a typical transfer system, the vaporizer characteristics calculated for the aforementioned vaporizer and typical transfer-line impedance curves are shown in Figure 4.8. The vaporizer characteristics are plotted for various values of the total head loss in the vaporizer control valve divided by the available liquid head in the storage vessel, which was assumed to be 30 inches of LH_2 in this example. From Figure 4.8 it can be seen that with control valves in the transfer line and in the vaporizer line a transfer can be made at any given pressure and rate within the capabilities of the vaporizer. At 100 psi the vaporizer characteristics cross over; that is, as the vaporizer valve is opened and the pressure drop across the valve is decreased, the transfer rate increases until a valve position is reached that corresponds to the maximum capability at 100 psi. Opening the valve wider will decrease the transfer rate in accordance with Figure 4.6. As this situation would not be desirable from a control standpoint, it is necessary to consider the vaporizer valve characteristics for proper design of a controllable system.

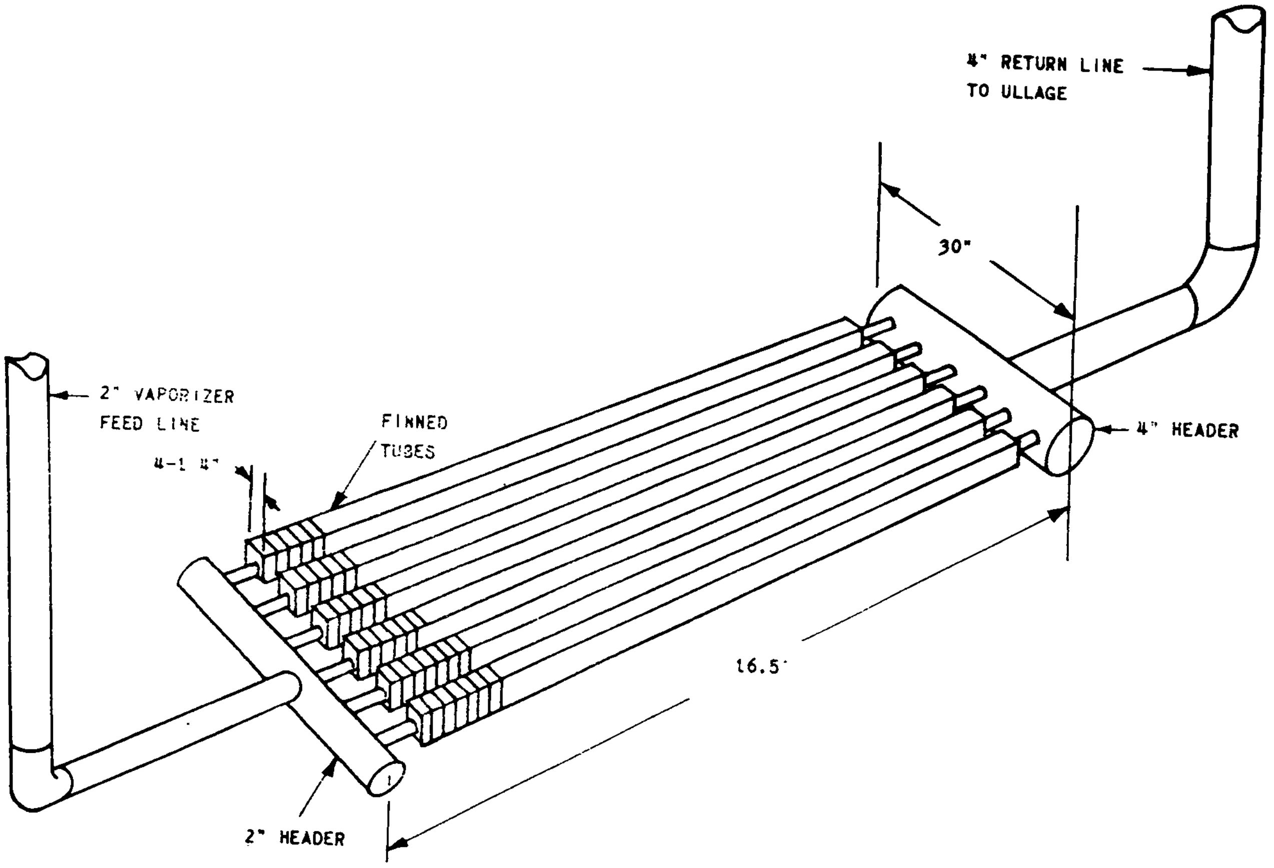
4" RETURN LINE
TO ULLAGE
30"
4" HEADER
2" VAPORIZER
FEED LINE
FINNED
TUBES
4-1 4"
16.5'
2" HEADER

FIGURE 4.7 Basic Natural-Convection Vaporizer Unit

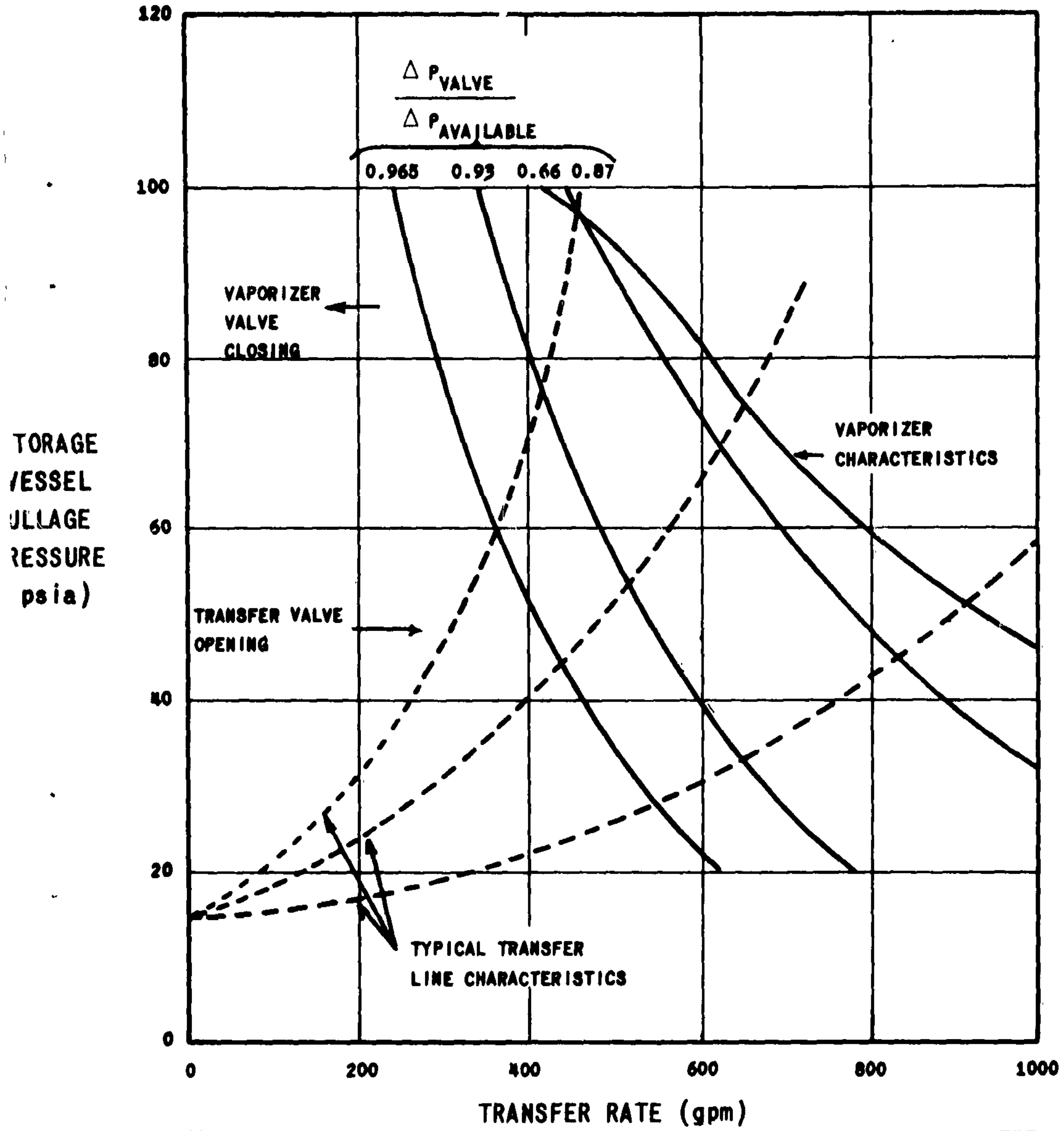

FIGURE 4.8 Transfer System Operating Conditions

In Figure 4.9 the transfer rate for the basic six-tube vaporizer is shown plotted as a function of the opening of the vaporizer valve for a given total head of liquid. The valve was conservatively sized to allow a maximum capability transfer at the design pressure of 100 psia (point A on Figure 4.6), and an "equal percentage" valve characteristic was used to obtain the C_V (valve flow coefficient) versus percent open relationship. From Figure 4.9 it is noted that if the ullage pressure is maintained constant at 100 psi, it is necessary to limit the vaporizer control valve opening to approximately 70 percent in order to remain within a controllable range. A fixed limit on the valve positioner would slightly reduce the transfer capability at 25 psi from the off-design figures quoted in a previous paragraph. Of course, one could specify a flow coefficient that would preclude the necessity for using a positioner limit, but it is recommended that a conservative valve size be used in conjunction with a valve positioner limit. The limit setting could easily be determined from initial trial runs with an actual system.

The vaporizer pressure drop calculation that was used to establish Figures 4.8 and 4.9 could be subject to some inaccuracies. These figures serve only to define the operating characteristics of a typical system. In a design application it is suggested that the vaporizer be mounted below the minimum necessary liquid head as calculated from the sum of the head losses associated with the feed line, return line, and vaporizer tube section.

5. Test Results

a. Introduction

To validate the theoretical analyses of a typical vaporizer system that have previously been outlined, tests were conducted to determine the heat transfer characteristics of a model finned tube vaporizer using liquid hydrogen. Other tests were completed using a natural-convection, regenerative vaporizer system to determine the liquid hydrogen transfer system capabilities, and the operating characteristics of a typical system. Schematic drawings of the test apparatus and a description of the test procedures are presented in Section D.

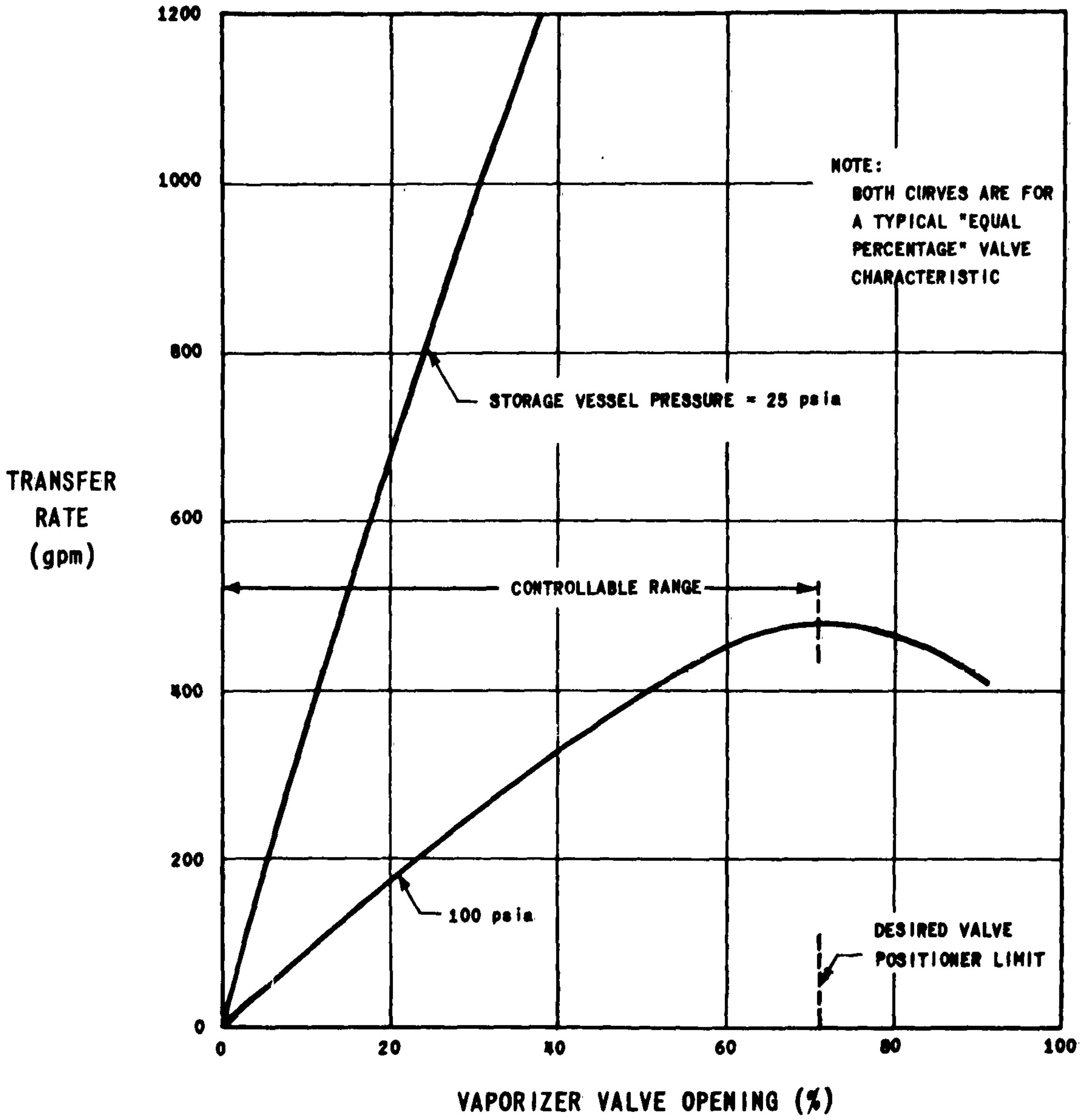

FIGURE 4.9 Vaporizer Valve Characteristics

b. Vaporizer Tests

To determine the heat-transfer characteristics of a typical liquid hydrogen vaporizer, approximately 20 tests were made to measure experimentally the steady-state temperature rise of the hydrogen as a function of the mass flow of hydrogen and average static pressure.

The vaporizer section used in the testing had the following dimensions:

Length (finned) L_{1-3} = 16.5 feet

Inside diameter D = 1.25 in.

Number tubes (parallel) N = 2

Fin size (rectangular) = 4-1/4 x 4-1/4 in.

Fin spacing = 40 per foot

Tube material = copper

Fin material = aluminum

The heat transfer data obtained in tests with the above vaporizer are presented in Figure 4.10. The average vaporizer exit gas temperature (measured approximately one inch from the end of the finned section) is shown plotted as a function of the vaporizer mass flow for a number of different vaporizer static pressures. The experimental points, in general, lie on a smooth curve. The effect of varying the static pressure on the temperature rise would appear to be negligible, as predicted by the theoretical analysis. Two theoretical curves obtained from calculations using eq. (8) are shown superposed on the experimental data. The curve for $\eta_{FIN} \times h_o = 0.60$ and $(\bar{q}/A)_{1-2} =$ 6000 Btu/hr-sq ft appears to fit the experimental data with reasonable accuracy, the curve for $\eta_{FIN} \times h_o = 0.75$ and $(\bar{q}/A)_{1-2} = 7000$ appears to be slightly conservative in predicting the temperature rise.

From Figure 4.10 one may conclude that the effect of pressure on the exit gas temperature of a vaporizer discharging superheated gas is negligible, and that eq. (8) can be used to predict the exit gas temperature with an accuracy sufficient for design purposes. Some caution, however, must be exercised in applying eq. (8) to a specific system design. Since the outside film coefficient of heat transfer controls the over-all heat flux to the vaporizer, wind velocity,

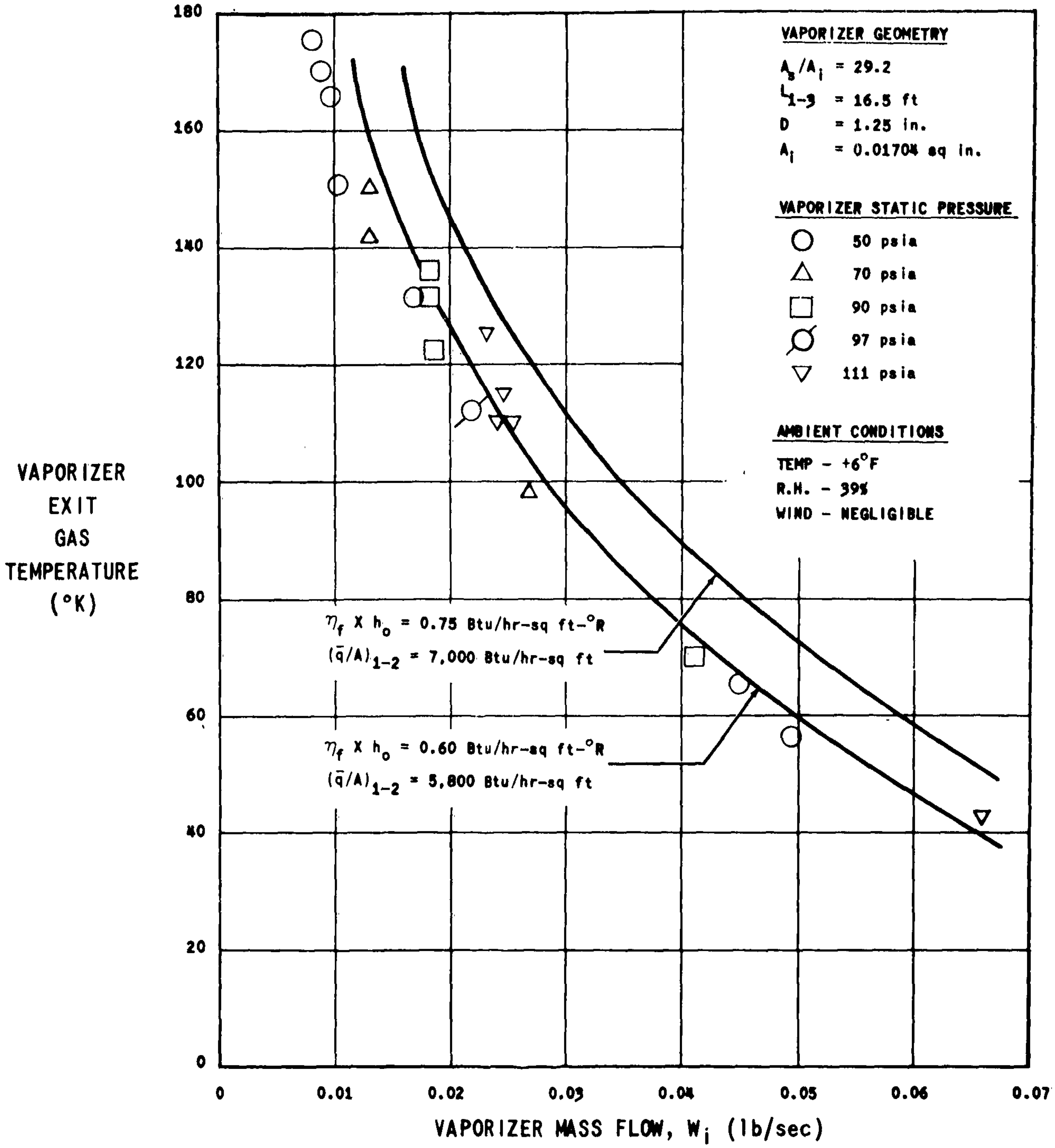

FIGURE 4.10 Vaporizer Heat Transfer Characteristics

humidity and the resulting frost accumulation on the vaporizer fins affect the heat transfer characteristics of the vaporizer. The performance of a vaporizer system operating under abnormal ambient conditions was not investigated in the test program described. Until such time as performance data under these conditions becomes available, a factor of safety should be applied to the transfer capability of the vaporizer system. Fortunately, it is relatively easy and inexpensive to utilize additional vaporizer units if required.

In the test program an unsuccessful effort was made to measure the static pressure drop in the vaporizer section. The extremely low pressure drops (less than 5 in. H_2O) associated with this type of vaporizer, coupled with the unsteady nature of the vaporization process, inherently limit the accuracy of measurements. An attempt was made to measure the pressure drop as a function of the mass flow with an extremely sensitive differential pressure transducer. It was found that a correlation of the test data was impossible, due to the large magnitude of the pressure fluctuations and the poor repeatability of test results.

c. Transfer Tests

In addition to the vaporizer tests described previously, a number of transfer tests were conducted to determine the performance of a typical natural-convection regenerative vaporizer system similar to that shown in Figure 4.1.

The experimental results obtained from a typical transfer test with no "hold period" are shown in Figure 4.11. The pressurizing gas temperature measured at the diffuser entrance, the vaporizer exit temperature, liquid transfer rate and ullage pressure are shown plotted as a function of the elapsed time from the opening of the flow control valve mounted in the vaporizer feed line. In this particular test the storage vessel was pressurized to approximately 80% of the desired steady-state pressure before the transfer valve was opened. The transfer and vaporizer valves were opened to a pre-set position and remained at that position throughout the test.

From the temperature data it can be seen that approximately 3.5 minutes are required for the temperature to reach a steady-state value. It is interesting to note that a temperature rise of approximately 45°K was produced by heating of the pressurizing gas in the 4-inch vaporizer return line, which had a length of approximately 30 feet. Also, the steady-state values of the ullage pressure and transfer rate were achieved in approximately 2 and 0.5 minutes

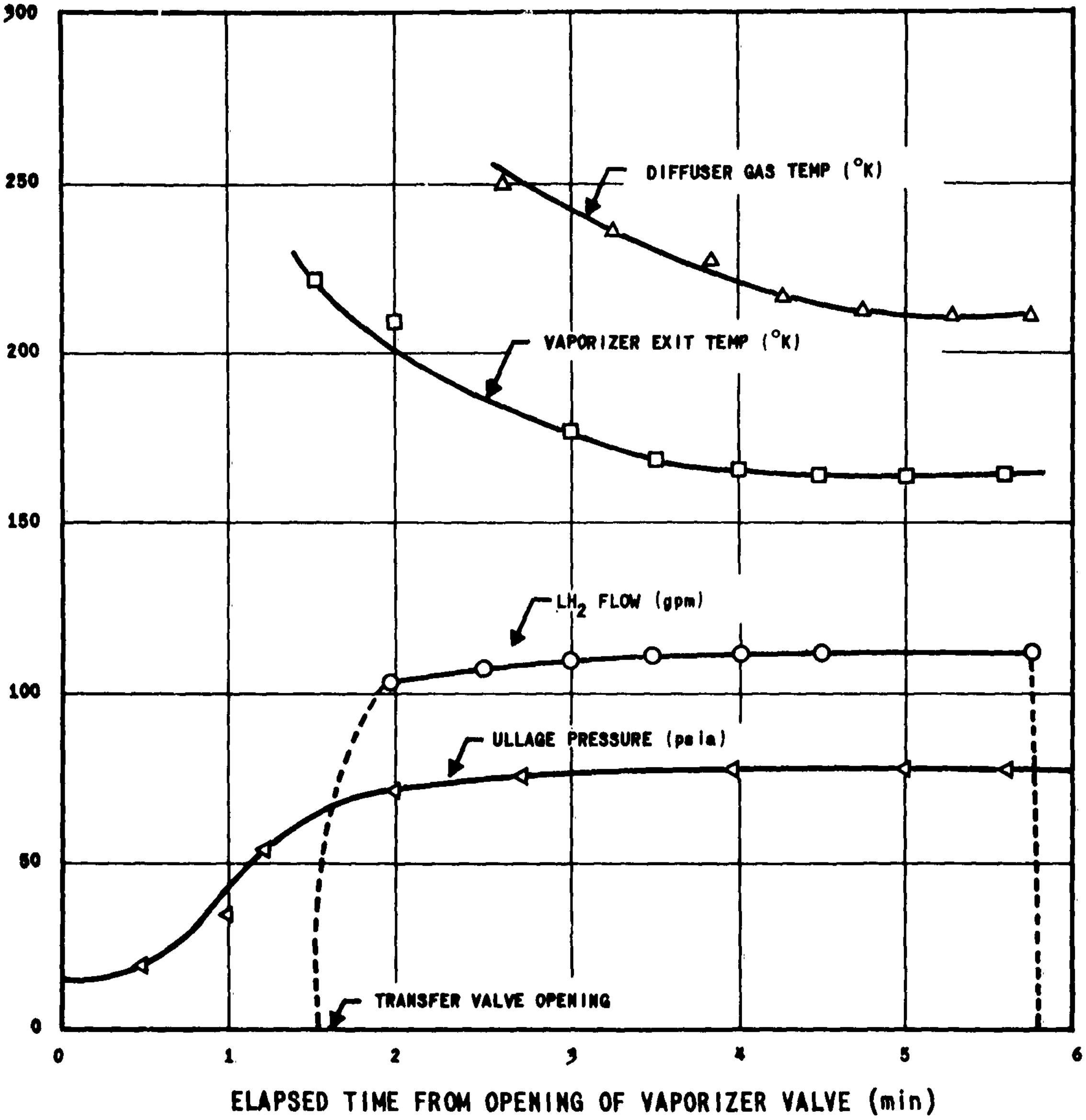

FIGURE 4.11 | Typical System Operating Characteristics

respectively. The time required to reach a steady-state transfer rate depends primarily upon the cooldown time of the transfer line. The time required to reach a steady-state ullage pressure is determined by the initial ullage volume, the head of liquid available and the temperature-flow characteristics of the vaporizer system during the transient cooldown process. With a storage vessel initially full, one can expect a 2-minute pressurization time to be typical of transfer systems using vaporizers of the type described.

Perhaps the most important design parameter for a pressurized transfer system is the amount of pressurizing gas required to effect a transfer of liquid at a given rate. In Figure 4.12 measured values of the ratio of liquid transfer mass flow to the pressurizing gas mass flow are compared to the theoretical minimum values for eight transfer tests. In each of these tests the transfer rate was maintained constant (with no "hold period") until the storage vessel was out of liquid. The test data plotted in Figure 4.12 include test runs in which the liquid transfer rate was varied from 75 to 140 gpm at ullage pressures ranged from 48 to 110 psia. The measured values of W_0/W_i are compared with theoretical values of W_0/W_i calculated from eq. (24), which was derived on the basis of a "no heat transfer model" (i.e., no heat transfer occurred between the pressurizing gas and the ullage surfaces). This is the minimum gas requirement. The ratios of measured to calculated values are shown plotted as a function of the pressurizing gas temperature measured at the diffuser inlet. The data indicate that good agreement with theory is maintained at pressurizing gas temperatures of less than 220°K. At higher temperatures, eq. (24) does not accurately predict the pressurizing gas requirements. This effect is most likely due to the fact that at higher gas temperatures the driving force for heat and mass transfer between the entering gas and the surfaces of the ullage volume is increased, and condensation of the pressurizing gas plays an important role in governing the pressurizing gas flow requirements. The data obtained for the higher pressurizing gas temperatures are in qualitative agreement with the results obtained for pressurization with room temperature gas as reported in Reference 1. Those results indicated that when room-temperature pressurizing gas was used, the pressurizing gas requirements were greater than the requirements calculated from a "no heat-transfer" model, but less than the requirements calculated from a "thermal equilibrium" model. In any particular case it is recommended that the methods described in Section II of this report be used to estimate the pressurizing gas requirements.

In the tests that were conducted, it was impossible to determine the maximum transfer capability of the two-tube vaporizer that was used, due to the fact that the storage vessel had a pressure limitation of 100 psi. For this reason the liquid flow to the vaporizer was throttled by the control valve in the vaporizer feed line to maintain an ullage pressure of less than 100 psi. At this ullage pressure the combined impedance of the transfer line (line, valves and orifice) limited the transfer rate to approximately 140 gpm. This would be approximately 85% of the theoretical transfer capability for a two-tube vaporizer as calculated in Section D for the same vaporizer tube geometry.

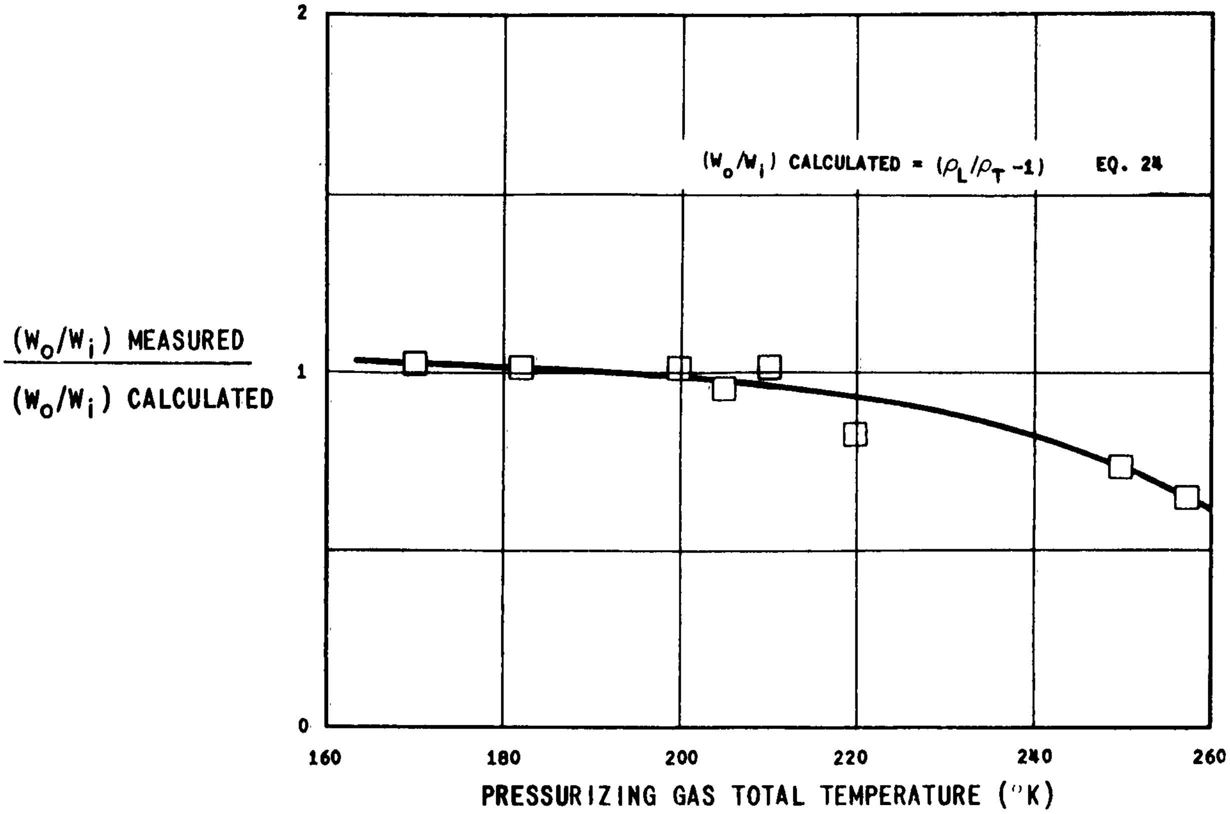

FIGURE 4.12 Comparison of Experimental and Theoretical Pressurizing Gas Requirements

d. Operating Experience

As discussed in Reference 1, one of the major problem areas encountered in the incorporation of a vaporizer in a transfer system is the control of the ullage pressure in the storage vessel. The control system for the transfer operation must be capable of maintaining a desired transfer flow rate and must also be capable of maintaining the ullage gas pressure at or below the design working pressure of the storage vessel. In large storage vessels designed for rapid propellant loading systems the vaporizer system would, of necessity, be capable of vaporizing large amounts of liquid, and ullage pressure control with small ullage volumes could definitely be a problem.

Several schemes for controlling the vaporizer flow were discussed in Reference 1. Of these, flow control valves in the vaporizer feed line and the transfer line would appear to satisfy the operating requirements of most systems It is suggested that in high-capacity vaporizer systems a control valve be used in the vaporizer line to sense a pressure build-up in the ullage volume and modulate the vaporizer flow to prevent an overpressure condition. In low-capacity vaporizer systems it would be possible to use a manual valve in the vaporizer loop. This type of control has been used successfully in liquid transfer systems such as those currently found in liquid delivery vehicles. In any system using a vaporizer, however, the storage vessel should be equipped with adequate pressure relief devices to preclude the danger associated with valve failures and a resulting overpressurization. Also, in a closed-loop vaporization system, wherein a control valve is located in the vaporizer feed line, the vaporizer and vaporizer return line constitute a portion of the ullage volume. During long "hold" periods these uninsulated lines are subject to large heat leaks and give rise to an increase in the ullage pressure. Automatic pressure relief devices would be necessary.

The following discussion relates to the operating experience that was accumulated during a series of transfer tests with a 600-gallon storage vessel and a vaporizer system schematically illustrated in Figure 4.1. The reader is referred to Reference 1 for the details of the experimental apparatus.

To determine the pressure rise characteristics of a transfer system similar to one that might be utilized in a rapid loading system, a test was conducted with the 600-gallon storage vessel filled to capacity. The ullage volume was, therefore, the volume of the room-temperature gas in the vaporizer tubes and the vaporizer return line. This volume constituted less than 4% of the total system volume. With an ambient-temperature vaporizer and return line, the flow control valve (which had an opening time of less than 2 seconds) to the vaporizer was opened to allow liquid to flow into the vaporizer. All vents and the transfer valve were closed. A pressure transducer was connected to the ullage space to record the pressure rise. After the ullage volume reached 50 psi, the transfer valve was opened; this allowed liquid to flow out of the tank, thereby increasing the ullage volume.

The results of a typical test are shown in Figure 4.13. From the slope of the plotted data the maximum rate of ullage pressure increase was approximately 90 psi/min with the storage vessel initially full. Using the initial pressure and the pressure at the initiation of transfer, the pressure rise was approximately 40 psi/min. It should be noted that the transfer valve was opened before the ullage pressure reached a steady-state value, i.e., during the initial pressurization period. (Opening the transfer valve increases the ullage volume and thereby decreases the slope of the pressure rise curve. For some operating conditions it may be undesirable to initiate a transfer before the ullage pressure reaches a steady-state value. Then, the ullage pressure rise time will be considerably less than the time shown in Figure 4.13, and provisions must be made in the valve system to sense and control the rather rapid rise that can occur in a storage vessel that is full.) After transfer had been initiated, the vaporizer valve was closed for a period of approximately 1/2 minute to determine the response of the system when the ullage volume was approximately 50% of the system capacity. During this interval the ullage pressure decreased 30 psi, indicating that during a transfer operation the ullage pressure can be controlled by a flow control valve in the vaporizer feed line.

In conclusion, the experience cited has indicated that the operation of a closed-loop vaporizer system can be controlled using the system shown in Figure 4.1. In high-capacity transfer systems, the rate of pressurization is quite rapid with a full storage vessel, and automatic pressure-relieving devices should be incorporated into the system. Flow control valves in the vaporizer feed line and the transfer line can be used to control the ullage pressure and transfer rate. In high-capacity systems it is recommended that these valves be automatically controlled and that automatic pressure-relief devices be installed to minimize the danger of an overpressure condition.

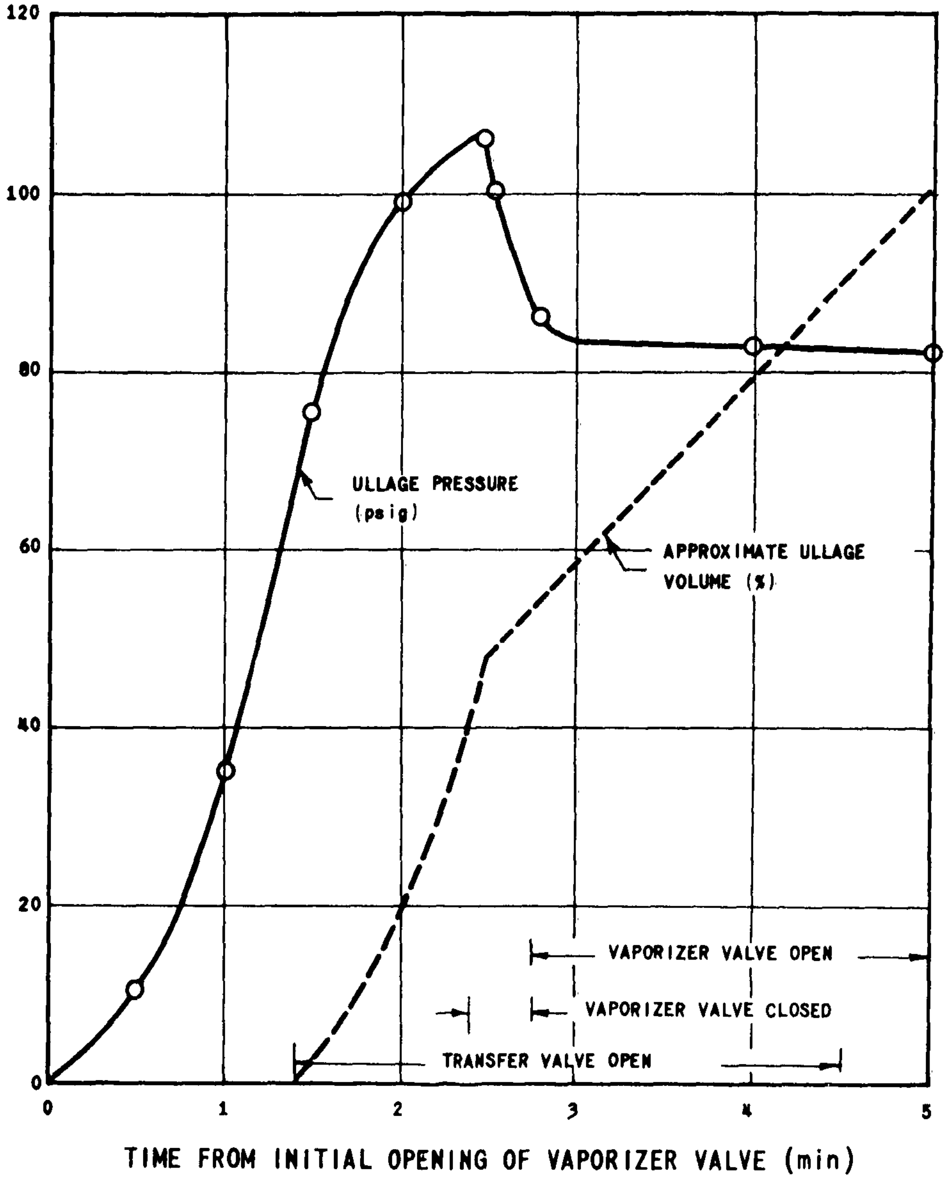

FIGURE 4.13 System Pressure Rise Characteristics

C. NATURAL-CONVECTION VAPORIZER WITH AN AUXILIARY STORAGE SYSTEM

1. Introduction

In Reference 1, the concept of a vaporizer system with an auxiliary storage vessel was discussed. The system consists of an auxiliary liquid storage vessel that is pressurized by gas bottles and discharges liquid into a vaporizer connected to the ullage volume of the main storage vessel. A typical system is illustrated in Figure 4.14. In this system it would be desirable to superheat the gas in the vaporizer and to utilize a vaporizer with inherently high pressure-drop characteristics. The main promise of this system compared to the regenerative system previously discussed would be in a reduced vaporizer size and improved control of the transfer operation. The system is complicated, however, by the necessity for a separate liquid storage vessel and gas storage facilities. It is nevertheless possible to consider substituting a pump for the auxiliary pressurization system.

The following discussion will apply several of the theoretical results derived in Part A to the design of a typical vaporizer for an externally pressurized system. In addition, the experimental results obtained from a liquid hydrogen test program will be compared with a theoretical analysis.

2. Theoretical Analysis

a. Analytical Model

For this vaporizer system the analytical model chosen will be essentially the same as that used in the previous analysis of a regenerative system. Of course, in this system the pressure drop in the vaporizer will be many times greater than in a regenerative system; however, on the pressure-enthalpy diagram in paragraph IV-A-3-a it is noted that for identical transfer pressures the enthalpy change necessary to superheat the pressurizing gas is approximately independent of the vaporizer pressure drop.

In the following section we will consider, as before, the flow of equilibrium hydrogen in a vaporizer tube, with the liquid entering the tube subcooled and leaving as a superheated gas.

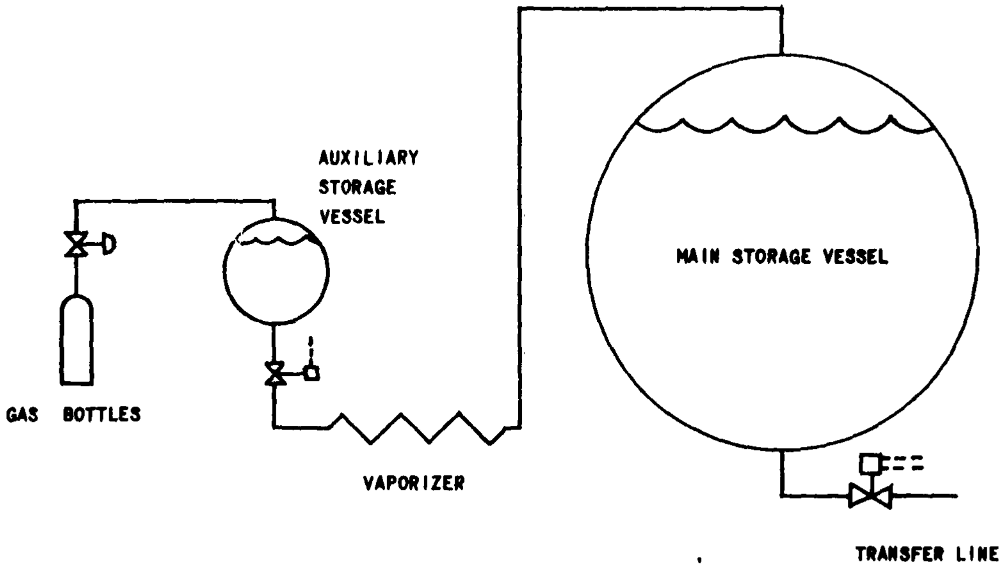
AUXILIARY
STORAGE
VESSEL
MAIN STORAGE VESSEL
GAS BOTTLES
VAPORIZER
TRANSFER LINE

FIGURE 4.14	Schematic Diagram of an Externally Pressurized Transfer System

b. Calculation of Vaporizer Temperature Rise

The equations derived in paragraph IV-A-3-b are applicable to the present case; eq. (8) relates the vaporizer exit temperature to the mass flow of hydrogen and the heat transfer characteristics of a natural convection unit:

$$T_3 = T_a + (T_2 - T_a) \exp \left[\frac{\overline{U}_{2-3}}{\overline{C}_{p_{2-3}}} \left(\frac{\Delta h_{1-2}}{(\overline{q}/A)_{1-2}} - \frac{4L_{1-3}}{Dw/A_i} \right) \right] \qquad (8)$$

The vaporizer exit temperature as a function of the mass flow per unit area and the average heat flux between points 1 and 2 is shown plotted in Figure 4.15 for a vaporizer tube configuration that might be typical of those used in an externally pressurized system. The following values were used in calculating the results shown in Figure 4.15:

L_{1-3}	-	vaporizer length	62.1 ft
D	-	vaporizer tube ID	0.435 in.
A_s/A	-	area ratio of surface to inside	23.48
T_a	-	ambient air temperature	466°R
$(\overline{q}/A)_{1-2}$	-	heat flux in subcooled and two-phase flow regions	10, 000 and 12, 000 Btu/hr-sq ft
η_{FIN}	-	fin effectiveness	0.50
h_o	-	outside surface coefficient of heat transfer	1.6 Btu/hr-sq ft-°F
Δh_{1-2}	-	enthalpy change from subcooled liquid to saturated vapor	208 Btu/lb

As discussed previously, the effect of pressure on the heat transfer characteristics is small since the outside film coefficient of heat transfer is controlling. The results indicate that the exit temperature is a strong function of the mass flow and that changes in the assumed value of the heat flux between points 1 and 2 are relatively unimportant. Note that we have assumed an average heat flux in this region approximately twice as large as the value assumed for the regenerative vaporizer system, because of the increased velocities

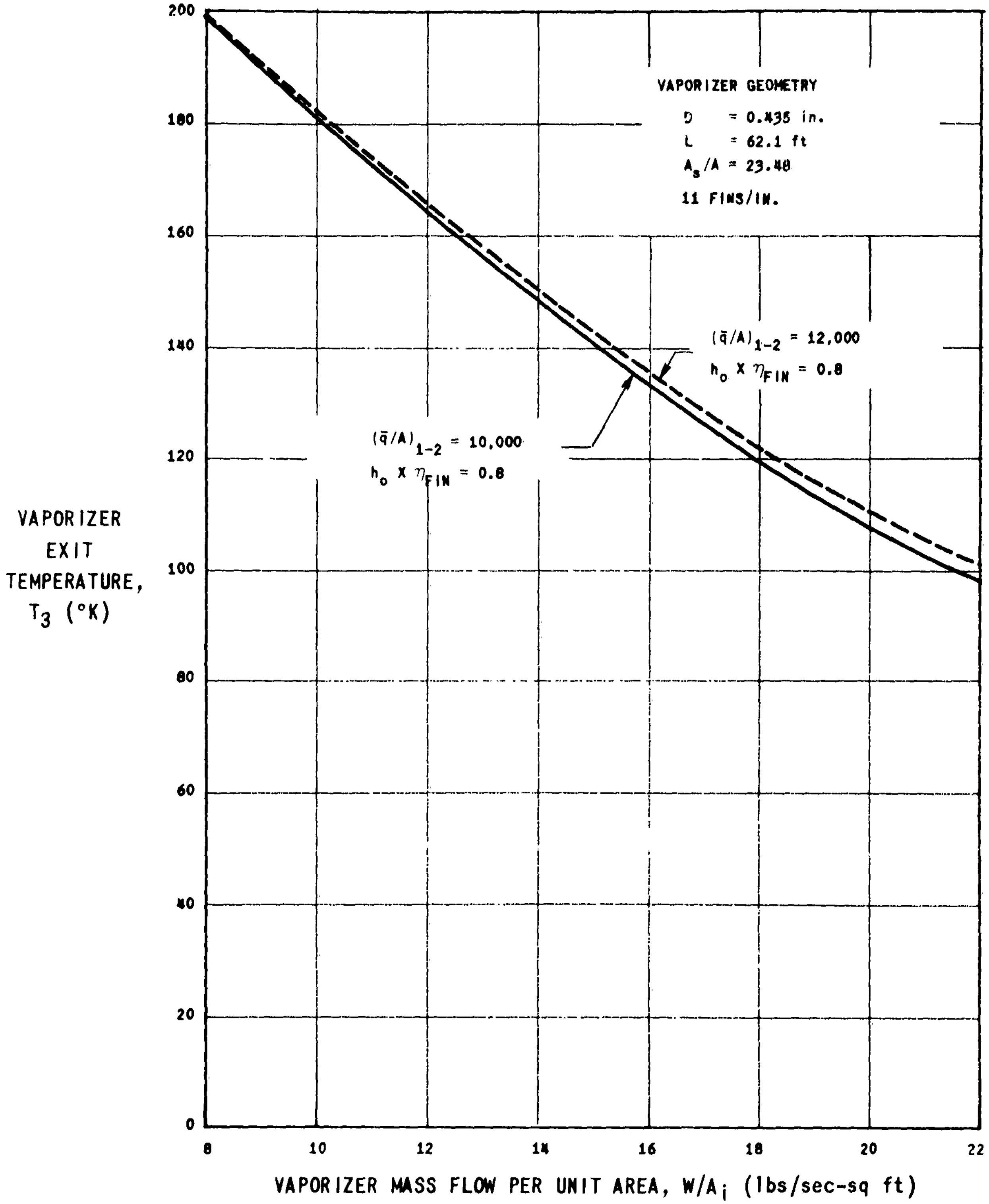

FIGURE 4.15 Vaporizer Temperature Rise Characteristics

typical of system with a higher pressure drop. In support of the assumption relating to the boiling heat flux, it should be noted that for systems discharging superheated vapor, a major portion of the heat is added in the superheated section, and the value chosen for the boiling heat flux does not appreciably alter the temperature rise characteristics.

c. Calculation of Vaporizer Pressure Drop

We can apply the equations derived in paragraph IV-A-3-c to calculate the vaporizer pressure drop between points 1 and 3. For the two-phase flow region we can use eq. (9), which relates the pressure drop to the friction parameter, densities and the inlet velocity to the tube.

$$\Delta P_{1-2} = 4f\left(\frac{L_{1-2}}{D}\right)\left(\frac{\rho_1}{\rho_2}\right)\left(\frac{\rho_1 V_1^2}{2g}\right) + \left(\frac{\rho_1}{\rho_2} - 1\right)\left(\frac{\rho_1 V_1^2}{g}\right) \qquad (9)$$

The pressure drop in the superheated region can also be obtained from the previous analysis, providing it is assumed that the local Mach number within the tube is always less than approximately 0.2. The pressure drop between points 2 and 3 of the tube can be calculated from the expression

$$\frac{P_3^2}{P_2^2} = 1 - 2\left(\frac{R\,T_a}{g\,P_2^2}\right)\left(\frac{w}{A_1}\right)^2\left[\left(\frac{T_a - T_2}{T_a}\right)\left(1 - e^{-\alpha L_{2-3}}\right)\left(1 - \frac{2f}{\alpha D}\right) + \frac{2f\,L_{2-3}}{D}\right] \qquad (23)$$

where

$$\alpha = \frac{\overline{U}_{2-3}\ \rho D}{W\,\overline{C}_{p_{2-3}}} \qquad (15)$$

and

$$L_{2-3} = \frac{(w/A_i)\,D\,\overline{C}_{p2-3}}{4\,\overline{U}_{2-3}}\ \ln\left(\frac{T_a - T_2}{T_a - T_3}\right) \qquad (6a)$$

The total pressure drop is the sum of the pressure drops calculated from eqs. (9) and (23). The vaporizer pressure drop calculated from the above equations for inlet pressures of 75 and 100 psi is shown plotted in Figure 4.16 as a function of the mass flow per unit area. The tube geometry and heat transfer characteristics used to calculate the pressure drop were identical to those listed in paragraph b preceding.

d. Transfer Capabilities of an Externally Pressurized System

The theoretical maximum transfer capability for a system of this type has been derived in Reference 1. The result indicates that if a "no heat-transfer model" is utilized, the ratio of the transfer flow rate to the pressurizing gas flow rate is proportional to the density ratio of the liquid to the pressurizing gas. The result is

$$\frac{W_o}{W_i} \propto \frac{\rho_L}{\rho_T} \tag{25}$$

For pressurizing gas temperatures lower than approximately 200°K. it has been shown from the test results with the regenerative system that the "no heat-transfer" model can be used to predict the gas requirements. Therefore. we would expect that eq. (25) would quite accurately predict the pressurizing gas requirements.

The ratio of transfer to pressurizing gas flow rate is plotted in Figure 4.17 as a function of the ullage pressure and the pressurizing gas temperature. A comparison of Figures 4.5 and 4.17 shows that at high pressurizing gas temperatures the amount of pressurizing gas required for an externally pressurized system is almost identical with the amount required in a regenerative system to effect the same transfer rate.

3. Design of a Basic Vaporizer System

We will now consider the design of a basic unit vaporizer with a transfer capability of approximately 500 gpm. The vaporizer system will be similar to that illustrated schematically in Figure 4 14 An auxiliary storage vessel will be pressurized with gas, and liquid hydrogen will be forced through the vaporizer. The resulting superheated gas will then be used to pressurize the main storage vessel

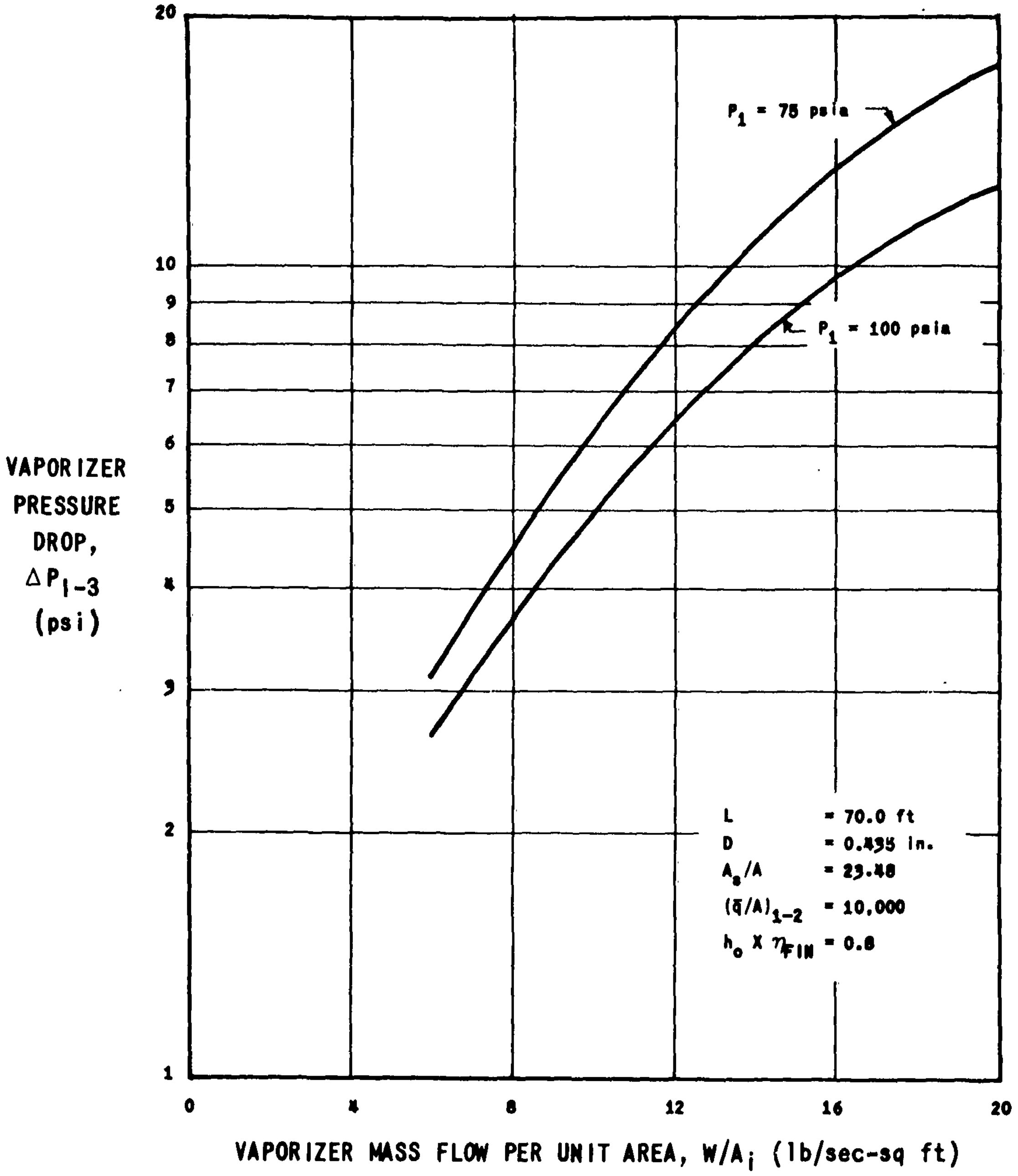

FIGURE 4.16 Vaporizer Pressure Drop Characteristics

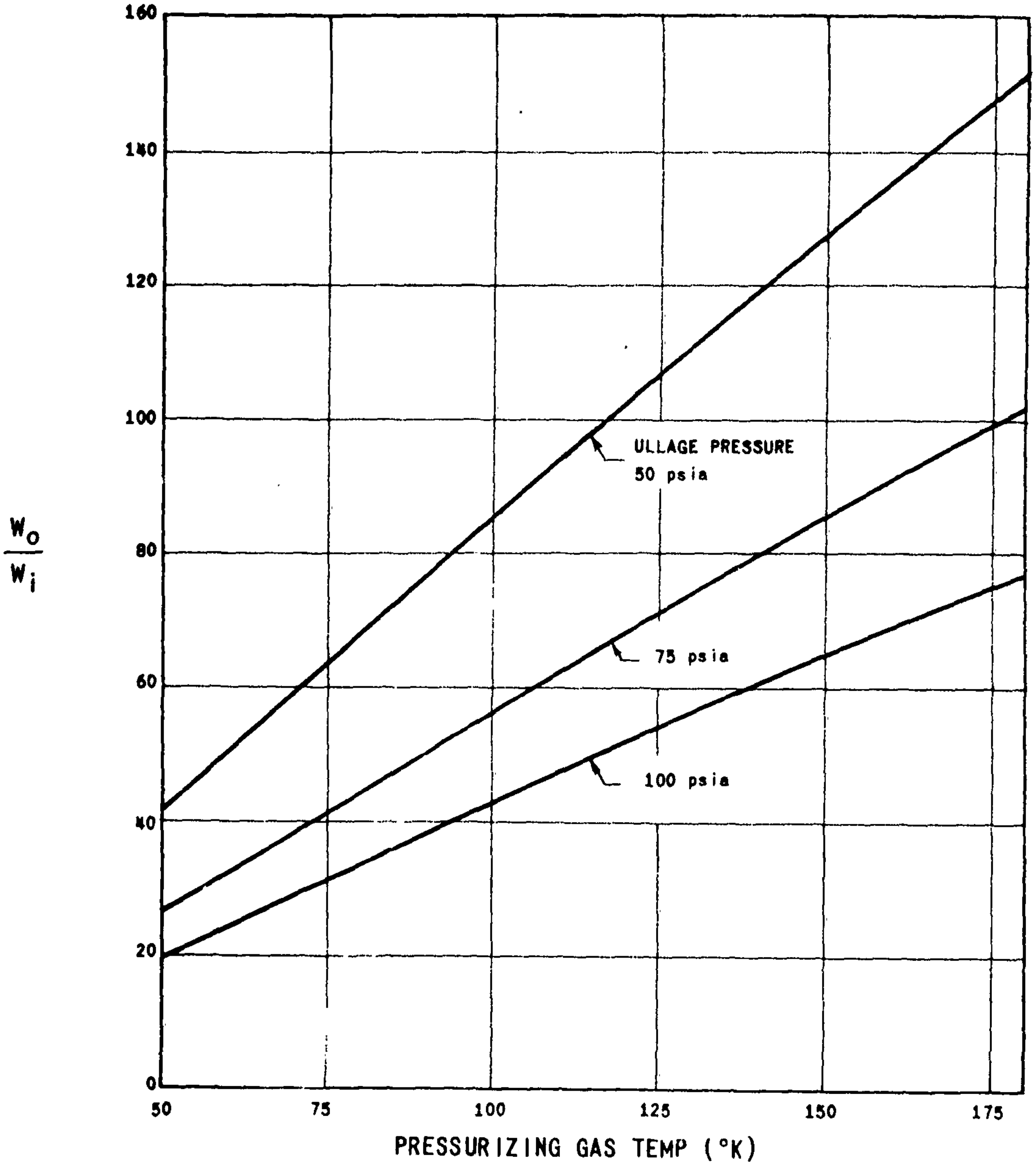

FIGURE 4.17 Maximum Theoretical Transfer Capabilities--Externally Pressurized System

Assume that it is desired to effect transfers from the main storage vessel at a maximum pressure of 100 psi. From Figure 4.17 we can obtain the ratio of transfer flow to vaporizer flow for any given pressurizing gas temperature. To prevent condensation of the pressurizing gas within the main storage vessel, we limit the maximum pressurizing gas temperature to 200°K in accordance with the experimental results presented in Figure 4.12. Since this vaporizer system is not pressure-drop limited, we will select several pressurizing gas temperatures and calculate the size and number of vaporizer tubes required to effect a transfer of 500 gpm at 100 psi.

The maximum transfer capability at a given temperature is obtained from Figure 4.17. For a transfer rate of 500 gpm, the required flow of pressurizing gas can be obtained. Using the temperature rise characteristics in Figure 4.15 for an externally finned vaporizer tube 62.1 feet long, with an ID of 0.435 inch and a surface-to-inside-area ratio of 23.48, the mass flow per tube can be calculated. Knowing the mass flow per tube, the total number of tubes required is obtained from the pressurizing gas requirements. The vaporizer pressure drop for "N" parallel tubes is then obtained from Figure 4.16.

The results of calculations similar to those described above are presented in Table 4.1. To be conservative, we have neglected any additional superheating in the line from the vaporizer exit to the ullage volume; i.e., the pressurizing gas temperature is assumed equal to the vaporizer exit temperature.

TABLE 4.1

CALCULATED DESIGN PARAMETERS

Pressurizing Gas Temp. (°K)	$\frac{W_o}{W_i}$	W_i (gpm)	(W/A_i) per Tube (lb/sec-sq ft)	No. of Tubes	ΔP_{1-3} (psi)	P_3 (psi)
200	85	5.89	8	7	4	100
150	65	7.70	14	6	8	100
100	43	11.60	22	5	14	100

From the above table it can be seen that an increase in pressurizing gas temperature decreases the required amount of pressurizing gas but increases the number of tubes required. It would appear that the selection of a design would be somewhat arbitrary and would depend on such factors as the cost of the auxiliary storage vessel, the size and cost of the vaporizer, and the amount and storage capacity of the gas system used to pressurize the auxiliary vessel.

For comparative purposes, we will select the five-tube design having an exit temperature of 100°K with a total flow of 11.6 gpm. This basic unit would effect a transfer of approximately 500 gpm at an ullage pressure of 100 psi. The required size of the vaporizer feed line would be approximately one-half inch, and the discharge line to the ullage volume of the main storage vessel would have to be approximately one inch in diameter for pressure drops of less than 10 psi. The total pressure drop in such a system would be in the order of 30 psi, assuming a conservative value for the vaporizer pressure drop. The five tubes, each approximately 60 feet long, would be arranged for parallel flow, and each tube could be folded in a "trombone" configuration. Using this arrangement with a single bank of tubes, the vaporizer would occupy an area approximately 12.5 feet long (between headers) and 4 feet wide.

It is of interest to compare the above vaporizer, which would be used in an externally pressurized system, with the basic vaporizer described in Part A, which has approximately the same transfer capability but is designed for a regeneratively pressurized system. In the former, the tube diameter is smaller, since the pressure drop limitations are not dictated by the available liquid head in the storage vessel. However, the total surface area of finned vaporizer tubing required for the regenerative vaporizer system is only slightly greater than that required by the external pressurization system, because of the fact that in any vaporizer discharging superheated gas the over-all heat transfer is controlled by the forced convection coefficient to the outer finned surfaces. In conclusion, it appears that the choice of an externally pressurized system versus a regeneratively pressurized system will not be influenced by the size or cost of the vaporizer, but will be influenced by the control characteristics, the simplicity, and the over-all costs as applied to a particular transfer requirement.

4. Test Results

An experimental program was undertaken to determine the heat transfer and pressure drop characteristics of a vaporizer section which might be typical of one used in an externally pressurized system. In addition, a transfer of liquid hydrogen was completed using an auxiliary liquid storage vessel and vaporizer to supply pressurizing gas to the ullage volume of the main storage vessel. Schematic drawings of the test apparatus and a description of the test procedures are presented in Section D following.

The vaporizer configuration was an externally-finned tube with an ID of 0.435 inch and had a finned length of 62.1 feet. The area ratio of the finned tubing from the outside surface to inside surface was 23.48. This commercially available tubing had a linear fin spacing of 11 per inch.

A limited amount of experimental data on the vaporizer temperature rise and pressure drop was obtained for the above vaporizer configuration. Measured values of the vaporizer exit temperature plotted against the vaporizer mass flow per unit area are shown in Figure 4.18 for six test runs. The solid curve represents the results of a theoretical calculation of the exit temperature using eq. (8), with an assumed value of the two-phase flow heat flux equal to 10,000 Btu/hr-sq ft. Comparing the experimental points with the theoretical curve indicates that eq. (8) can be used to predict the vaporizer temperature rise with an accuracy sufficient for design purposes.

In conjunction with the temperature rise determinations, the vaporizer static pressure drop was measured using a differential pressure transducer. The measured pressure drop and the theoretical value calculated from eq. (23) are compared in Table 4.2.

TABLE 4.2

COMPARISON OF MEASURED AND THEORETICAL PRESSURE DROPS

Run	W/A_i (lb/sec-sq ft)	P_3 (psia)	ΔP_{1-3} (psia) (measured)	$\frac{\Delta P_{1-3} \text{ (measured)}}{\Delta P_{1-3} \text{ (theoretical)}}$
S1	9.4	55	16	2.67
S2	12.0	71	15	2.05
S3	14.4	50	20	1.67
S4	15.3	75	19	1.98
S5	18.5	85	22	1.96
S6	18.7	87	24	2.20

The results indicate that the measured pressure drop is considerably higher than the value calculated from eq. (23) for the same operating conditions. In an attempt to resolve this discrepancy, the theoretical values calculated from eq. (23) were re-examined and then compared with a numerical solution for the pressure drop using "non-perfect" gas property relationships. No error of this

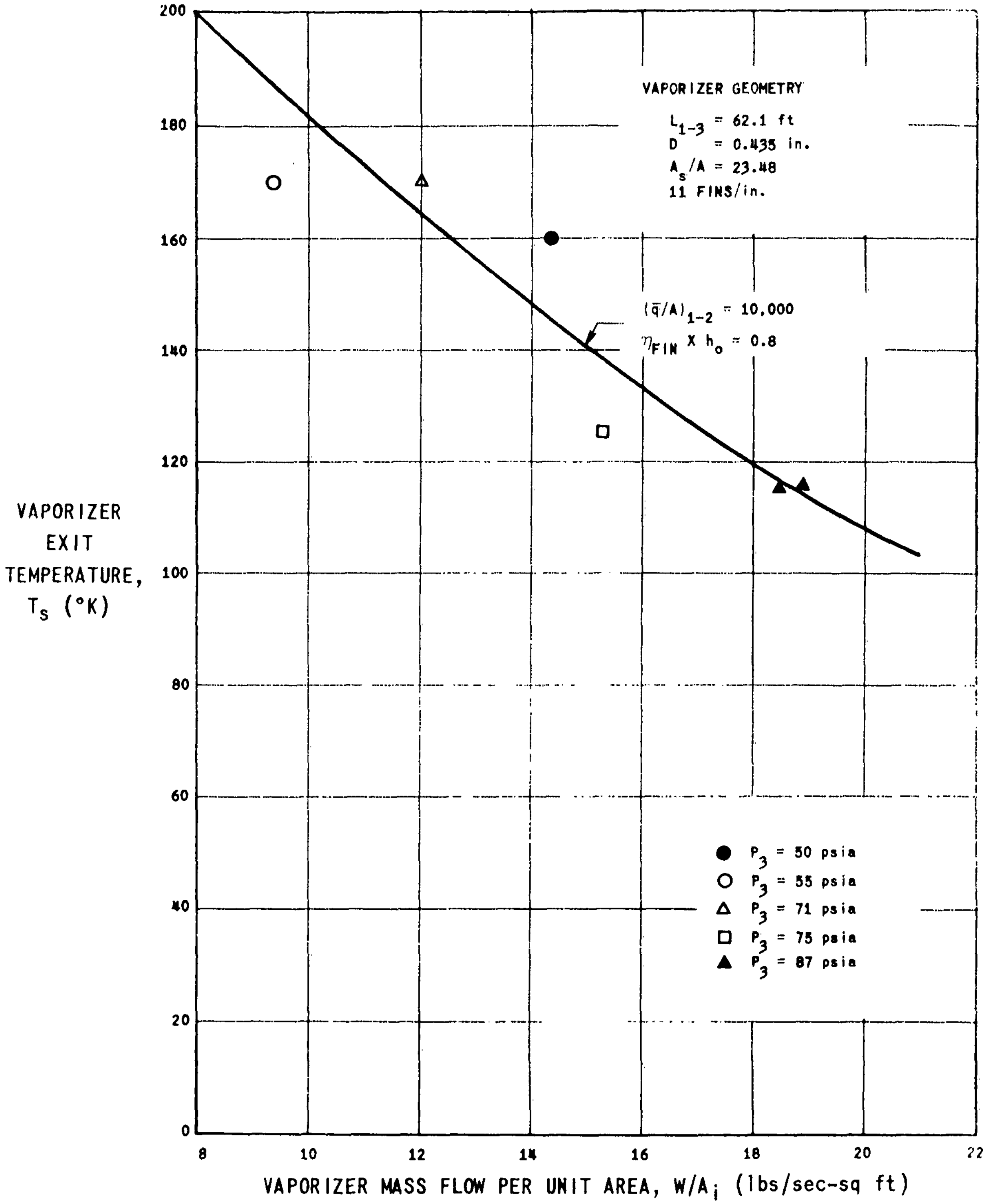

FIGURE 4.18 Vaporizer Heat Transfer Characteristics

magnitude could be attributed to the theoretical analysis, and therefore, the error was probably due to experimental inaccuracies. Unfortunately, the scope of the test program was limited, and the test data could not be repeated to determine the true cause of the discrepancy.

A single transfer run was made with the single-tube vaporizer described in the previous paragraphs. The test set-up, shown schematically in Figure 4.14, consisted of the main 600-gallon storage vessel, and a 110-liter auxiliary storage vessel. A description of the instrumentation and test procedure used in these tests is presented in Section D. The theoretical and experimental results obtained in this transfer test are compared in Table 4.3. (The measured quantities represent average steady-state values obtained after the transient cooldown of the vaporizer and transfer line.)

TABLE 4.3

TRANSFER TEST - EXPERIMENTAL VS THEORETICAL RESULTS

Transfer rate, W_o	68 gpm
Ullage pressure, P_u	83 psig
Vaporizer return gas temperature measured at diffuser inlet, T_D	222°K
Vaporizer exit temperature, T_3	192°K
Vaporizer flow, W	0.0098 lb/sec
Experimental transfer capability, $(W_o/W_i)_{exp.}$	68.7
Calculated maximum transfer capability (Figure 4.17), (W_o/W_i)	87.0

The table shows that the measured transfer capability is approximately 80% of the theoretical maximum capability calculated from an analytical model (which assumed that no heat transfer occurs between the pressurizing gas and the ullage interface). With a return gas temperature of 222°K, one would expect that a portion of the pressurizing gas would condense, as supported by the experimental data in Reference 1 for ambient pressurizing gas temperatures. Note that the ratio of the experimental to calculated maximum capability of 0.79, obtained at a temperature of 222°K, is in agreement with the experimentally determined curve (Figure 4.12) presented in Section A for data obtained with a regenerative vaporizer system at various pressurizing gas temperatures. Since it has been established experimentally that condensation of the pressurizing gas occurs when the temperature is above approximately 200°K (Figure 4.12), it is recommended that at temperatures above 200°K a conservative factor of safety be applied to the theoretical maximum capability calculated from eq. (25).

The operating characteristics of the transfer system described above were not investigated thoroughly, since the test program was limited in scope. Although no difficulty was encountered in effecting a transfer with the system, it is recommended that in a large-scale, rapid-transfer installation, some consideration be given to the control requirements necessary to prevent an over-pressurization of the main storage vessel.

D. TEST PROCEDURES AND APPARATUS

1. Vaporizer Tests

The heat transfer characteristics of the two vaporizer tube configurations shown in Figure 4.19 were determined. Configuration "A" was an externally finned tube with a finned length of 16.5 feet and an ID of 1.25 inches. The surface area ratio from outside to inside was 29.2 for this tube. The tube material was copper, and the fins were aluminum. Configuration "B" was an externally finned tube with a finned length of 62.1 feet and an ID of 0.435 inches. The area ratio for this tube was 23.48. The fins were integral with the tube body, and the material was copper.

The apparatus used in the vaporizer tests is shown in Figure 4.20. Liquid hydrogen (of equilibrium concentrations) was stored in a 600-gallon, vacuum-jacketed vessel. The storage vessel was protected from an overpressure by several rupture discs, relief valves and a remotely operated solenoid vent valve. The storage vessel was pressurized with gaseous hydrogen from a bank of high-pressure gas cylinders. The pressure was controlled by a remotely operated flow control valve. Liquid entered the vaporizer through a section of 2-inch stainless steel line in which a manually operated and an air-operated remotely controlled valve were located. This entire section of line was insulated with approximately two inches of glass foam with an aluminum foil vapor barrier. The hydrogen gas discharging from the vaporizer passed through an ASME orifice and was vented to the atmosphere.

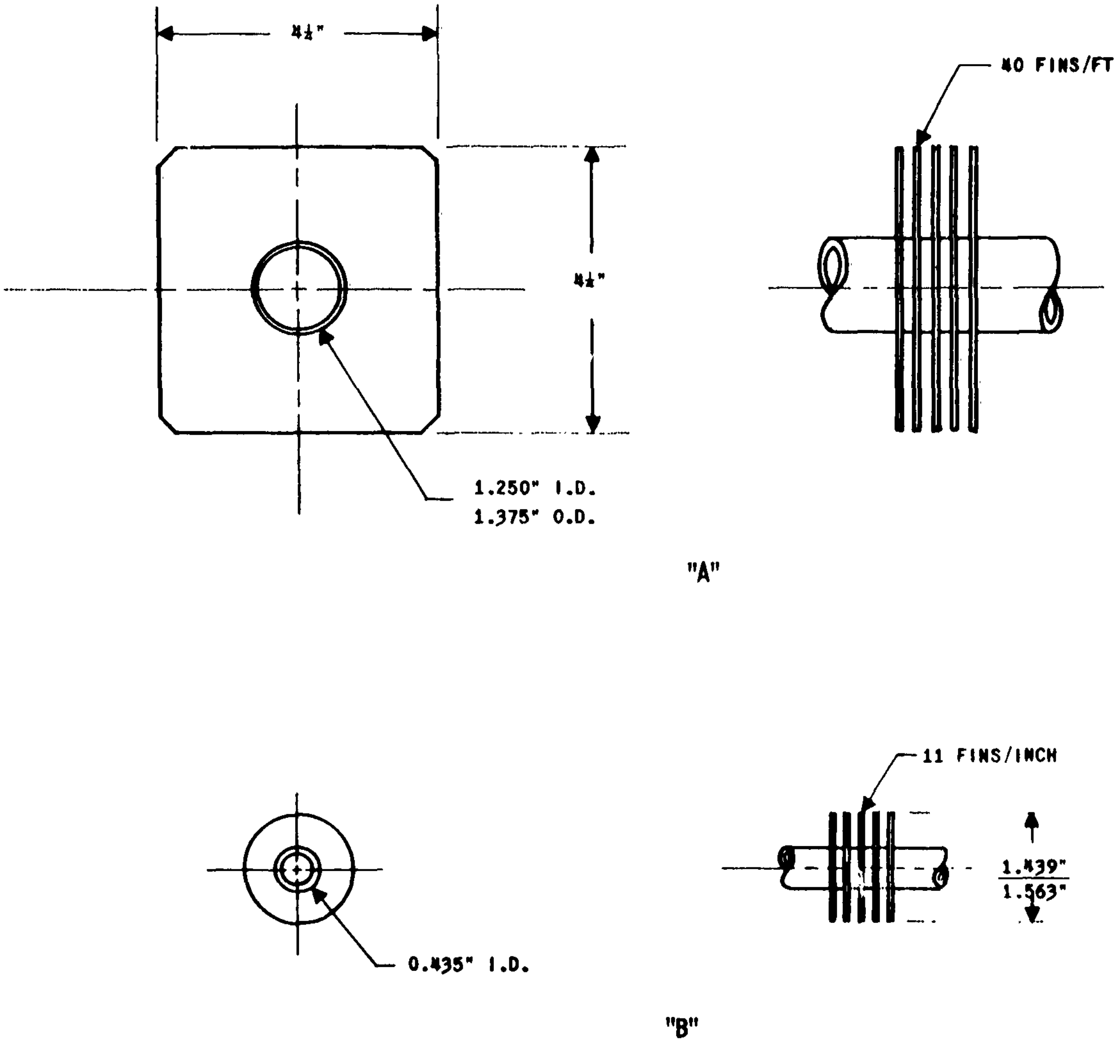
4½"
40 FINS/FT
4½"
1.250" I.D.
1.375" O.D.
"A"
11 FINS/INCH
1.439"
1.563"
0.435" I.D.
"B"

FIGURE 4.19	Vaporizer Tube Configurations

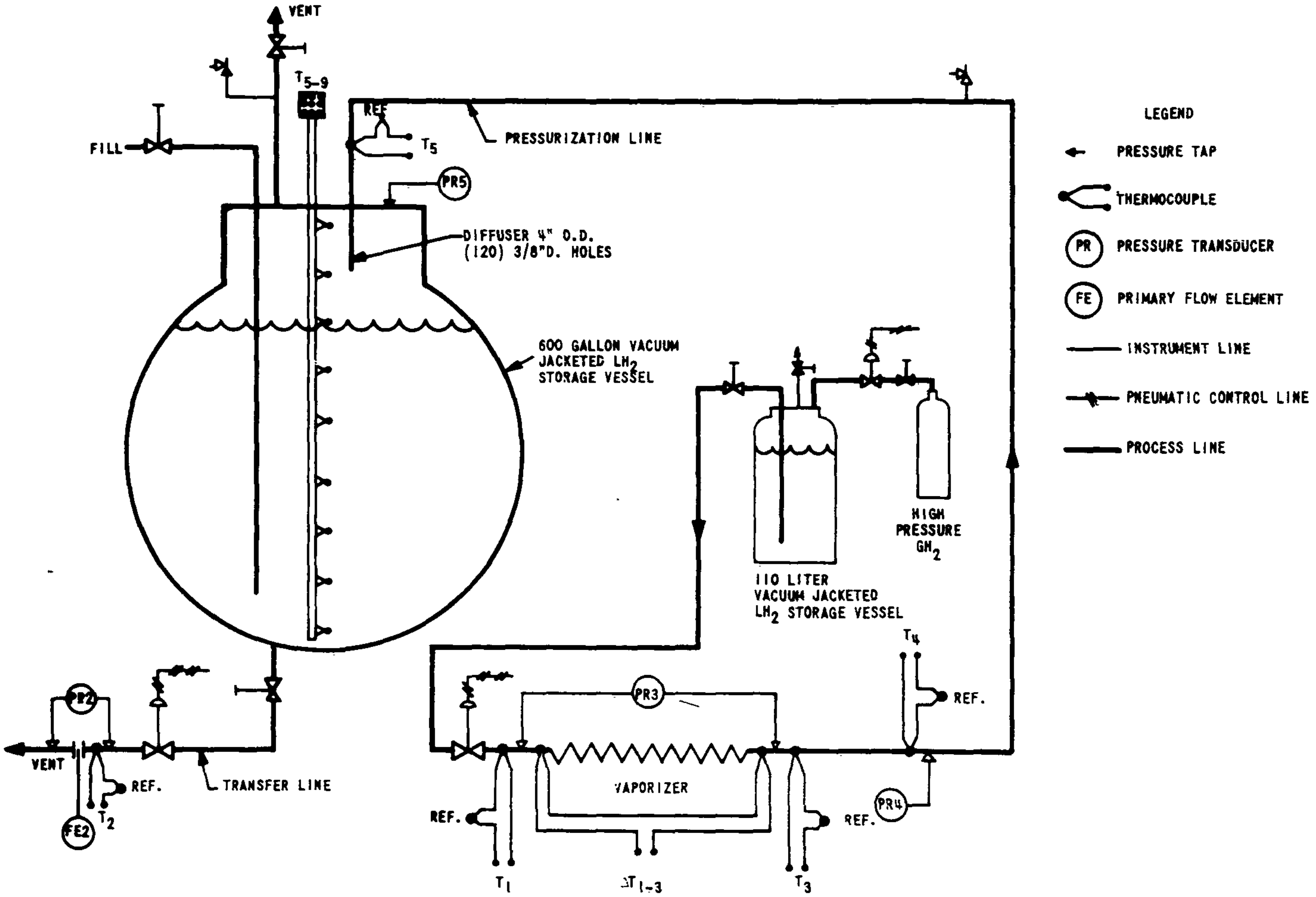
VENT
T_{5-9}
FILL
REF
T_5
PRESSURIZATION LINE
PR5
DIFFUSER 4" O.D.
(120) 3/8"D. HOLES
600 GALLON VACUUM JACKETED LH_2 STORAGE VESSEL
110 LITER VACUUM JACKETED LH_2 STORAGE VESSEL
HIGH PRESSURE GH_2
T_4
REF.
PR2
VENT
REF.
T_2
FE2
TRANSFER LINE
PR3
VAPORIZER
REF.
T_1
ΔT_{1-3}
T_3
REF.
PR4
LEGEND
PRESSURE TAP
THERMOCOUPLE
PR PRESSURE TRANSDUCER
FE PRIMARY FLOW ELEMENT
INSTRUMENT LINE
PNEUMATIC CONTROL LINE
PROCESS LINE

FIGURE 4. 20

Schematic Diagram of Vaporizer Test Apparatus

The primary instrumentation used in the tests consisted of a number of copper-constantan thermocouples with bare wire junctions. These thermocouples had ice-water reference junctions and strain-gauge type pressure transducers. The outputs were remotely recorded on several multi-channel, null-balanced recording potentiometers. Pressure gauges and manometers (photographed by a remotely operated movie camera) provided secondary measurements of the pressures. The arrangement and location of the instrumentation relative to the vaporizer is shown in Figure 4.20. Of prime concern were measurements of the vaporizer temperature rise, the pressure drop in the vaporizer and the hydrogen mass flow through the vaporizer. The temperature rise was measured in two ways: 1) by a differential thermocouple and 2) by two thermocouples, one located at the vaporizer inlet and one at the vaporizer outlet. The vaporizer static pressure drop was measured by differential pressure transducers, an inclined draft gauge (for low pressure drops) and a U-tube manometer. The vaporizer pressure taps were 1/16-inch holes drilled in the vaporizer tube adjacent to the first and last fins. The flow measuring orifice plates were designed to ASME code and located in a standard orifice flange having flange pressure taps. The instrument lines connecting the pressure taps to the transducers were of copper tubing and were sufficiently long to permit the transducers to operate at or near ambient temperature.

Prior to each series of tests the primary instrumentation was calibrated. The thermocouples were calibrated at ice-water, liquid nitrogen, and liquid hydrogen temperatures. These calibrations were marked directly on the instruments of each temperature recording channel. The pressure transducers were calibrated on the recording instruments by use of pressurized nitrogen and a laboratory test gauge. The differential pressure transducers were calibrated against water and mercury manometers. In the reduction of data from the recording instruments, a curve of temperature vs EMF (for copper-constantan thermocouples) in Reference 3 was used to interpolate between the temperature calibration points. The pressures were obtained directly from the pressure calibrations using a linear interpolation. In all cases, it was found that the transducers were linear, in their design range, to within approximately 1/2%. (The linearity, zero pressure balance, and the EMF output of all of the transducers agreed with the calibration curve and specifications supplied by the manufacturer.)

Other pre-test procedures included the purging, cooldown, and filling of the storage vessel, and the purging of the vaporizer and instrument lines. The storage vessel was cooled with liquid nitrogen; after this liquid was discharged, the vessel was purged with hydrogen gas before liquid hydrogen entered the system. The vaporizer and instrument lines were purged with nitrogen, followed by hydrogen gas to eliminate water vapor and any residual air.

The vaporizer tests were conducted in the following manner: Liquid hydrogen flow to the vaporizer was established by opening the remotely operated control valve in the vaporizer feed line, and the storage vessel was pressurized with hydrogen gas from a high-pressure manifold. (The maximum storage vessel pressure was limited to approximately 100 psi by the design of the inner vessel.) The vaporizer temperatures were monitored during cooldown until they reached a steady state at a given mass flow and vaporizer inlet static pressure. When a steady state was reached, the pertinent data was recorded. The same process was repeated at other vaporizer inlet static pressures and mass flow rates to obtain data over as wide a range of pressure and flows as possible. The mass flow through the orifice was calculated by use of the flow coefficients reported in Reference 4.

An exact analysis of the errors involved in each of the determinations was not completed; however, it was estimated that the maximum error in measuring the vaporizer exit temperature, including recording instrument error, was approximately ±3°K. The maximum error in the mass flow determinations, accounting for the uncertainties in measurements of temperature, pressure, flow coefficient and orifice diameter, was estimated to be approximately ±8%.

In the vaporizer tests described, no attempt was made to control the ambient air temperature, the relative humidity, or the air velocity across the fins of the vaporizer sections. However, the experimental data presented in Figures 4.10 and 4.18 were obtained at essentially a constant ambient temperature and relative humidity. The wind velocity during these tests was negligible.

2. Transfer Tests - Regenerative Transfer System

A number of tests were conducted to determine the operating characteristics and performance of a transfer system using a regenerative vaporizer. The apparatus used in these tests is shown schematically in Figure 4.21. Two vaporizer tubes (configuration "A," Figure 4.19), each 16.5 feet long, were connected in parallel and mounted approximately four feet below the bottom of the 600-gallon storage vessel. A 2-inch insulated vaporizer feed line and a 4-inch uninsulated vaporizer return line completed the vaporizer loop. A diffuser was attached to the return line and mounted in the permanent ullage space at the top of the storage vessel. The diffuser was a length of 4-inch tubing, blanked-off at the end, and had 120 3/8-inch holes drilled in a radial pattern. A 2-inch transfer line, which discharged to the atmosphere, was

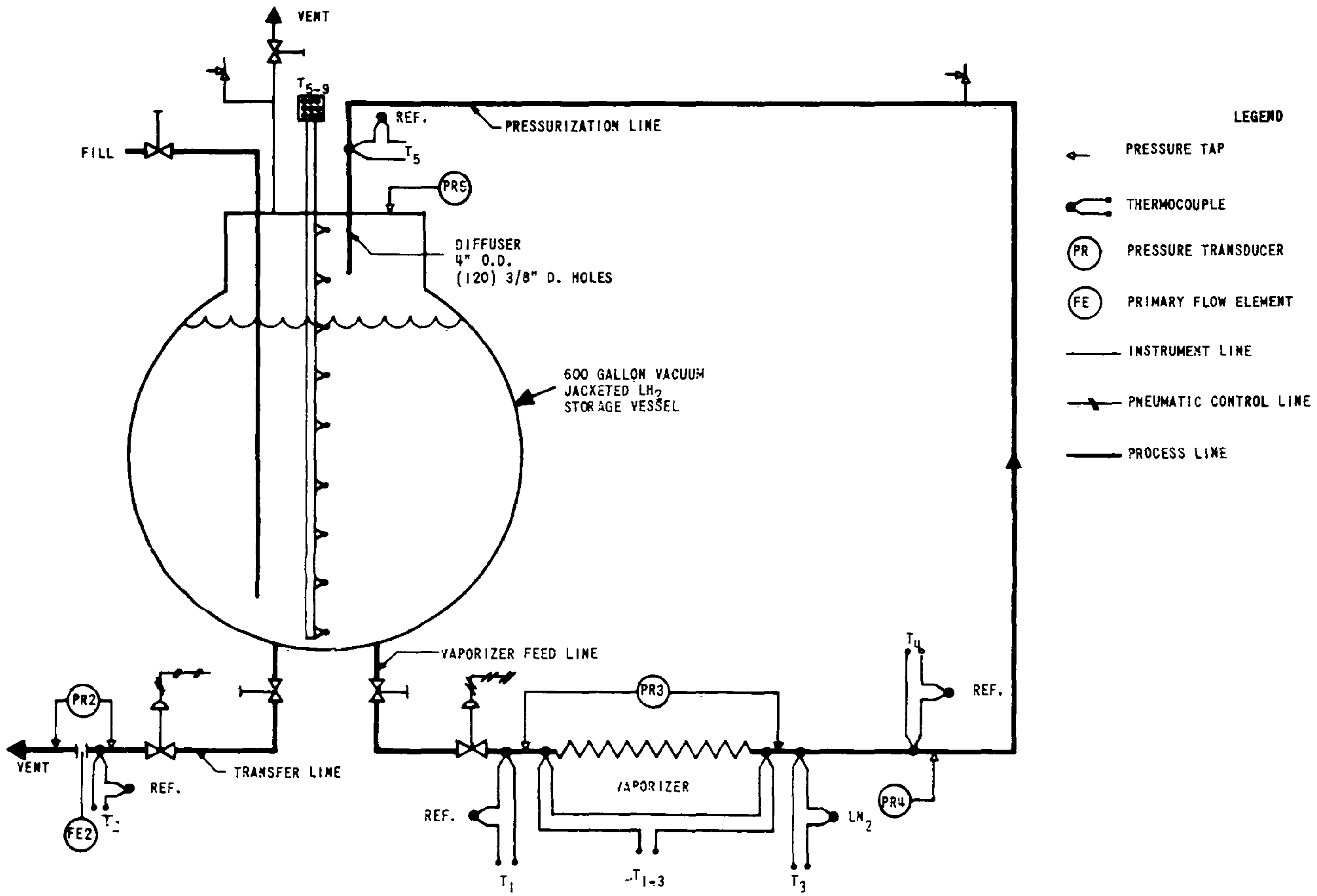
VENT
FILL
T5-9
REF.
T5
PRESSURIZATION LINE
PR5
DIFFUSER
4" O.D.
(120) 3/8" D. HOLES
600 GALLON VACUUM
JACKETED LH2
STORAGE VESSEL
VAPORIZER FEED LINE
PR2
VENT
REF.
FE2
TRANSFER LINE
PR3
VAPORIZER
REF.
T1
T1-3
T3
LN2
PR4
T4
REF.
LEGEND
PRESSURE TAP
THERMOCOUPLE
PR
PRESSURE TRANSDUCER
FE
PRIMARY FLOW ELEMENT
INSTRUMENT LINE
PNEUMATIC CONTROL LINE
PROCESS LINE

FIGURE 4.21

Schematic Diagram of Transfer System with Regenerative Vaporizer also connected to the storage tank. A remotely operated control valve and an ASME orifice were used to control and measure the liquid being transferred. To insure single-phase flow at the orifice (after line cooldown) the transfer line was insulated with approximately two inches of foam.

Additional instrumentation required for the transfer tests included a measurement of the differential pressure across the transfer line orifice. A strain-gauge type transducer connected to a recording potentiometer was used for primary measurements. A mercury U-tube manometer was photographed with a remotely operated movie camera as a secondary measurement. A thermocouple "tree," consisting of nine bare-wire copper-constantan junctions was used to obtain an approximate indication of the liquid level in the storage vessel. In addition, another copper-constantan thermocouple was used to measure the vaporizer return gas temperature at the inlet to the diffuser.

A pre-test procedure, identical to that used in the vaporizer tests, was used to calibrate the instrumentation and to purge the system. The thermocouple "tree" instrumentation was not calibrated, since the data was merely used to indicate the approximate liquid level.

In the transfer tests the entire amount of liquid in the storage vessel (600 gallons) was discharged to permit the recording of data during the steady-state operation of the vaporizer. In a typical test the vaporizer flow control valve was opened to a pre-set position. When the ullage pressure rose to approximately 80% of the desired transfer pressure, the transfer line flow control valve was opened to a pre-set position. In this manner, transfers could be effected at any desired ullage pressure and transfer flow rate. Transfer tests were conducted at ullage pressures ranging from 48 to 110 psia and transfer flows from 75 to 140 gpm.

The instantaneous transfer flow rate (after the transfer line cooldown) was determined from the orifice differential pressure measurement and the flange tap flow coefficients presented in Reference 5. The vaporizer mass flow rate was obtained indirectly from experimental data on the temperature rise-flow characteristics developed in the vaporizer tests (plotted in Figure 4.10).

An exact error analysis of the measurements of liquid hydrogen transfer rate and the vaporizer flow rate was not attempted. In several tests the measured transfer flow was integrated over the total transfer time and compared with the total amount of liquid used, as determined from a volumetric storage vessel measurement. Allowing for the ullage gas remaining in the storage vessel (but neglecting the liquid required for line cooldown), the comparison indicated that the transfer flow rate as determined from the orifice measurements was accurate to within approximately ± 10%.

3. Transfer Tests - Auxiliary-Fed Vaporizer

In addition to the transfer tests with the regenerative system, several transfers of liquid were made with the test apparatus shown in Figure 4.22. A 110-liter liquid hydrogen storage vessel was pressurized with hydrogen gas from a high-pressure bottle manifold through a pressure regulating valve. Liquid hydrogen from this auxiliary storage vessel was fed to a single-tube vaporizer (Configuration "B," Figure 4.19) having a finned length of 62.1 feet. The hydrogen vapor discharging from the vaporizer was used to pressurize the main storage vessel through the 4-inch diffuser described previously. Liquid flow to the vaporizer was controlled by a remotely-operated valve located in the insulated transfer line from the auxiliary dewar. The maximum vaporizer static pressure was limited to approximately 125 psi by the safe working pressure of the auxiliary dewar, which was approximately 140 psi.

The instrumentation used in this test apparatus, the operating procedure and the measurements were essentially the same as those described previously for the transfer tests with a regenerative vaporizer system.

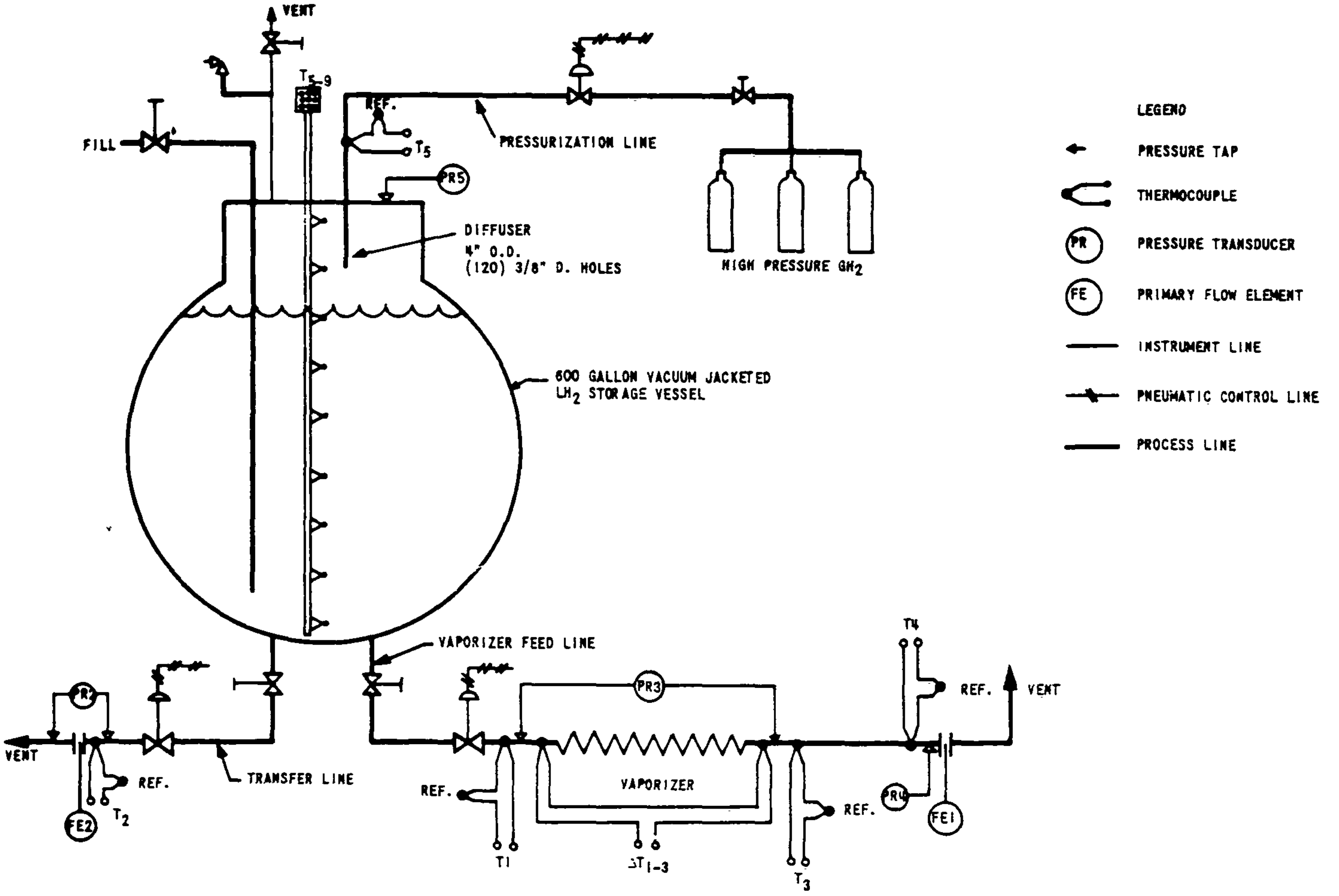
VENT
FILL
T_{5-9}
REF.
T_5
PRESSURIZATION LINE
PR5
DIFFUSER
4" O.D.
(120) 3/8" D. HOLES
HIGH PRESSURE GH_2
600 GALLON VACUUM JACKETED
LH_2 STORAGE VESSEL
VAPORIZER FEED LINE
PR2
VENT
REF.
FE2
T_2
TRANSFER LINE
PR3
REF.
VAPORIZER
T1
ΔT_{1-3}
REF.
T_3
T4
REF.
VENT
PR4
FE1
LEGEND
PRESSURE TAP
THERMOCOUPLE
PR
PRESSURE TRANSDUCER
FE
PRIMARY FLOW ELEMENT
INSTRUMENT LINE
PNEUMATIC CONTROL LINE
PROCESS LINE

FIGURE 4. 22

Schematic Diagram of Transfer System with Auxiliary Fed Vaporizer

E. REFERENCES

1. Bailey, B. M., et al., Handbook for Hydrogen Handling Equipment, WADC Technical Report 59-751 (February 1960).

2. Shapiro, A. H., The Dynamics and Thermodynamics of Compressible Fluid Flow, Vol. I, Ronald Press Co., New York (1953).

3. Chelton, D. B., and Mann, D. B., Cryogenic Data Book, National Bureau of Standards, Cryogenic Engineering Laboratory, Boulder, Colorado (May 15, 1956).

4. Cunningham, R. G., Orifice Meters with Supercritical Compressible Flow, ASME Paper No. 50-A-45 (August, 1950).

5. ASME, Power Test Codes, Part 5, Measurements of Quantities of Materials (April, 1949).

V. ECONOMIC COMPARISON OF VARIOUS MEANS FOR TRANSFERRING LIQUID HYDROGEN

A. INTRODUCTION

In Reference 1 an economic comparison of three liquid hydrogen transfer systems was completed. The systems studied were:

1. System B_1 - pressure transfer utilizing bottled gas furnished by pump-vaporizer units
2. System C_1 - pressure transfer utilizing a gravity-fed vaporizer with a saturated vapor exit temperature
3. System D-B_1 - pump transfer utilizing System B_1 to maintain tank ullage at 5 psig for pump NPSH requirements.

The costs of these various systems were estimated for various transfer rates, quantities and pressures on the basis of a "one-shot" batch transfer, which was selected as a field operation of some interest. The results indicated that for transfer quantities of less than 500, 000 gallons and transfer pressures of 100 psi or less, System C_1 was competitive with the other systems; in several cases studied, it had a definite economic advantage.

In view of the analytical and experimental investigations reported in Section IV, it is of considerable interest to add to the comparisons presented in Reference 1 by comparing variations of a vaporizer system. Utilizing again the "one-shot" batch transfer mode of operation, the following systems will be compared:

1. System C_1 - pressure transfer using a regenerative vaporizer system with a saturated vaporizer exit temperature
2. System C_{1A} - identical with C_1 except that the vaporizer exit temperature is arbitrarily fixed at 100°K
3. System C_3 - pressure transfer using an auxiliary storage vessel to supply the pressurizing gas at 100°K.

Schematic diagrams of the above systems are shown in Figure 5.1 for reference.

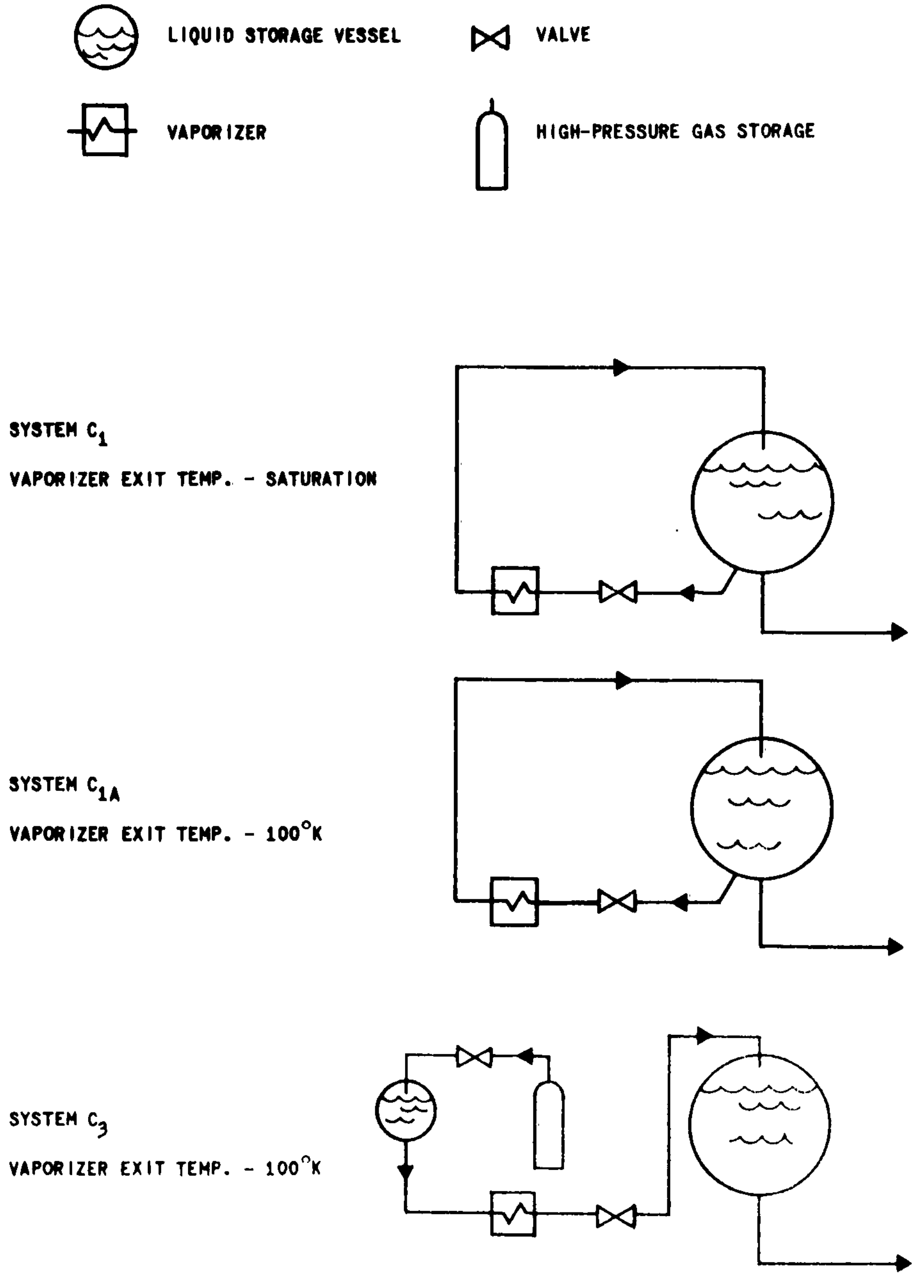
LIQUID STORAGE VESSEL
VALVE
VAPORIZER
HIGH-PRESSURE GAS STORAGE
SYSTEM C_1
VAPORIZER EXIT TEMP. - SATURATION
SYSTEM C_{1A}
VAPORIZER EXIT TEMP. - 100°K
SYSTEM C_3
VAPORIZER EXIT TEMP. - 100°K

FIGURE 5.1	Liquid Transfer Systems

In the economic comparison that follows, the effects of the following variables on the system costs were investigated:

1. System transfer capacity (gal) 80, 000 and 400, 000
2. System transfer pressure (psig) 5 (C_1 only), 50, 100, and 150

In each of the above cases the transfer rate was chosen as 10, 000 gpm.

B. BASIS OF COMPARISON

To allow a direct comparison to be made with Figures 4.14 and 4.15 of Reference 1, the gas required to pressurize the transfer storage vessel was assumed to be obtained by vaporized liquid hydrogen. A liquid cost of 60¢ per gallon was assumed. The costs of storage vessels, pressurizing lines, and the gas storage system used in System C_3 were obtained from the prices developed in Reference 1. These costs include such items as fabrication, erection, inspection, foundations, etc.

The storage vessel capacities were developed from the analysis presented in Section IV, which described the pressurizing gas requirements for various ullage pressures and vaporizer exit temperatures. For System C_3 the gas requirements for pressurizing the auxiliary dewar were obtained from the experimental results reported in Reference 1.

For each system considered, a basic unit vaporizer was designed to effect a transfer rate of 500 gpm. The cost of the basic unit was estimated for fabrication and installation. The number of basic units required for transfer at higher rates was obtained from the curves in Section IV relating the required vaporizer flow to the transfer rate. The total vaporizer cost was obtained from the product of the unit cost and the minimum number of units required.

C. COMPARISON OF SYSTEMS C_1, C_{1A}, and C_3

The estimated costs of the three systems considered are shown in Figure 5.2 for transfer quantities of 80, 000 and 400, 000 gallons and transfer pressures up to 150 psi. The cost of the C_1 system is greater than the C_{1A} and C_3 systems for all pressures and the two transfer quantities due to pressurizing gas requirements. As illustrated in Figure 4.5, the maximum transfer capabilities of a vaporizer system increase with an increase in the pressurizing gas temperature. Therefore, the cost of the C_1 system is strongly influenced by the increase in the storage vessel capacity and additional liquid required to supply the pressurizing gas at the saturation temperature corresponding to the transfer pressure. At high transfer pressures the cost of this additional capacity becomes more dominant.

Note that the costs presented in Figure 5.2 were estimated for a transfer rate of 10, 000 gpm. Lower transfer rates would tend to decrease the costs of all three systems by reducing the number of "basic" vaporizer units required and decreasing in the size of the pressurization return line and related valves. This effect is demonstrated in Figures 4.13, 4.14, and 4.15 of Reference 1 for System C_1.

For a transfer quantity of 400, 000 gallons the estimated costs of System C_{1A} are lower than System C_3 for the range of transfer pressures investigated. The costs of the auxiliary storage vessel and the gas charging system required to store high-pressure gas in System C_3 outweigh the savings that result from the use of a somewhat smaller vaporizer and vaporizer return line. For an 80, 000-gallon quantity the costs of the C_{1A} and C_3 Systems are equal. At this quantity, the savings in vaporizer and pressurization line costs for the C_3 system balance the additional costs involved in the auxiliary storage vessel and gas charging system.

System C_3, which is described in Reference 1, is similar to C_1 and C_{1A} except that instead of using the storage vessel liquid head, a liquid pump is used to overcome pressure losses in the vaporizer and return line. The use of a pump permits a smaller and therefore less expensive vaporizer and pressurizing line than those used in Systems C_1 and C_{1A}. However, the relatively high costs of liquid pumps, combined with maintenance costs, would offset the potential savings associated with the decreased vaporizer and pressurizing line costs.

D. CONCLUSIONS

The cost estimates of the three transfer systems investigated indicate that savings can be realized by using vaporizer systems that pressurize the ullage volume with gas temperatures above the saturation temperature, namely, Systems C_{1A} and C_3 . A comparison of Systems C_{1A} and C_3 for transfer quantities of less than 400, 000 gallons indicates that the costs are comparable and, therefore, that the choice of a system would be dependent on its operational characteristics as applied to a particular transfer requirement.

The preceding discussion has been confined to an economic comparison of vaporizer systems. For a comparison between these and other transfer systems, the reader is referred to Figures 4.13, 4.14, and 4.15 of Reference 1. Since the publication of Reference 1, no new data has been uncovered that would warrant refinement of the economic comparisons.

E. REFERENCES

1. Bailey, B. M., *et al.*, *Handbook for Hydrogen Handling Equipment,* WADC Technical Report 59-71 (February 1960).

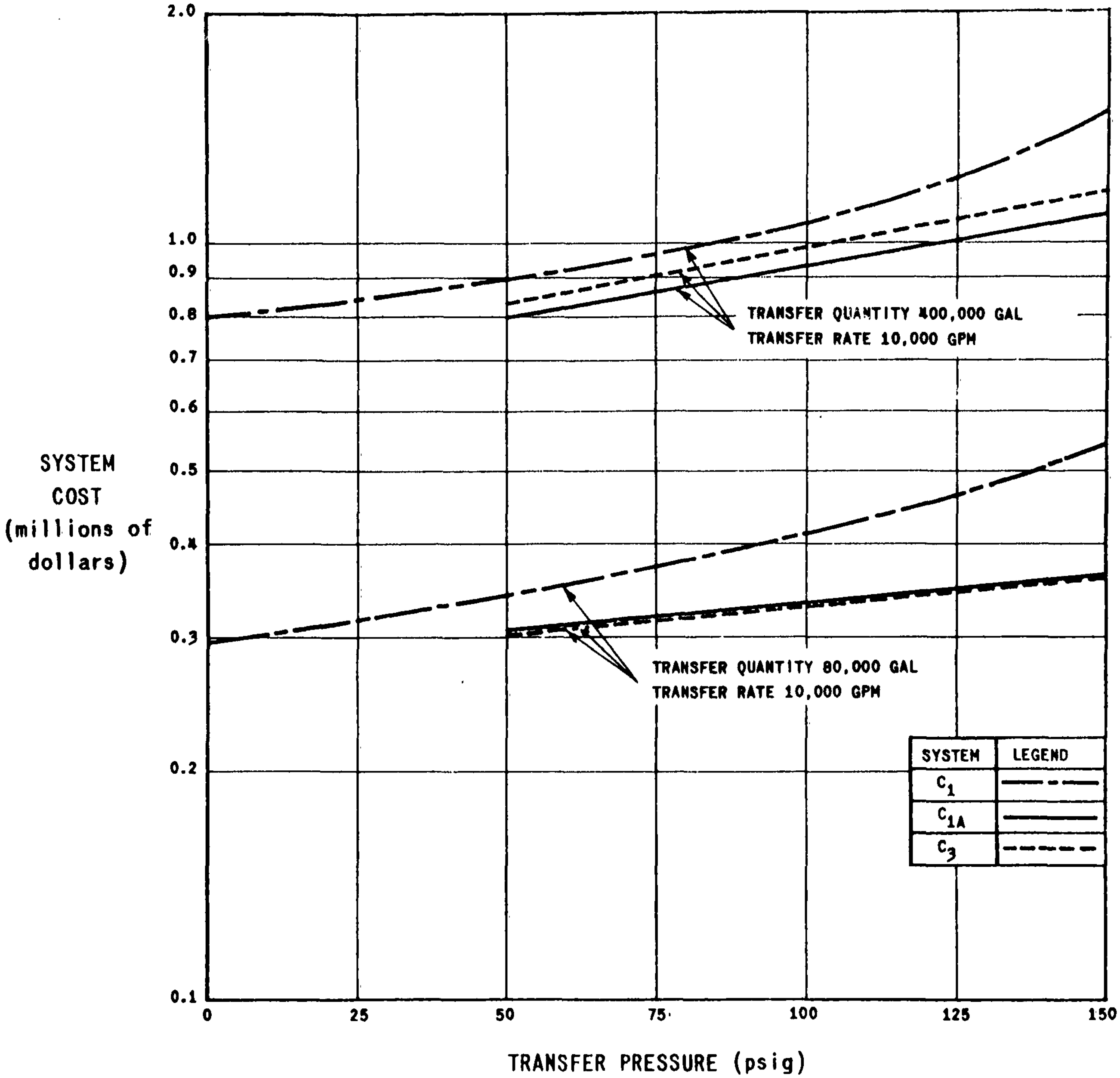

FIGURE 5.2 Cost Comparison of Vaporizer Systems

VI. DEVELOPMENT OF A COUPLING FOR A VACUUM-JACKETED LINE

A. INTRODUCTION

When disconnectable joints are needed in commercial, vacuum-jacketed cryogenic lines, bayonet-type couplings are usually supplied. Although the bayonet joint has been commonly accepted, it has some disadvantages when considered as an ultimate standard. Among these, one may cite:

1. The two mating elements of a coupling are not identical; male and female parts are necessary to make one joint.
2. To disassemble a joint requires that the piping be moved 10 to 12 inches in the axial direction.

Under AF 33(616)-5641 Arthur D. Little, Inc., undertook to develop a better coupling for vacuum-jacketed lines. This coupling would have two principal advantages:

1. It would consist of two identical parts, thus decreasing the inventory of parts and eliminating the problem of matching coupling elements.
2. It could be parted in a direction perpendicular to its axis, so as to facilitate the assembly or removal of a section of the line.

Such a coupling was designed, and an experimental model was constructed and tested.(1) The tests proved the design to be feasible but showed that the high loads necessary to seal the gasket at the cold joint were beyond the capabilities of spring members made of 304L stainless steel. Design changes were recommended to correct this shortcoming. These changes were incorporated in a prototype unit, which was built and tested under Contract AF 33(616)-7330, as described below.

B. DESIGN DESCRIPTION

The proposed design of a 2-inch coupling developed as a result of analyses and tests to date is shown in Figure 6.1. In this design, the cold seal is effected by the compression of a flat gasket between rings attached

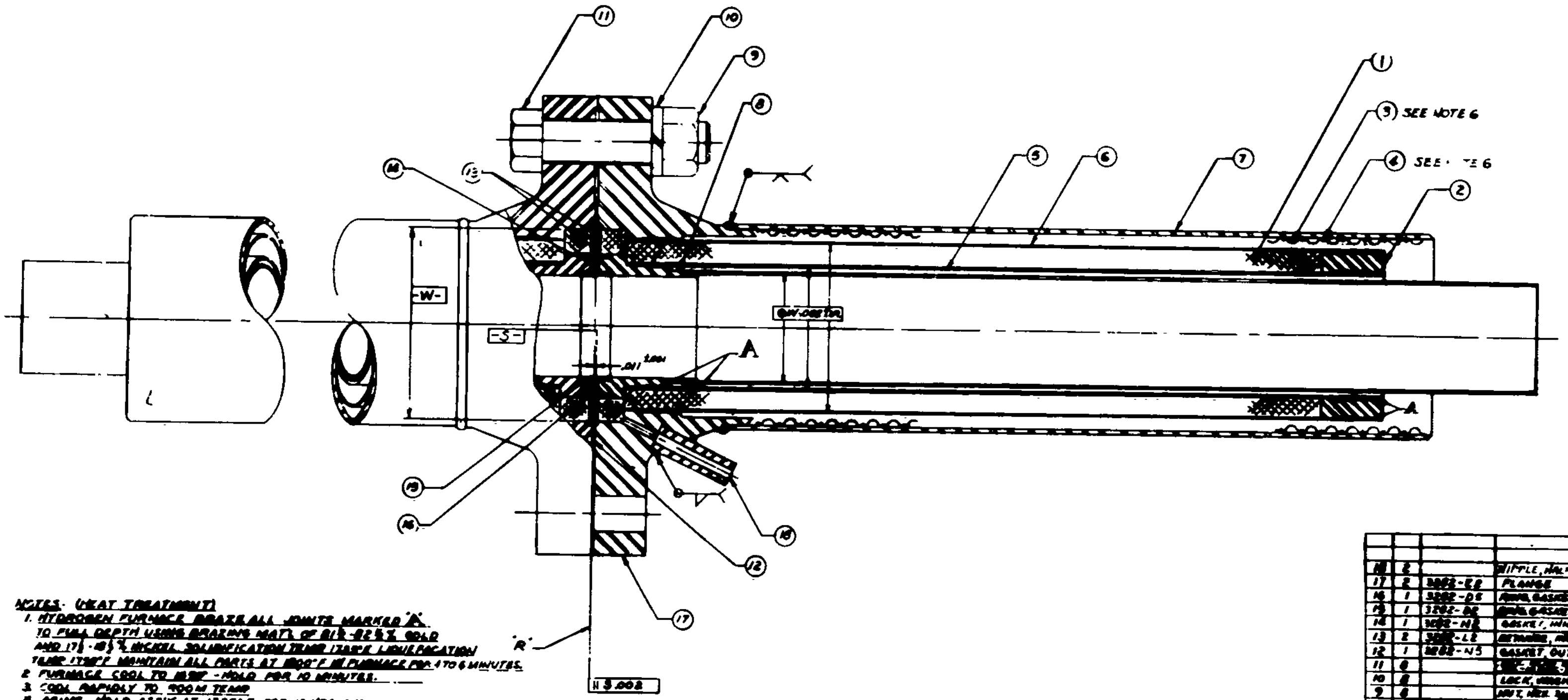

NOTES- (HEAT TREATMENT)
1. HYDROGEN FURNACE BRAZE ALL JOINTS MARKED 'A' TO FULL DEPTH USING BRAZING MAT'L OF 81½-82½% GOLD AND 17½-18½% NICKEL. SOLIDIFICATION TEMP 1735°F LIQUEFACATION TEMP 1740°F MAINTAIN ALL PARTS AT 1800°F IN FURNACE FOR 4 TO 6 MINUTES.
2. FURNACE COOL TO 1650°F - HOLD FOR 10 MINUTES.
3. COOL RAPIDLY TO ROOM TEMP.
4. AGING - HOLD ASS'Y AT 1325°F FOR 16 HRS. AND AIR COOL.

(ASSEMBLY NOTES)
5. SURFACE 'S' MUST BE .011 ±.001 BELOW SURFACES 'R' (SURFACE 'S' IS MEASURED FROM TOP OF SERRATIONS.
6. ALUMINUM FOIL IS WRAPPED THE FULL LENGTH OF ITEM AND SECURED WITH PIANO WIRE.

18	2		NIPPLE, HALF [illegible]	SST	
17	2	3282-E2	FLANGE	SST	
16	1	3282-D5	RING, GASKET [illegible]	SST	[illegible]
15	1	3282-D2	RING, GASKET RETAINING	SST	[illegible]
14	1	3282-N2	GASKET, INNER	LEAD	
13	2	3282-L2	RETAINER, INSULATION	MICARTA	
12	1	3282-N5	GASKET, OUTER	LEAD	
11	8		[illegible]	SST	
10	8		LOCK, WASHER (¾)	SST	
9	8		NUT, HEX ¾-10UNC-2B	SST	
8	2	3282-[illegible]	COLD FLANGE ASSY	SST	[illegible]
7	2	3282-F2	TUBE, OUTER	SST	
6	2	3282-J2	TUBE, OUTER SUPPORT	SST	
5	2	3282-K2	TUBE, INNER SUPPORT	SST	
4	[illegible]		PIANO WIRE	STL	
3	[illegible]		ALUMINUM FOIL		
2	2	3282-G2	RING, JUNCTION	SST	[illegible]
1	[illegible]		[illegible]		
[illegible]	[illegible]	[illegible]	[illegible]	[illegible]	[illegible]

FIGURE 6.1 Development Coupling for Vacuum-Jacketed Liquid Hydrogen Transfer Line

to the inside diameter of the mating transfer lines. These rings are attached to the outer flange through joined, concentric tubes. The warm seal is produced by a flat gasket compressed between bolted flanges.

To produce and maintain a positive cold seal requires a proper combination of gasket, gasket pressure, and surface finish on the metal part at the gasket-metal interface. In this design, a chemical lead gasket squeezed between concentrically serrated surfaces is used. The gasket is further restrained by rings at its OD and ID; these rings also act to align the two halves of the coupling. Proper gasket loads for the cold seal are produced by tightening the outer flange and straining the concentric tube members by an amount determined by the offset between the gasket-ring interfacial plane and the parting line of the outer flange. In effect, the tubes are designed to act as springs to maintain minimum gasket sealing pressure, while compensating for manufacturing tolerances and dimensional changes accompanying cooldown.

To make the performance of the cold seal less sensitive to manufacturing tolerances, the design permits the cold flange to undergo a large axial displacement with respect to the warm flange. Since the gasket load must be large for effective sealing, a large energy storage in the spring member is required. In the loaded state, the inner tube of the two concentric tubes is in direct compression, and the outer tube is in direct tension. This is the stress condition for a most efficient spring. The spring force is a function of the tubes' cross-sectional area and allowable stress. The length of the tubes determines the spring rate and also provides the long conductive path necessary to minimize heat leak as well as to seal off the vacuum at the joint.

The warm seal is provided by a weather-resistant, flat rubber gasket that needs to seal against only a small pressure difference. It is readily compressible and allows a line-to-line contact of the outer flanges, thereby eliminating the influence of the warm-seal dimensional variations on the cold-seal requirements.

The bolted outer flange (shown in Figure 6.2) was selected as a good, rugged, proven connection, but the use of quick-disconnect types could be considered where the service warrants. A pipe connection communicating to the space between the warm and cold seal permits attachment of a pressure relief valve.

The ability to maintain a positive cold seal is a critical feature of the coupling design. This ability is enhanced by the use of high unit gasket loads, which, in turn, demand the use of a material for the tube members that has a high yield point and is serviceable at low temperatures. A heat-treated A-286 steel is used for the concentric spring members shown in Figure 6.1. The

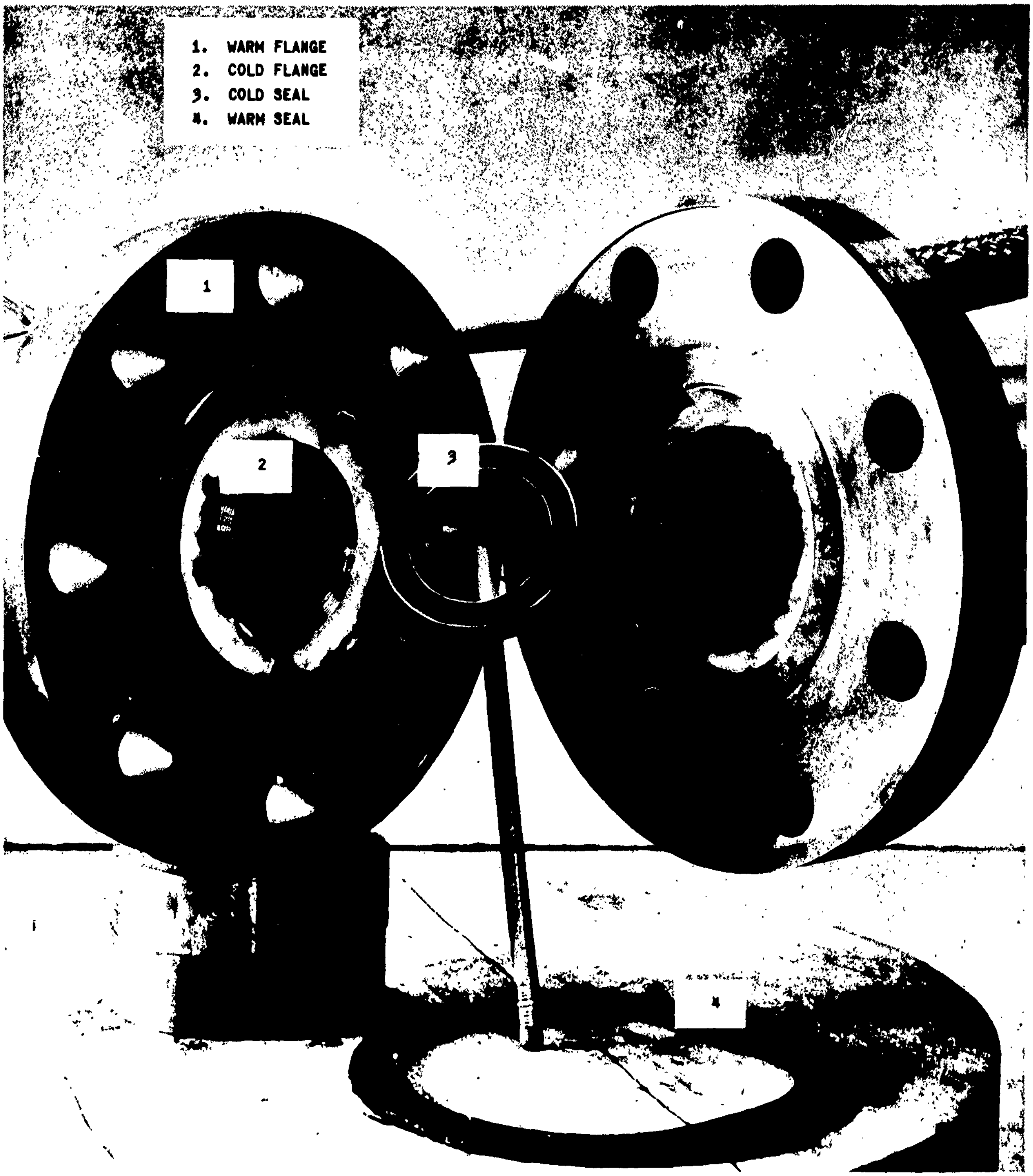
1. WARM FLANGE
2. COLD FLANGE
3. COLD SEAL
4. WARM SEAL
1
2
3
4

FIGURE 6.2 Warm and Cold Flanges of Liquid Hydrogen Transfer Line Coupling

brazed assembly provides the strength to carry the large shear loads. The elongated ring at the junction of the concentric tube members resists the large twisting stresses and deflections at this joint. Brazed assemblies of A-286 have not been strength-tested at temperatures lower than that of liquid nitrogen, but extrapolation indicates that they would give satisfactory service at liquid-hydrogen temperatures.

Insulation is placed between the two cylinders that form the connection between the cold seal and the warm flange. Without this insulation, a large (over 100 Btu/hr in the 2-inch size) heat inleakage would occur at the joint. In effect, the heat transfer between these cylinders short-circuits the resistance provided by the long cylinders themselves. Tests have shown that the installation of a Micro-fiberglas blanket with aluminum-foil radiation shields in this region provides a satisfactory insulation as long as the warm and cold seals are vacuum-tight. In such an arrangement, the pressure in the insulation space is reduced upon cooldown with liquid hydrogen to the degree necessary to make the effectiveness of the insulation satisfactory. A 1/4-inch NPT connection is provided to evacuate the space filled with Micro-fiberglas wool if the pipe is used in liquid nitrogen or LOX service or to attach a relief valve in case the cold seal begins to leak. A thin Micarta diaphragm is used to retain the insulation at the open end. The cold and warm flanges, the outside jacket and the inside pipe carrying the liquid are made of 321 stainless steel.

Full sets of detailed AFCON drawings for the coupling of 1-inch, 2-inch and 4-inch sizes are supplied under this contract. The sizes designate the inside diameter of the liquid-carrying tube.

C. MANUFACTURING

Our first attempt to braze the coupling assembly was made in accordance with the following recommendations received from the producer of the A-286 alloy:

1. Hydrogen-furnace or vacuum-furnace braze all joints with AMS 4775 Nicrobraze at 2100°F for 4 to 6 minutes.
2. Furnace-cool to 1650°F and hold for 5 minutes.
3. Cool rapidly to room temperature.
4. Age at 1325°F for 16 hours and air-cool.

The recommended gap between assembled parts prior to brazing was set at 0.001-.003 inch. After being brazed and heat treated as described above, the coupling proved to have vacuum leaks in the brazed joints. Attempts to correct this deficiency were unsuccessful. One of the coupling halves was broken during repeated handling. When we dissected this coupling half, we found signs of corrosion of the A-286 alloy next to the joint, evidence of brittle fracture of the A-286 alloy tube, and poor penetration of the brazing material into the joint. With further investigation, it became apparent that little is known about the brazing of A-286. References 2 and 3 describe some difficulties in brazing A-286 alloy that are very similar to those we experienced.

According to some investigators,(2) the microscopic structure of A-286 alloy changes at temperatures of 2100°F and above, causing brittleness at room temperature. The use of 82%-18% gold-nickel alloy allows performance of the brazing operation below the critical temperature. AMS 4775, which was originally recommended to us as a brazing compound, contains boron. Investigation showed that it may cause corrosion of the A-286 alloy.(3) Nickel plating prevents the attack of brazing material on A-286 alloy and also provides for a better bond between brazed parts.

Adopting these suggestions and some offered by several companies specializing in brazing, we modified the specifications for brazing as follows:

1. Control the dimensions of parts to be brazed to insure a gap of 0.0004 to 0.0020 prior to brazing.
2. Plate the areas to be brazed with a 0.0004-.0006-inch layer of nickel.
3. Hydrogen-furnace braze all joints with 82% gold-18% nickel alloy at 1800°F for 4 to 6 minutes.
4. Furnace-cool to 1650°F and hold for 10 minutes.
5. Cool rapidly to room temperature.
6. Hold assembly at 1325°F for 16 hours and air-cool.

In the fabrication procedure all parts were carefully inspected after machining and nickel plating to insure that the tolerances were maintained according to the design specifications. The coupling produced by these methods proved sound when tested as described below.

D. TESTS

1. Results

A test to determine the structural integrity of the coupling and the tightness of its seals and joints was made. No leaks were discovered through either of the two gaskets or through any of the brazed joints when the coupling was filled with liquid nitrogen and pressurized to 180 psig.

In the heat inleakage tests, the coupling was filled with liquid nitrogen; its boil-off rate was measured, and the heat losses were calculated from this rate. Two tests were conducted: in one, the space between cold and warm gaskets was evacuated; in the other, the space was filled with gaseous nitrogen. With the space between the warm and cold gaskets evacuated, the heat loss was 33 Btu/hr. When the space was not evacuated, the heat loss was 82 Btu/hr. In both tests the temperature of the warm flange was very close to the ambient.

The heat leak for other sizes may be estimated from analysis. A heat-transfer analysis of couplings of this family predicts a heat leak proportional to line size. For liquid hydrogen service, the estimated heat leaks are 80, 40, and 20 Btu/hr for the 4-inch, 2-inch, and 1-inch sizes, respectively.

2. Equipment

A photograph of the coupling test system is shown in Figure 6.3.

A major element of the test system is the supply dewar (Figure 6.4), which is essentially an insulated, stainless steel cryogen container. To minimize the heat leak to this vessel, it is placed in a vacuum chamber and surrounded by a liquid nitrogen jacket. The vessel is supported by Micarta columns. A thin-walled, stainless steel bellows is used for the fill and vent neck to the vessel. The vent is connected to a wet-test gas meter when the heat inleakage to the coupling is measured, or it is connected to a nitrogen gas bottle when the pressure retention capabilities of the coupling are to be determined. A horizontal run of 1-inch OD tubing is attached at the bottom of the measuring vessel. The test coupling is mounted on the other end of the tubing through an adapter. This line, which permits a cryogenic fluid to fill the test coupling, is surrounded by a copper thermal radiation shield attached to the liquid nitrogen jacket. The radiation shield is, in turn, surrounded by an outer tube. The spaces on both sides of the radiation shield are evacuated. When the coupling is attached to the adapter, it is possible to evacuate one coupling half and the spaces about the cryogen vessel with the same pumping apparatus. Provision is made to evacuate the other half of the coupling and the space between the warm and cold flanges.

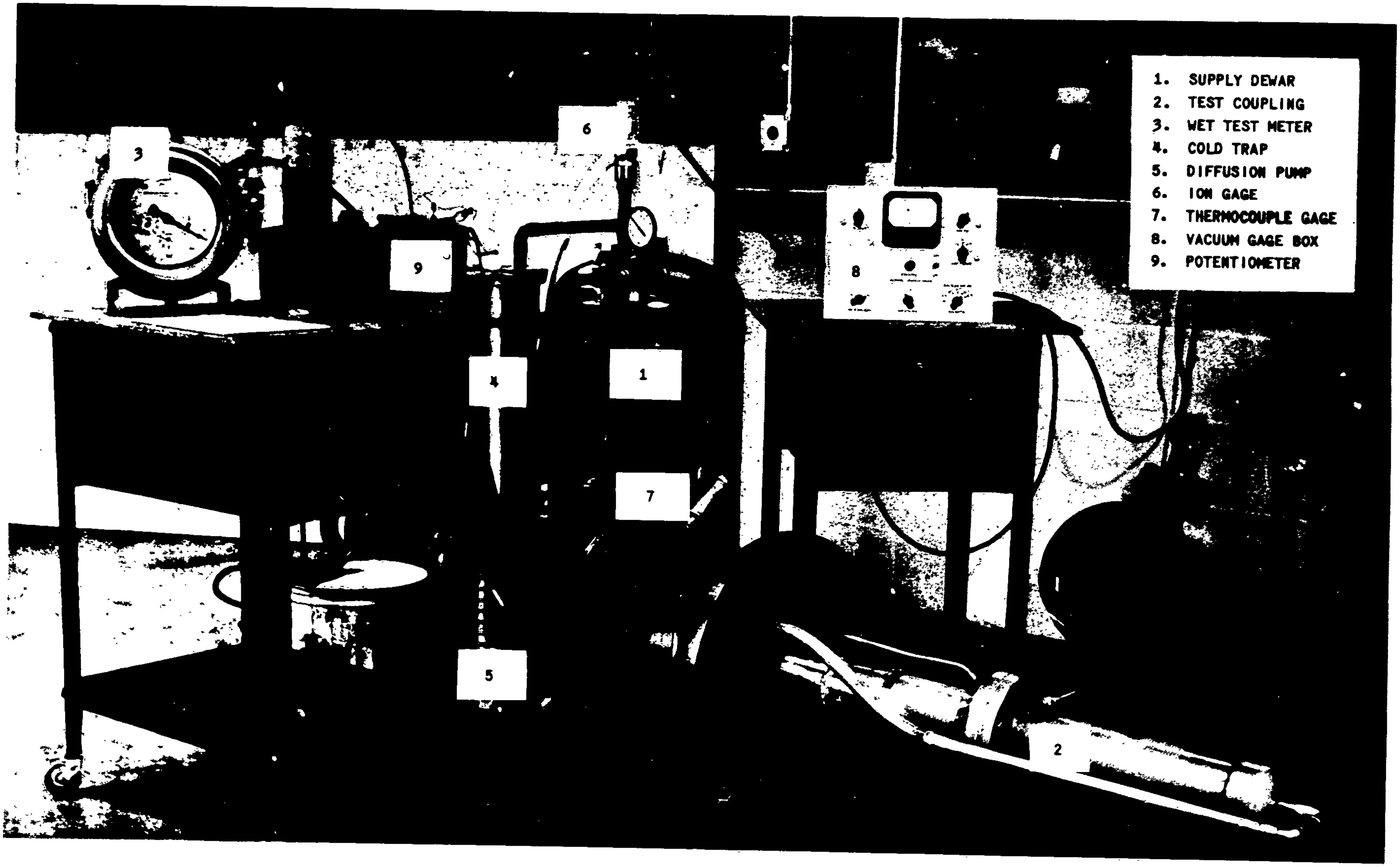
1. SUPPLY DEWAR
2. TEST COUPLING
3. WET TEST METER
4. COLD TRAP
5. DIFFUSION PUMP
6. ION GAGE
7. THERMOCOUPLE GAGE
8. VACUUM GAGE BOX
9. POTENTIOMETER
1
2
3
4
5
6
7
8
9

FIGURE 6.3 Coupling Test Apparatus

A 2-inch diffusion pump with a single-stage forepump was used to evacuate the system. The vacuum was measured by a thermocouple gage and an ionization gage. A system of valves was used to separate any part of the vacuum system for leak checking.

Four thermocouples were installed to check the outer flange temperature and the temperature of the outer tube of the coupling 6 inches from the flange.

The following commercially available equipment was used in the test system:

1. NRC Diffusion Pump, Type 113-VI, H-2-D.
2. Welch Vacuum Forepump, 1403-B
3. NRC Ionization Gage, 05-0700
4. NRC Thermocouple Gage, 05-0100
5. American Wet Test Gas Meter, 7420
6. Lunkenheimer Relief Valve, Figure 1227
7. Minneapolis-Honeywell Potentiometer, Model No. 2732
8. U. S. Gage Company Compound Pressure Gage, Figure 5058

3. Procedure

a. Test Stand Calibration

Before the heat leak of the coupling could be evaluated, it was necessary to determine the tare heat leak of the supply dewar and connecting tube. This was done by sealing the end of the connecting tube between the coupling and measuring vessel at the adapter and filling both the measuring vessel and nitrogen jacket with liquid nitrogen.

Readings of the gas meter attached to the vent of the measuring vessel were recorded every half hour. After a 4-1/2-hour cooldown period, the system had reached a state of equilibrium. The half-hour readings were constant for a period of two hours, at which point the test was terminated. The heat leak to the measuring vessel was calculated from the gas meter readings corrected for temperature and pressure.

1

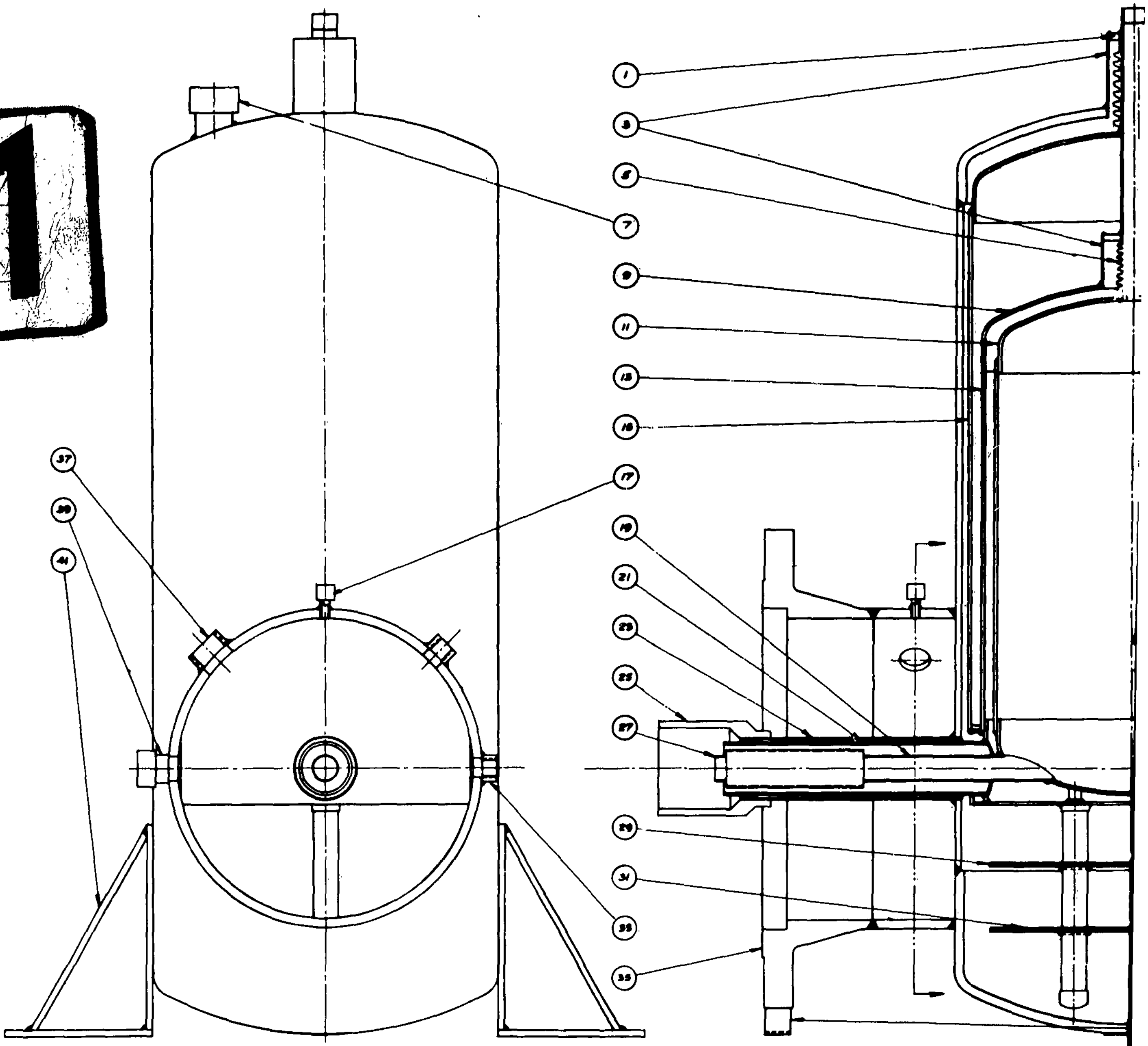
1
3
5
7
9
11
13
15
17
19
21
23
25
27
29
31
33
35
37
39
41

FIGURE 6.4

Supply Dewar for C

2

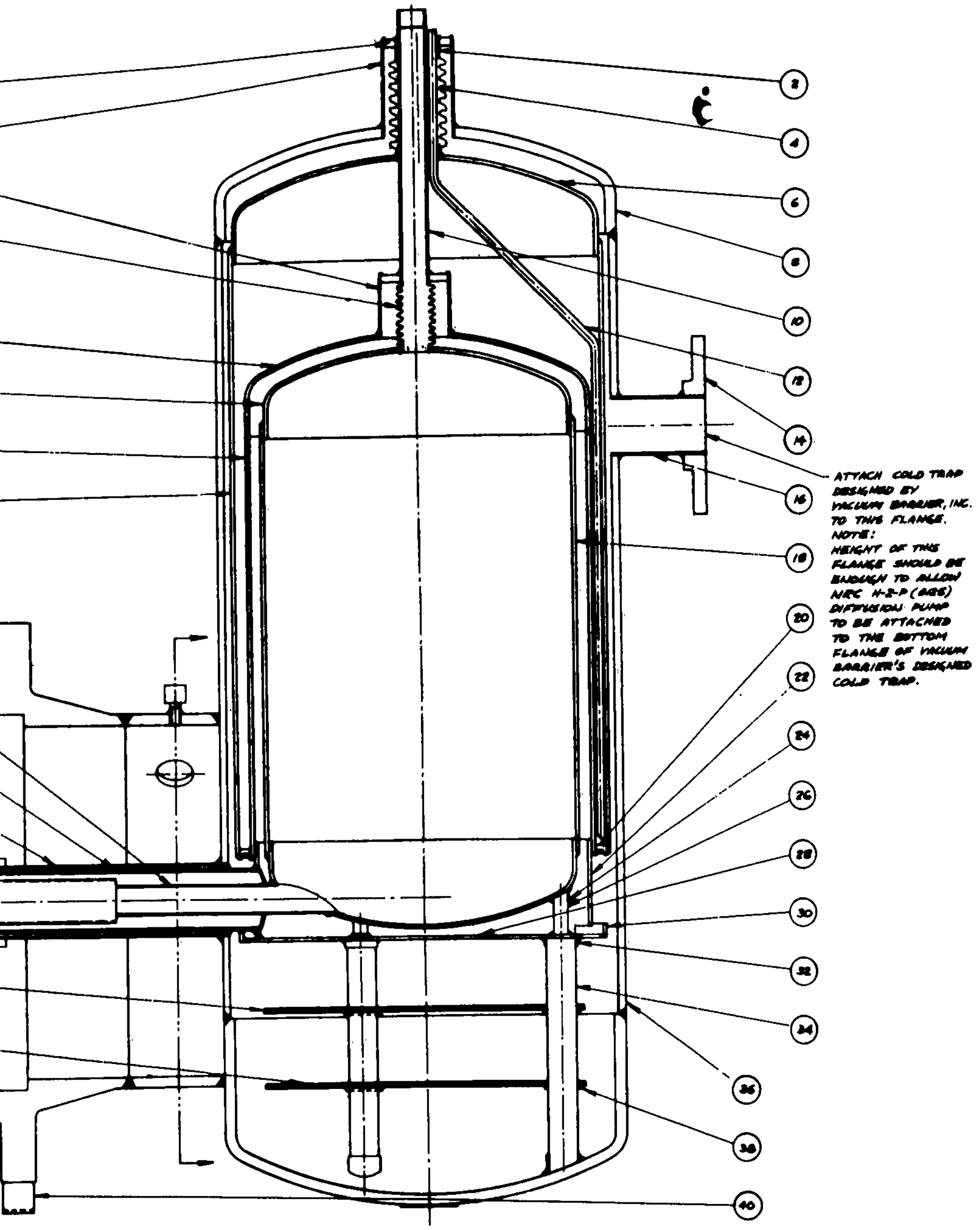
2
4
6
8
10
12
14
16
18
20
22
24
26
28
30
32
34
36
38
40
ATTACH COLD TRAP DESIGNED BY VACUUM BARRIER, INC. TO THIS FLANGE.
NOTE:
HEIGHT OF THIS FLANGE SHOULD BE ENOUGH TO ALLOW NRC H-2-P (ABE) DIFFUSION PUMP TO BE ATTACHED TO THE BOTTOM FLANGE OF VACUUM BARRIER'S DESIGNED COLD TRAP.

Item No.	Part Name
1	Disc-Pant Leg
2	Neck-Guard Tank
3	Pant Leg
4	Bellows-Guard Tank
5	Bellows-Inner Tank
6	Cap-Guard Tank
7	Universal Seal
8	Cap-Outer Jacket
9	Cap-Tubing
10	Neck-Inner Tank
11	Cap-Inner Tank
12	Nitrogen Fill Line
13	Shell-Guard Tank
14	Flange
15	Shell-Guard Tank
16	Vacuum Outlet
17	Quick Vacuum Coup.
18	Shell-Inner Tank
19	Transfer Line
20	Weld Ring
21	Copper Tubing
22	Radiation Shield
23	Jacket-Transf. Line
24	Seat
25	Adapter
26	Support-Inn. Tank
27	Vibration Elimin.
28	Radiation Shield
29	Spacer
30	Radiation Shield
31	Aluminum Foil
32	Seat
33	Half Coupling
34	Support-N_2 Tank
35	Flange
36	Shell-Outer Jack.
37	Half Coupling
38	Pin
39	Quick Vac. Coupl.
40	Stand
41	Stand

Supply Dewar for Coupling Test

b. Coupling Heat Leak

The heat-leak test on the coupling was made in a manner similar to the one described for the test stand calibration. After the test coupling was joined to the test stand, the system was evacuated to 6 x 10^{-5} mm Hg, and the measuring vessel and nitrogen jacket were filled with liquid nitrogen. After a one-hour cooldown period, both vessels were refilled and the gas meter was attached to the vent of the measuring vessel. Gas meter readings were taken every half hour. When the reading did not change, it was assumed that thermal equilibrium was reached.

The gas meter readings, in cubic feet per hour, after correction for temperature and pressure, were converted to the heat leak in Btu per hour. The heat leak of the coupling was computed by subtracting the test stand heat leak from the total measured heat leak.

The procedure described above was used to measure the heat inleakage to the coupling under two conditions. In one, the space between cold and warm flanges was evacuated; in the other, the space between two flanges was pressurized with gaseous nitrogen to 15 psia.

c. Product Leak

The product leak, as used in this report, refers to the leakage through the cold seal or warm seal into the insulated area. In the application of the ADL coupling to liquid hydrogen service, this area becomes evacuated because the condensables above hydrogen temperature migrate to the cold surface and freeze. In liquid nitrogen or LOX service, this space should be evacuated through the pipe nipples provided.

Two tests were performed to investigate the product leak. In both these tests the vacuum jackets of the supply dewar and coupling were evacuated to below 10^{-5} mm Hg, and the supply dewar and coupling were filled with liquid nitrogen and pressurized to 180 psig.

In the first test the space between the cold and warm flanges was filled with gaseous nitrogen to atmospheric pressure. The space was valved off, and the pressure in this space was monitored with a pressure gage and recorded for a half-hour period.

The same procedures were followed in a second test, except that the space between the cold and warm flanges was evacuated to 10^{-2} mm Hg.

E. CONCLUSION

The screening tests with liquid nitrogen indicate that the coupling under development has satisfactory performance and design characteristics. However, extensive performance and service tests with liquid hydrogen are necessary before its adoption for regular service can be recommended.

F. REFERENCES

1. Arthur D. Little, Inc., Storage, Transfer and Servicing Equipment for Liquid Hydrogen, WADC Technical Report 59-386 (July 1959).

2. "Metallurgical Characteristics of A-286 Alloy," Battelle Memorial Institute DMIC Memo #59 (July 26, 1960).

3. Aggen, G., Long, R. A., and Reynolds, E. E., "Ni-Cr-B Brazing of a High-Temperature Alloy," Welding Research Supplement, p. 366-S (August 1957).

DISTRIBUTION LIST
AFFTC TR-61-18

	NR. COPIES
DCAS (DCLMT) AF Unit Post Office Los Angeles 45 Calif	1
Lewis Research Center National Aeronautics & Space Administration Attn: Mr. Paul Ordin 21000 Brookpark Rd. Cleveland 35, Ohio	3
National Bureau of Standards Cryogenic Laboratory Attn: R. B. Scott, Chief Boulder, Colorado	1
University of California Attn: Mr. R. E. Schrieber P.O. Box 1663 Los Alamos, New Mexico	4
Armed Services Technical Information Agency Arlington Hall Station Arlington 12, Virginia	68
Federal Aviation Agency Bureau of Research & Development Attn: Records Officer Wash 25 DC	1
The Martin Company Denver Division Attn: Mr. M.S. Robinson Denver 1, Colo.	1
Air Products, Inc. Attn: Mr. J. A. Snyder P. O. Box538 Allentown, Pa.	1
Boeing Airplane Company Pilotless Aircraft Division Engineer Div - 5-7000 Attn: Mr. J. C. Drury Seattle, Wash.	1

Rocketdyne Division of North American Aviation Company Attn: Dr. Stanley Gunn Dept. 596 Group II Canoga Park, Calif	1
Pesco Products Division of Borg Warner Attn: Louis J. Schafer, Jr. 24700 N. Miles Road Bedford, Ohio	11
Aerojet-General Corp Attn: Dr. C. H. Trent 6352 Trwindale Road Azusa, Calif	1
Aerojet-General Corp Liquid Rocket Plant Attn: Mr. J. T. Paul for Mr. P.S. Gakle Sacremento, Calif	1
Convair Astronautics Attn: Mr. G. Drake San Diego, Calif	1
Bell Aircraft Corp Attn: Mr. A. Kimball Buffalo, New York	1
Pratt & Whitney Aircraft Florida Research & Development Center Attn: Mr. C. D. Robin United, Florida	1
Bogue Electric Manufacturing Company Attn: Mr. P. Turkheimer 52 Iowa Avenue Patterson 3, New Jersey	1
Linde Company Division Of Union Carbide Attn: P. P. Huffard, Jr. 30 E. 42 Street New York 17, New York	1
LPIA Johns Hopkins University Applied Physics Laboratory 8621 Georgia Ave. Silver Spring, Maryland	3

U.S. ATOMIC ENERGY COMMISSION 1
Tech. Information Service Extension
Attn: Margaret L. Pflueger
P. O. Box 62
Oak Ridge, Tenn.

General Dynamics Corp 1
Liquid Carbonic Div.
Attn: Mr. H. A. Koester
4400 W. 45th Street
Chicago 32, Ill.

U. S. Dept of Commerce 1
National Bureau of Standards
Attn: Mr. L. W. Scott (File #4200)
Washington 25, D. C.

American Clanamid Company 1
Attn: Mr. T. A. Ventrone
Bound Book, New Jersey

Dynamic Research, Inc. 1
Attn: Mr. W. C. Gates
6701 So. Sepulveda Blvd
Los Angeles 45, Calif

Office of the Chief of Engineers 1
Dept of the Army
Attn: Eng SD
Washington 25, D. C.

J. C. Carter Company 1
Attn: Mr. W. W. Saxton
671 W. 17th Street
Costa Mesa, Calif

Jet Propulsion Laboratory 1
Calif Institute of Technology
Attn: Mr. I. E. Newlan, Chief, Rpts Grp.
4800 Oak Grove Drive
Pasadena 3, Calif

Boeing Airplane Company 1
Aero-Space Division
Attn: Mr. F. C. Meer
P.O. Box 3707, Mail Stop 14-82
Seattle, Wash

Airesearch Manufacturing Company 1
Attn: Mrs. M. Stein
9851-9951 Sepulveda Blvd.
Los Angeles 45, Calif

General Dynamics Corp Convair (Astronautics) Division AFMTC Field Office Attn: Mr. B. G. MacNabb P. O. Box #999 Cocca Beach, Florida	3
Beechcraft Research & Development, Inc. Attn: Mr. B. Cooper Boulder, Colorado	1
U.S. Atomic Energy Commission Attn: HSSFP:RBS (Mr. D.F. Hayes) Washington 25, D. C.	1
ARMY Ballistic Missile Agency Missile Flying Laboratory Attn: ORDAB-DMMP (Mr. J. Deese) Titusville, Florida	1
NASA 1520 H Street Northwest Washington (25), D. C.	12
Pan American World Airways, Inc. Guided Missile Range Division Attn: AFMTC Tech. Library M.U. 135 Patrick AFB, Florida	1
General Electric Company Attn: Whitney Library, *Mrs. Jean Dado) P.O. Box 1088 Schenectady, New York	1
Office of Technical Services U.S. Dept of Commerce Washington 25, D.C.	100
ASD(WWDNS, Mr. B. C. Dunnam) Wright Patterson AFB, Ohio	1
ASD(WWDNSG, Mr. A.M. Paulson) Wright Patterson AFB, Ohio	1
ASD(WWRMFS, Mr. C. R. Martel) Wright Patterson AFB, Ohio	1

ASD(WWOA) Wright Patterson AFB, Ohio		1
ASD(WWT) Wright Patterson AFB, Ohio		1
ASD(WWDTC) Wright Patterson AFB, Ohio		1
ASD(WWE) Wright Patterson AFB, Ohio		1
6593d Test Gp (Dev) (DGRP) Edwards, Calif		60
ASD(WWRCEF) Wright Patterson AFB, Ohio		1
AFFTC (FTOTL) Edwards AFB, Calif		10
	TOTAL	311